OULU 2017
C 641

ACTA UNIVERSITATIS OULUENSIS


*Ari Vuokila*

# CFD MODELING OF AUXILIARY FUEL INJECTIONS IN THE BLAST FURNACE TUYERE-RACEWAY AREA

*UNIVERSITY OF OULU GRADUATE SCHOOL;*
*UNIVERSITY OF OULU,*
*FACULTY OF TECHNOLOGY*

ACTA UNIVERSITATIS OULUENSIS
C Technica 641

*ARI VUOKILA*

# CFD MODELING OF AUXILIARY FUEL INJECTIONS IN THE BLAST FURNACE TUYERE-RACEWAY AREA

Academic dissertation to be presented with the assent of the Doctoral Training Committee of Technology and Natural Sciences of the University of Oulu for public defence in the Arina auditorium (TA105), Linnanmaa, on 19 December 2017, at 12 noon

UNIVERSITY OF OULU, OULU 2017

Acta Univ. Oul. C 641, 2017

Supervised by
Professor Riitta Keiski
Docent Esa Muurinen

Reviewed by
Professor Björn Hjertager
Professor Anders Brink

Opponent
Professor Timo Hyppänen

ISBN 978-952-62-1769-7 (Paperback)
ISBN 978-952-62-1770-3 (PDF)

ISSN 0355-3213 (Printed)
ISSN 1796-2226 (Online)

Cover Design
Raimo Ahonen

JUVENES PRINT
TAMPERE 2017

**Vuokila, Ari, CFD modeling of auxiliary fuel injections in the blast furnace tuyere-raceway area.**
University of Oulu Graduate School; University of Oulu, Faculty of Technology
*Acta Univ. Oul. C 641, 2017*
University of Oulu, P.O. Box 8000, FI-90014 University of Oulu, Finland

***Abstract***

The blast furnace process is the most common way throughout the world to produce pig iron. The primary fuel and reducing agent in a blast furnace is coke. Coke is a fossil fuel and the most expensive raw material in iron production. Blast furnace ironmaking is an energy-intensive process, which results in high energy costs. Auxiliary fuels are injected into the blast furnace to replace expensive coke. They provide energy for the blast furnace operation and act as a source of reduction agents for iron oxides. Coke replacement with high auxiliary fuel injection levels leads to permeability changes in a blast furnace shaft, because of the increased amount of unburnt coal.

In this thesis, fuel injection with two different auxiliary fuels, heavy oil and pulverized coal, was studied using computational fluid dynamics (CFD) modeling. The aim was to improve the combustion of auxiliary fuels by increasing the understanding of the phenomena in the blast furnace tuyere-raceway area. The atomization model for modeling the heavy oil combustion was selected and validated using the results of an experimental rig from the literature. The atomization model was applied to study the effect of different nozzles on heavy oil mixing with the air blast. In addition, the model was used to study the effect of lance position on the combustion efficiency of heavy oil. A pulverized coal combustion model was developed and validated with experimental data from the literature. Pulverized coal combustion was modeled with different lance positions to evaluate its effect on combustion efficiency.

Based on the results, heavy oil mixing in the air blast can to a great extent, be boosted by the nozzle design. Furthermore, the heavy oil combustion is more efficient when the lance position is farthest from the tuyere nose. But the increasing temperature inside the tuyere causes ablation of the tuyere walls, which creates a constraint for the lance position. The results from the pulverized coal combustion study show that the model works well for the tuyere-raceway area. In addition, the effect of lance position on the combustion efficiency of the pulverized coal is very small, and the lance should be positioned as close to the tuyere nose as possible to avoid fouling of the tuyere walls and the ignition inside the tuyere.

*Keywords:* blast furnace, combustion, gasification, heavy oil, pulverized coal, raceway, tuyere

**Vuokila, Ari, Masuunin lisäpolttoaineinjektioiden virtausmallinnus hormin ja palo-onkalon alueella.**
Oulun yliopiston tutkijakoulu; Oulun yliopisto, Teknillinen tiedekunta
*Acta Univ. Oul. C 641, 2017*
Oulun yliopisto, PL 8000, 90014 Oulun yliopisto

## *Tiivistelmä*

Suurin osa maailman raakaraudasta valmistetaan masuuniprosessilla. Masuunin ensisijainen polttoaine ja rautaoksidien pelkistin on koksi. Koksi on fossiilinen polttoaine ja kallein raaka-aine masuunissa. Raudanvalmistus on erittäin energiaintensiivistä, joten valmistuksen energiakustannukset ovat korkeat. Lisäpolttoaineinjektiota käytetään masuunissa korvaamaan osa koksista sekä energian tuottajana että pelkistimenä. Injektiomäärät pyritään kasvattamaan mahdollisimman suuriksi, mutta injektiomäärien kasvaessa palamattoman kiinteän polttoaineen määrä kasvaa ja koksipatjan kaasunläpäisevyys heikkenee.

Väitöskirjatutkimuksessa luotiin virtauslaskentamalli hormin ja palo-onkalon alueelle kahta lisäpolttoainetta (raskas polttoöljy, kivihiilipöly) varten. Sen avulla tutkittiin palamista hormin ja palo-onkalon alueella tavoitteena lisätä tietoa palamista rajoittavista tekijöistä. Pisaroitumismalli valittiin ja validoitiin kirjallisuusdatan perusteella raskaan polttoöljyn toimiessa lisäpolttoaineena. Mallia käytettiin tutkittaessa erilaisia suuttimia palamisilman ja polttoaineen sekoittumisen tehostamiseen. Lisäksi sitä käytettiin mallinnettaessa lanssin sijainnin vaikutusta raskaan polttoöljyn palamistehokkuuteen. Kivihiilipölylle luotiin palamismalli, joka validoitiin olemassa olevan kokeellisen datan perusteella. Tätä mallia hyödynnettiin tutkittaessa kaksoislanssin sijainnin vaikutusta palamistehokkuuteen.

Tulosten perusteella voidaan todeta, että öljylanssin suuttimella on suuri vaikutus palamisilman ja polttoaineen sekoittumiseen. Lisäksi voidaan päätellä, että raskaan polttoöljyn palaminen tehostuu siirrettäessä lanssia syvemmälle hormiin, mutta syttyminen tapahtuu liian aikaisin ja kasvava lämpötila voi sulattaa hormin seinämät. Tämä aiheuttaa rajoituksen lanssin sijainnille hormissa. Kivihiilipölyn palamisen mallin todettiin toimivan erittäin hyvin hormin ja palo-onkalon alueilla. Tämän ohella havaittiin, että lanssin sijainnilla oli hyvin pieni vaikutus palamisasteeseen, jolloin lanssi kannattaa sijoittaa mahdollisimman lähelle hormin suuta, jotta vältetään hormiin kohdistuva ylimääräinen lämpökuorma ja hormin likaantuminen.

*Asiasanat:* hormi, kaasutus, kivihiilipöly, masuuni, palaminen, palo-onkalo, raskas polttoöljy

# Acknowledgements

The research work presented in this thesis was conducted in the Environmental and Chemical Engineering research unit (ECE) of the University of Oulu. I would like to thank my supervisors Prof. Riitta Keiski and Docent Esa Muurinen for the opportunity to work as a part of their research group. I also want to thank them for their support and guidance during the doctoral studies. I would also like to acknowledge Dr. Tiina Pääkkönen for her valuable comments on the thesis and for good collaboration during these years. I am thankful to Mr. Markus Riihimäki for his guidance at the beginning of my doctoral studies and his valuable remarks on my first journal paper as a co-author. Furthermore, I am thankful to Dr. Tuomas Paloposki from Aalto University for the material and data regarding the first journal article as well as the discussion about the experimental work on atomization and its CFD modeling.

I want to express my gratitude to Prof. Bjørn Hjertager from the University of Stavanger and Prof. Anders Brink from Åbo Akademi for their pre-examination of this thesis and their valuable comments on it.

During this work, I had the pleasure of working with industrial partners from SSAB Raahe. The blast furnace tuyere-raceway area proved to be a very interesting and challenging subject. I am grateful to Mr. Olli Mattila and Mr. Jarmo Lilja from SSAB Raahe for providing the necessary information for the CFD modeling and for all the interesting discussions we had about the subject. I appreciate their continued interest in this area, which made the thesis possible.

I would like to acknowledge my follow-up group– Prof. Timo Fabritius, Dr. Timo Paananen and Dr. Mika Ruusunen –for their guidance during the thesis work. We had good discussions about the thesis work and ideas for the future as well.

For financial support, I would like to thank the Finnish Funding Agency for Technology and Innovation, the Council of Oulu Region for the financing from the European Regional Development Fund and the Technology Industries of Finland Centennial Foundation.

Furthermore, I would like to thank my co-workers in the ECE research unit for collaboration and many nice moments during these years. I'm thankful for Auli Turkki for the help with the thesis bureaucracy and all the good discussions about renewable energy. I am also thankful for my former ECE colleague Dr. Timo Kulju for the numerous interesting discussions about CFD modeling. I would like to give warm thanks to my officemates during these years. I have had plenty of good conversations, nice moments, and heartfelt laughs with my former officemate, Dr.

Ari Väliheikki, and my current officemate, Mr. Esa Turpeinen. Many thanks for Mr. Tuomas Nevanperä for his friendship and peer support during these years.

Finally, my warmest expression of gratitude is given to my family. My parents Liisa and Pertti together with my brothers Arto, Miika, and Panu for their support and all the debates we have had during my life.

Oulu, December 2017 Ari Vuokila

# List of symbols and abbreviations

*Latin symbols*

| | |
|---|---|
| $a$ | particle volume/internal surface ratio, gas absorption coefficient |
| $a_p$ | equivalent absorption coefficient of particles |
| $a_{\varepsilon,i}$ | emissivity weighting factor for the *i*th gray gas |
| $A$ | area [$m^2$], modeling constant |
| $A_0$ | model constant for $C_\mu$ |
| $A_c$ | reaction constant [m/(s·K)] |
| $A_{coke}$ | coke particle surface area [$m^2$] |
| $A_i$ | pre exponential factor for the reaction i |
| $A_p$ | particle/droplet surface area [$m^2$] |
| $A_s$ | Gibb constant, model parameter for $C_\mu$ |
| $A_T$ | area of the tuyere nose [$m^2$] |
| $B$ | burnout [%], modeling constant |
| $B_0$ | droplet size constant |
| $B_1$ | droplet breakup time constant |
| $B_m$ | Spalding mass number |
| $B_T$ | Spalding heat transfer number |
| $c$ | speed of sound [m/s] |
| $c_p$ | specific heat capacity of droplet [J/(kg·K)] |
| $c_{p,i}$ | specific heat capacity of component i [J/(kg·K)] |
| $c_{p,\infty}$ | specific heat capacity of the gas [J/(kg·K)] |
| $C_1$ | empirical constant for diffusion-limited reaction rate, model parameter for Realizable κ-ε model |
| $C_{1\varepsilon,3\varepsilon}$ | constants for dissipation generation |
| $C_2$ | constant for Realizable κ-ε model |
| $C_d$ | constant for mixture fraction variance conservation equation |
| $C_g$ | constant for mixture fraction variance conservation equation |
| $C_p$ | specific heat capacity of the gas mixture [J/(kg·K)] |
| $C_D$ | drag coefficient |
| $C_{EBU}$ | Eddy-Break-Up constant |
| $C_L$ | constant for time scale of dissipation |
| $C_\mu$ | turbulent viscosity coefficient |
| $C_\xi$ | volume fraction constant |

| | |
|---|---|
| $C_\tau$ | time scale constant |
| $d_c$ | char particle diameter [m] |
| $d_{coke}$ | coke particle diameter [m] |
| $d_l$ | droplet diameter [m] |
| $d_p$ | particle diameter [m] |
| $d_R$ | raceway depth [m] |
| $d_{st}$ | particle diameter after breakup [m] |
| $d_T$ | tuyere diameter [m] |
| D | external diffusion coefficient [$m^2 \cdot s^{-1}$] |
| $D_{i,m}$ | mass diffusion coefficient for species i [$m^2 \cdot s^{-1}$] |
| $D_p$ | pore diffusivity [$m^2/s$] |
| $D_{ref}$ | dynamic diffusivity [kg/(m·s)] |
| $D_t$ | turbulent diffusivity [$m^2/s$] |
| $D_{T,i}$ | thermal diffusion coefficient for species i [$m^2 \cdot s^{-1}$] |
| E | energy [J] |
| $E_i$ | activation energy for the reaction i [J/kmol] |
| $E_p$ | equivalent emission of the particles |
| $F_D$ | drag force |
| $\vec{F}$ | additional acceleration [$m/s^2$] |
| g | gravity constant [$m/s^2$] |
| $G_b$ | buoyancy effects on the production of turbulent kinetic energy [$m^2/s^2$] |
| $G_k$ | production of turbulent kinetic energy [$m^2/s^2$] |
| h | sensible enthalpy [J/kg], convective heat transfer coefficient [$W/(m^2 \cdot K)$] |
| $h_i$ | enthalpy for species i |
| $h_{fg}$ | latent heat [J/kg] |
| $h_g$ | heat transfer coefficient [$W/(m^2 \cdot K)$] |
| $h_R$ | raceway height [m] |
| I | unit tensor, intensity [$W/m^2$] |
| $\vec{J}_i$ | species diffusion flux [$mol/(m^2 s)$] |
| k | thermal conductivity [W/(m·K)] |
| $k_c$ | chemical rate coefficient [kg/s], mass transfer coefficient [m/s] |
| $k_d$ | diffusion of oxidizing species [$m^2/s$] |
| $k_{eff}$ | effective conductivity [W/(m·K)] |
| $k_i$ | reaction rate constant for reaction i |
| $k_t$ | turbulent thermal conductivity [W/(m·K)] |

| | |
|---|---|
| $k_\infty$ | thermal conductivity of the gas [W/(m·K)] |
| l | characteristic length scale of the system [m] |
| $L_e$ | turbulent eddy length scale |
| $m_a$ | ash content of the current time step [kg] |
| $m_{a,0}$ | ash content of the initial coal particle [kg] |
| $m_c$ | char mass [kg] |
| $m_{coke}$ | coke mass [kg] |
| $m_p$ | particle mass [kg] |
| $m_{p,0}$ | initial particle mass [kg] |
| $m_v$ | volatile mass [kg] |
| $M_t$ | turbulent Mach number |
| $M_w$ | molecular weight [g/mol] |
| n | refractive index |
| Nu | Nusselt number |
| Oh | Ohnesorge number |
| p | pressure [Pa] |
| $p_A$ | atmospheric pressure [Pa] |
| $p_g$ | air blast pressure [Pa] |
| $p_{op}$ | operating pressure [Pa] |
| $p_{ox}$ | partial pressure of oxygen [Pa] |
| $p_s$ | static pressure [Pa] |
| $p_x$ | sum of the partial pressures of all absorbing gases [Pa] |
| Pr | Prandtl number |
| Q | heat flow rate [W] |
| r | random number |
| $\vec{r}$ | position vector |
| $r_0$ | initial droplet radius [m] |
| $r_{coke}$ | coke particle radius [m] |
| $r_d$ | droplet radius [m] |
| $r_p$ | particle radius [m] |
| R | universal gas constant [J/(kmol·K)] |
| $R_{diff}$ | diffusion-limited reaction rate [kg/s] |
| Re | Reynolds number |
| $Re_{crit}$ | critical Reynolds number |
| $Re_d$ | particle Reynolds number |
| $Re_t$ | turbulent Reynolds number |
| $R_i$ | net rate of production of species i by chemical reaction [kg/s] |

| | |
|---|---|
| $R_I$ | inertial resistance [1/m] |
| $R_{kin}$ | kinetic-limited reaction rate [kg/s] |
| $R_v$ | viscous resistance [1/m$^2$] |
| $\vec{s}$ | direction vector [m] |
| $\vec{s}$' | scattering direction vector [m] |
| S | modulus of the mean rate of strain tensor [1/s] |
| $Sc_t$ | turbulent Schmidt number |
| $S_d$ | rate of creation by addition from the dispersed phase [kg/(m$^3$·s)] |
| $S_h$ | source term for the chemical reactions, heat sources and sinks, and radiation heat sources [W/m$^3$] |
| $S_i$ | source term for the momentum equation [N/m$^3$] |
| $S_{ij}$ | mean strain rate tensor [1/s] |
| $S_m$ | source term for the mass addition [kg/(m$^3$·s)] |
| t | time [s] |
| T | temperature [K], integral time scale [s] |
| $T_c$ | Field char oxidation model reaction parameter [K] |
| $T_{coke}$ | coke temperature [K] |
| $T_e$ | characteristic lifetime of the eddy [s] |
| $T_g$ | gas temperature [K], air blast temperature [K] |
| $T_L$ | Lagrangian integral time scale [s] |
| $T_p$ | particle temperature [K] |
| $T_{ref}$ | reference temperature [K] |
| $T_s$ | Gibb char oxidation model reaction parameter [K] |
| $T_0$ | coke bed temperature [K] |
| $T_\infty$ | continuous phase temperature [K] |
| Ta | Taylor number |
| u | velocity [m/s] |
| $u_i$ | velocity in direction i [m/s] |
| $\overline{u_i'}$ | temporal average of the fluctuating velocity in suffix notation |
| $\overline{u_j'}$ | temporal average of the fluctuating velocity in suffix notation |
| $u_{mag}$ | velocity magnitude [m/s] |
| $\vec{u}_p$ | particle velocity [m/s] |
| u' | velocity fluctuation [m/s] |
| $\overline{u}$ | mean fluid phase velocity [m/s] |
| U$^*$ | model parameter for $C_\mu$ [1/s] |
| $v_s$ | speed of sound [m/s] |
| $\vec{v}$ | velocity vector [m/s] |

| | |
|---|---|
| $v'_{kl}$ | stoichiometric coefficient for the reactant |
| $v''_{kl}$ | stoichiometric coefficient for the product |
| $V_g$ | volume flow of air blast [$m^3/s$] |
| $w_R$ | raceway width [m] |
| We | Weber number |
| $x_j$ | position vector [m] |
| $X_g$ | mole fraction of the oxidizing species |
| $y^+$ | dimensionless wall distance |
| $Y_i$ | mass fraction of component i |
| $Y_i^*$ | fine-scale species mass fraction after reacting over time $\tau^*$ |
| $Y_{i,s}$ | vapor mass fraction at the surface |
| $Y_{i,\infty}$ | vapor mass fraction in the bulk gas |
| $Y_M$ | fluctuation dilatation |
| $\overline{Y_p''^2}$ | variance of the product mass fraction |

### *Greek letters*

| | |
|---|---|
| $\alpha_{1,2}$ | yield factors |
| $\delta_{ij}$ | Kronecker delta |
| $\varepsilon$ | turbulent dissipation rate [$m^2/s^3$], total emissivity |
| $\varepsilon_{char}$ | char particle void fraction |
| $\varepsilon_i$ | porosity of zone i |
| $\varepsilon_{ijk}$ | Levi-Civita permutation symbol |
| $\varepsilon_p$ | particle emissivity |
| $\eta$ | time scale ratio of the turbulence to the mean strain |
| $\theta_R$ | radiation temperature [K] |
| $\kappa$ | turbulence kinetic energy [$m^2/s^2$] |
| $\kappa_i$ | absorption coefficient of the i*th* gray gas [1/m] |
| $\Lambda$ | wavelength of the fastest growing wave [m] |
| $\rho$ | density [$kg/m^3$] |
| $\bar{\rho}$ | mean time averaged fluid density [$kg/m^3$] |
| $\rho_c$ | char density [$kg/m^3$] |
| $\rho_{coke}$ | coke density [$kg/m^3$] |
| $\rho_g$ | gas density [$kg/m^3$] |
| $\rho_{g0}$ | gas density under standard condition [$kg/m^3$] |
| $\rho_l$ | liquid density [$kg/m^3$] |
| $\rho_p$ | droplet/particle density [$kg/m^3$] |

| | |
|---|---|
| $\rho_\infty$ | bulk gas density [kg/m$^3$] |
| $\mu$ | dynamic viscosity [kg/(m·s)] |
| $\mu_{eff}$ | effective viscosity [kg/(m·s)] |
| $\mu_t$ | turbulent viscosity [kg/(m·s)] |
| $\nu$ | kinematic viscosity [m$^2$/s] |
| $\xi^*$ | length scale fraction of the fine scales |
| $\sigma$ | Stefan-Boltzmann constant [W/(m$^2$·K$^4$)] |
| $\sigma_l$ | surface tension [N/m] |
| $\sigma_p$ | equivalent particle scattering factor |
| $\sigma_\varepsilon$ | turbulent Prandtl number for turbulence kinetic energy |
| $\sigma_\varepsilon$ | turbulent Prandtl number for turbulent dissipation rate |
| $\tau$ | droplet breakup time [s] |
| $\tau^*$ | time scale of the reaction time in fine structures [s] |
| $\tau_{cross}$ | particle eddy crossing-time [s] |
| $\tau_l$ | mean life time for turbulent eddies [s] |
| $\overline{\overline{\tau}}_{eff}$ | effective viscous stress tensor [s] |
| $\tau_l$ | time scale of dissipation [s] |
| $\overline{\phi}_i$ | density-weighted mean variable of species i |
| $\Phi$ | phase function |
| $\psi$ | sphericity of the coke particle |
| $\omega_k$ | angular velocity [rad/s] |
| $\overline{\omega_p}$ | turbulent mean reaction rate of products [kg/s] |
| $\Omega$ | maximum wave growth rate |
| $\Omega$' | solid angle [rad] |
| $\Omega_{ij}$ | rotation rate viewed from the absolute frame of reference [rad/s] |
| $\widetilde{\Omega}_{ij}$ | extra rotation term [rad/s] |
| $\overline{\Omega}_{ij}$ | mean rotation rate viewed from the rotating frame of reference [rad/s] |

### *Acronyms*

| | |
|---|---|
| BF | Blast Furnace |
| BOFG | Basic Oxygen Furnace Gas |
| CFD | Computational Fluid Dynamics |
| COG | Coke Oven Gas |
| DEM | Discrete Element Method |

| | |
|---|---|
| EBU | Eddy-Break-Up |
| EHO | Extra Heavy Oil |
| FVM | Finite Volume Method |
| NG | Natural Gas |
| PC | Pulverized Coal |
| PCI | Pulverized Coal Injection |
| RR | Replacement Ratio |
| VM | Volatile Matter |
| VMD | Volume Median Diameter |

# List of original publications

This thesis is based on the following publications, which are referred throughout the text by their Roman numerals:

I Vuokila A, Riihimäki M & Muurinen E (2014) CFD-modeling of heavy oil injection into blast furnace – Atomization and mixing in raceway-tuyere area. *Steel Research International 85*(11): 1544-1551.

II Vuokila A, Mattila O, Keiski RL & Muurinen E (2017) CFD study on the heavy oil lance positioning in the blast furnace tuyere to improve combustion. *ISIJ International 57*(11): 1911-1920.

III Vuokila A, Mattila O, Keiski RL & Muurinen E (2016) CFD modeling of pulverized coal combustion in blast furnace test rig. *Industrial Combustion. Article No. 201603: 1.*

IV Vuokila A, Mattila O, Keiski RL & Muurinen E (2018) CFD modeling on the effect of double lance position on pulverized coal combustion in blast furnace tuyere-raceway area. Manuscript.

Vuokila was the main author of all Papers I-IV.

# Table of contents

# 1 Introduction

## 1.1 Background

Blast furnace (BF) is the most commonly used technology in ironmaking. It is a shaft furnace where raw materials, mainly iron ore and coke, are charged from the top. In the case of the collaborating partner, SSAB Raahe BFs, iron ore is in the form of pellets and briquettes. Coke acts as a reducing agent and the main source for the primary reducing agent carbon monoxide (CO) in BF, and it also provides heat for the BF operation via combustion reactions. To provide the required oxygen ($O_2$) for the combustion and gasification of fuels, a hot air blast is blown through tuyeres in the lower part of the BF. Auxiliary fuels (pulverized coal (PC), natural gas, extra heavy oil, tar, etc.) are injected into BF through tuyeres to reduce consumption of expensive coke, to decrease carbon dioxide ($CO_2$) emissions (higher H/C ratio), to stabilize the process and to increase productivity. Auxiliary fuels can replace coke in two ways–as a source of reducing agents for iron oxides (CO, $H_2$), and to provide energy for the blast furnace operation. (Ishii, 2000)

In the SSAB Raahe BF the injection is limited to 100–120 kg per ton of hot metal (thm) with the extra heavy oil injection and to 160 kg/thm with the PC injection. The target is to increase the heavy oil injection level to 160 kg/thm and the PC injection level to 235 kg/thm. The goal has not been reached yet, because of the challenges in combustion. Worldwide, the PC injection levels are increasing. For example, in Baosteel (Baosteel, 2017) several BFs have the injection rate between 220–250 kg/thm, and in Tata Steel's (Chatterjee, 2012) BFs 6 and 7, the injection rate is between 220–240 kg/thm.

The injection system should be improved to increase the amount of auxiliary fuel injection to gain the maximum benefit. Regardless of the fuel, the main problems arise from the poor mixing between the air blast and the fuel in the tuyere-raceway area. Auxiliary fuel combustion at high injection levels tends to be incomplete and it produces small char particles (soot, cenosphere, and/or char) in the raceway area, which plugs the porous coke bed and reduces the gas flow through the blast furnace. Permeability issues can be tackled with an adjusted charging program, but poor auxiliary fuel combustion will not enable cost-efficient substitution of coke with coal. The only way to overcome this limit is to improve conditions in the auxiliary fuel combustion. (Ishii, 2000; Moszkowicz, Witzel, & Claus, 1996)

Combustion efficiency has been improved using several different methods including various lance configurations (Majeski, Runstedtler, D'alessio, & Macfadyen, 2015), double lance systems (Ariyama, Sato, Yamakawa, Yamada, & Suzuki, 1994), tuyere modifications (Nozawa *et al*., 2011), oxygen enrichment of the air blast (Y. S. Shen, Yu, Austin, & Zulli, 2012), a more reactive coal type (Y. S. Shen, Guo, Yu, & Zulli, 2009c), and multi-fuel injections (Majeski *et al*., 2015).

Two different auxiliary fuels, extra heavy oil and PC, are studied in this thesis. Liquid and solid fuels require different approaches in modeling. Liquid fuels atomize into droplets, vaporize to a mixture of combustible gases, and in the case of extra heavy oil, leave a solid carbonaceous residue called cenosphere. In the solid fuel combustion, devolatilization releases a mixture of combustible gases leaving a residue called char, which contains carbon and ash-forming elements. Gas phase combustion is common with both fuels. Char and cenosphere combustion is heterogeneous combustion, which is much slower than the gas phase reactions. Therefore heavy oil droplet combustion is faster than that of a PC particle of the same size.

Effective combustion of auxiliary fuels requires good mixing as well as maximized residence time in the tuyere-raceway area. Therefore lance design and lance positioning are very important factors in effective combustion. There are several constraints in the design process; for example the fuel must not touch the tuyere walls, pressure losses should be as small as possible and combustion should not occur inside the tuyere. (Ishii, 2000)

Effective heavy oil combustion requires small droplets to maximize the vaporization surface. This can be affected by the nozzle design and the lance positioning. The PC particle size is also very important. Particles that are too small ignite too quickly inside the tuyere, but particles that are too large do not have time to react sufficiently. The PC volatile fraction is an important factor for the combustion rate; i.e., the higher the volatile fraction the faster the combustion. High volatile coals also have more reactive char. The coal lance position is important, because it affects the residence time and mixing of the fuel. The double lance system halves the PC injection velocity when compared to the single lance system even though the mass flow rate remains the same. This leads to an increase in the residence time of the PC particle. In addition, it enhances the particle dispersion throughout the cross section of the tuyere because of the two injection points. (Ariyama *et al*., 1994)

## 1.2 Objectives and scope

In this thesis, the main goal is to gain new knowledge about the limiting factors in blast furnace auxiliary fuel injection and to maximize the coke replacement ratio by increasing the amount and combustion degree of the injected fuel. The knowledge can be applied to the actual BF process to minimize existing problems in injection technologies. The objectives of the thesis are summarized in the following way:

- To gain knowledge about the modeling of secondary atomization of the extra heavy oil in the tuyere-raceway area and evaluate the suitability of the existing atomization models for auxiliary fuel injection.
- To improve the geometry of the injection nozzle to maximize the mixing of auxiliary fuel and the air blast.
- To develop a combustion model for the extra heavy oil injection and to validate the model.
- To develop a combustion model for the pulverized coal injection and to validate the model.
- To find out limiting factors for the auxiliary fuel combustion in BF with the created CFD models.

This thesis consists of three refereed journal articles and one manuscript. The scope of the original papers is shown in Fig. 1.

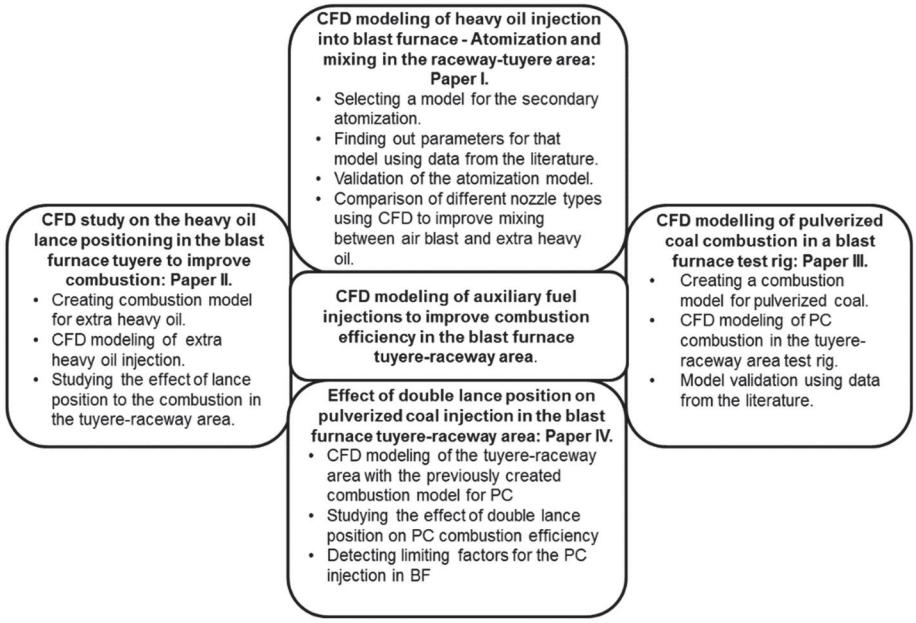


**Fig. 1. Scope and contribution of the original publications to the thesis.**

The scope of this thesis is to create a combustion model for extra heavy oil and pulverized coal and to apply CFD to improve auxiliary fuel combustion and to find out limiting factors for the high auxiliary fuel injection levels.

In Paper I, secondary atomization of extra heavy oil is modeled with CFD. The goal was to find out an atomization model and model constants that have a good fit with the experimental results. The model was validated with experimental data and later used to study the mixing between the air blast and the extra heavy oil.

The combustion model for the extra heavy oil is presented in Paper II. The secondary atomization model for the extra heavy oil, from Paper I, was used in the study. The maximum adiabatic flame temperature of the combustion model was calculated and compared to the temperature obtained by the probability density function (pdf) model. Furthermore, video data from SSAB Raahe was compared with the CFD results to assess the behavior of the combustion model. This combustion model was used to study the effect of lance position on the extra heavy oil combustion and the blast furnace operation. The coke bed combustion model was also applied in the CFD model to obtain more realistic temperatures and gas recirculation effects in the raceway area.

The pulverized coal injection is important because of the new injection system in the SSAB Raahe BFs. The development of the combustion model is presented in Paper III. The combustion model was created for the PC and was validated using data from the literature. An experimental rig and its boundary conditions were used as a basis for the CFD model.

In Paper IV, the previously created combustion model for PC is used to study the effect of double lance positioning on the blast furnace operation and the combustion efficiency of the fuel. The goal was to find out a good compromise for the new injection system, where tuyere walls stay clean, the pressure drop stays low, combustion does not melt tuyere walls, and combustion efficiency remains high. The coke bed model is also used in this study.

The auxiliary fuel models and their use in this thesis are given in Fig. 2. The models are divided between extra heavy oil and PC to clarify where the models were used.

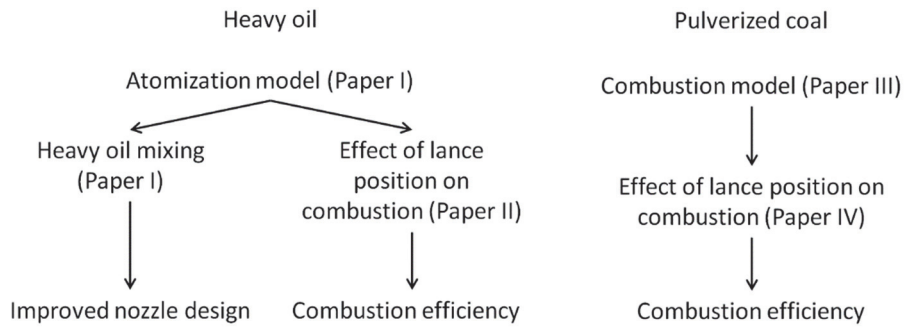


**Fig. 2. Auxiliary fuel models and their use in the thesis.**

# 2 Blast furnace process

## 2.1 Blast furnace

Blast furnace is the most common way worldwide to produce pig iron. A schematic drawing of the bottom part of the BF is presented in Fig. 3. BF is a counter-current reactor where gases rise up through the reactor while the iron ore and coke are descending down through the furnace. It is used to reduce iron oxides into hot metal. Iron ore and coke are charged into the BF in alternating layers from the top of the furnace. These layers remain separate from each other until heat softens and melts the ore in the cohesive zone. To provide the necessary heat and reducing agents for the operation, coke and auxiliary fuels are combusted and gasified in the BF. A hot air blast is blown into the BF through tuyeres, which are positioned in the lower part of the BF. Tuyeres are placed symmetrically around the furnace. There can be up to 42 tuyeres in the biggest blast furnaces. The air blast is pre-heated typically up to around 1100–1200 °C in Cowper stoves. The air blast pushes, burns, and gasifies the coke in the front of the tuyere and forms a cavity called the raceway. The temperature in the raceway area can reach 2000–2500 °C. Auxiliary fuels are injected into the air blast in tuyeres. These auxiliary fuels are used to lower the need for expensive coke, to stabilize the process and to reduce $CO_2$ emissions. (Geerdes, Chaigneau, & Kurunov, 2015)

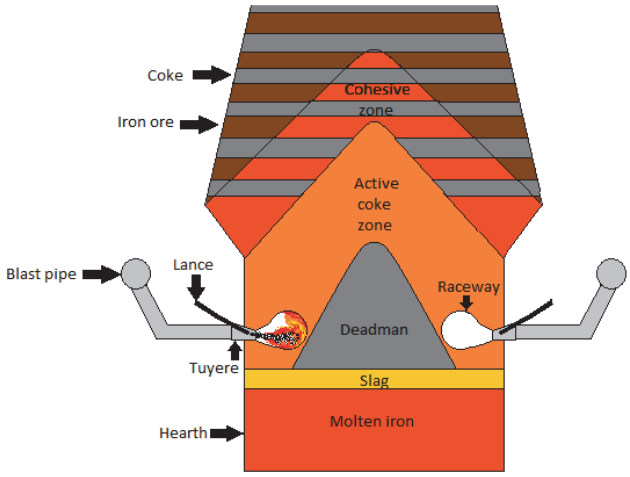


**Fig. 3. Schematic drawing of the bottom part of the blast furnace (Paper III, published by permission of IFRF).**

Coke is a solid fossil fuel which is produced via high temperature distillation of coal. It is the primary fuel of the BF and the most expensive raw material in ironmaking. Iron ore reduction is energy intensive, resulting in high energy costs. Coke's function is not only limited to fuel in the BF. It has other important tasks, because it is the only raw material that remains solid at high temperatures. Therefore, it acts as a support material in the BF, creating a porous bed and allowing gases to flow upwards. Coke cannot be fully substituted in the BF ironmaking, but it can be partially replaced with auxiliary fuels. These auxiliary fuels can be PC, heavy oil, natural gas, plastic waste or bio-char, for example. Auxiliary fuels have higher H/C ratio than coke, which results in lower $CO_2$ emissions. The coke to auxiliary fuel replacement ratio (RR) is a very important quantity when considering fuel efficiency. With an RR of 1, auxiliary fuel replaces an equal amount of coke (kg of coke per kg of auxiliary fuel). Typically, the RR values are between 0.8 and 1, but the value depends on the fuel and injection rate. For example, in coal combustion, the RR decreases linearly with the increasing volatile matter (VM) content in fuel. (Geerdes *et al*., 2015)

Iron ore pellets, which are used in the BF, contain hematite ($Fe_2O_3$) and a small percentage of magnetite ($Fe_3O_4$). Iron oxides are reduced by CO, $H_2$, or coke, and the reduction reactions produce $CO_2$ and $H_2O$. The reduction reactions begin at about 500 °C, where hematite is reduced to magnetite. At temperatures of 600–800 °C, magnetite is reduced to wüstite (FeO). In the temperature region of 800–

1150 °C wüstite reduces in partly metallic iron. The remaining iron oxides are reduced in a direct reduction with coke at temperatures above 1150 °C. (Geerdes *et al*., 2015)

The BF forms slag from the gangue and ash-forming elements in coal and coke. To achieve the desirable slag chemistry, limestone ($CaCO_3$) is also added to the burden. Limestone reacts to flux material CaO and $CO_2$ as temperature rises above 1000 °C. Molten iron and slag build up in the hearth at the bottom of the BF. Coke forms a porous deadman in the center of the furnace, which can either be floating on the liquids or sitting on the bottom of the hearth. Coke dissolves slowly from the deadman into the molten iron. Hot metal and slag are removed from the BF through a tap hole. (Geerdes *et al*., 2015)

## 2.2 Auxiliary fuels

The combustion modeling of different fuels requires fuel-specific models. The characteristics of the studied auxiliary fuels and their combustion stages are presented shortly in this section. The auxiliary fuels in the scope of this thesis are extra heavy oil and pulverized coal.

### *2.2.1 Extra heavy oil*

Extra heavy oil (EHO) is an undistillable side stream from the petroleum refining process. It is a highly viscous oil (viscosity higher than 10,000 cP), which requires increased temperatures to keep it flowing. Heavy oils are mixtures of hydrocarbons with high molecular weights and high boiling points. Typically these hydrocarbons contain more than 60 carbon atoms. By definition, extra heavy oil density is above 1000 kg/m$^3$. (K. Guo, Li, & Yu, 2016)

The steel industry used to buy extra heavy oil from the petrochemical industry, which avoided building of expensive facilities for the production of petroleum coke. With new refining methods, extra heavy oil gained a purpose that is more valuable for its use than as a fuel, leading to an increase in its price. This change forced the steel industry to search for alternatives and led to investment in a new PC injection system. The H/C ratio in extra heavy oil is higher than that in PC, which led to an increase in $CO_2$ emissions in the ironmaking process.

EHO combustion and gasification can be divided in three stages, vaporization, gas phase combustion, and cenosphere combustion. Cenosphere mass is about 8% of the total droplet mass.

### 2.2.2 Pulverized coal

Coal is an organic sedimentary rock that is composed of organic compounds, inorganic minerals, and moisture. The properties and chemical composition of coals vary with geological maturity (rank) and type. Relevant coal classes in the BF process are the highest rank coals, i.e., anthrasitic and bituminous. Anthrasitic coals have a high fixed carbon content between 86 and 98% and a low volatile matter content of 0–14% in dry mineral matter-free mass fractions. Bituminous coals, which are classified in terms of fixed carbon content, are coals that contain more than 69% but less than 86% fixed carbon. These are either low-volatile or medium-volatile bituminous coals. High volatile coals have less than 69% fixed carbon, but their calorific value is between 24.42 and 32.56 MJ/kg. The volatile fraction of a coal has a huge effect on coal combustion efficiency, because volatile releases are much faster than the char combustion rate. In addition, the lower-rank coal chars are more reactive than the higher-rank coals. Coal properties also affect the replacement ratio of coke. Lower-volatile coals have a better replacement ratio, but lower combustion efficiency. Therefore, optimization has to be made to find good coal for the BF process. (Bartok & Sarofim, 1991; Carpenter & IEA Coal Research, 1988)

The combustion model for PC can be divided into five steps, i.e., heating, drying, devolatilization, char combustion and gas phase combustion.

# 3 State of the art in CFD modeling of the blast furnace tuyere-raceway area

Experimental measurements in the blast furnace tuyere-raceway area are extremely difficult due to the harsh environment (high temperature, increased pressure, and solid and molten materials), which leads to the need for alternative research methods (Nightingale, Dippenaar, & Lu, 2000). For this, Computational Fluid Dynamics (CFD) modeling provides an interesting tool. In this section, studies related to CFD modeling of the BF tuyere-raceway area are reviewed. The most important models and results are presented and analyzed.

## 3.1 CFD modeling of the tuyere-raceway area

Several CFD studies with different combustion models have been made concerning the BF tuyere-raceway area. Studies with the combustion models are summarized in Table 1. Papers where auxiliary fuel does not contain coal or heavy oil have been dismissed as well as conference papers that do not contain all the needed information about the CFD models. These studies are reviewed with respect to their experimental rigs and the CFD models. The reviews are classified according to the research groups. The order of the research groups is from the most published to the single studies. At first, a general overview of the models used in these studies is made, and then the studies with their results are discussed. Models can be divided into two groups: (1) small-scale models based on experimental rigs, and (2) full-scale models based on some actual BF. Small-scale models are used for the validation of combustion models and to study the behavior of different fuels. Full-scale models are used to study the injection process and the effect of different parameters on the combustion of auxiliary fuel.

**Table 1. Comparison of different combustion models for coal and heavy oil in blast furnace studies.**

| Researchers | Fuel | Drying | Devolatilization | Gas phase | Char conversion |
|---|---|---|---|---|---|
| Almeida Santos *et al*. 2014 | Coal | - | Kobayashi | EDM | Gibb |
| Andahazy *et al*. 2006 | Heavy oil, COG | - | Spherical droplet | PDF | - |
| Du *et al*. 2006 | Coal | - | Kobayashi | PDF | PDF |
| Gu *et al*. 2008 | Coal | Droplet | Kobayashi | EBU/Arrhenius | Arrhenius |
| Gu *et al*. 2010 | Coal | Droplet | Kobayashi | EBU/Arrhenius | Arrhenius |
| Guo *et al*. 2005 | Coal | - | Kobayashi | EBU | Gibb |
| Li *et al*. 2014 | Coal | Droplet | Kobayashi | EBU/Arrhenius | Finite rate |
| Majeski *et al*. 2015 | Coal + NG | - | Arrhenius | EDM/Arrhenius | Arrhenius |
| Shen *et al*. 2008 | Coal | - | Kobayashi | EDM | Gibb |
| Shen *et al*. 2009 | Coal | - | Kobayashi | EDM | Gibb |
| Shen *et al*. 2009b | Coal | - | Kobayashi | EDM | Gibb |
| Shen *et al*. 2009c | Coal | - | Kobayashi | EDM | Gibb |
| Shen *et al*. 2011 | Coal | - | Kobayashi | EDM | Gibb |
| Shen *et al*. 2012 | Coal | - | Kobayashi | EDM | Gibb |
| Shen *et al*. 2012b | Coal | - | Kobayashi | EDM | Gibb |
| Shen *et al*. 2014 | Coal | - | Kobayashi | EDM | Gibb |
| Shen & Yu 2015 | Coal | - | Kobayashi | EDM | Gibb |
| Shen & Yu. 2016 | Coal | - | Kobayashi | EDM/Arrhenius | Gibb |
| Takeda & Lockwood 1997 | Coal | - | Single rate | EDM | Kin/diff |
| Yeh *et al*. 2012 | Coal | - | Kobayashi | PDF | Kin/diff |
| Zhou 2008 | Coal | Droplet | Kobayashi | EBU/Arrhenius | Arrhenius |

The most actively publishing group in tuyere-raceway area modeling is the Laboratory for Simulation and Modeling of Particulate Systems at the University of New South Wales (UNSW) in Australia. They do their work together with BlueScope Steel, where the experimental equipment for model validation is located. Publications are written by Guo *et al*. (2005) and Shen *et al*. (2008, 2009, 2009a, 2009b, 2009c, 2011, 2011b, 2012, 2012b, 2014, 2015, 2016). Their CFD models have remained similar since 2005, when Guo *et al*. (2005) made a CFD study on PC combustion in a blast furnace test rig. The turbulence model was RNG κ-ε in that study, and all the later studies have applied the standard κ-ε model. All of their studies use the Euler approach to model the continuous phase and the Lagrangian method to model the dispersed phase. Radiation is modeled with the Discrete Transfer Model (DTM), which takes into account particles and gray gases as well as surface-to-surface radiation. The group has modeled coal devolatilization with a

two competing rates model, also known as the Kobayashi model (Kobayashi, Howard, & Sarofim, 1977). The combustion model for the gas phase was the Eddy Break-Up model (EBU) in Guo *et al*. (2005) and was changed to the Eddy Dissipation Model (EDM) in later studies. (B. Guo, Zulli, Rogers, Mathieson, & Yu, 2005)

In the EBU (Spalding, 1971), the chemical reaction rate is controlled with the mixing of fuel and oxidizer on the molecular level or mixed-is-burnt combustion models. The turbulent mean reaction rate of products, $\overline{\omega_p}$, is solved from

$$\overline{\omega_p} = \rho C_{EBU} \frac{\varepsilon}{\kappa} \left(\overline{Y_p''^2}\right)^{0.5} \quad (1)$$

where ρ is the density, $C_{EBU}$ is the Eddy-Break-Up constant, ε is the turbulent dissipation rate, κ is the turbulence kinetic energy, and $\overline{Y_p''^2}$is the variance of the product mass fraction. EDM (Magnussen & Hjertager, 1976) is a modification based on EBU. In the EDM, the reaction rate is the minimum of the reactants limiter for

$$R_k = A \frac{\varepsilon}{\kappa} min\left(\frac{[i]}{v'_{ki}}\right) \quad (2)$$

where the modeling constant A=4.0, [i] is the molar concentration of reactant components and $v'_{kl}$is the stoichiometric coefficient for the reactant. The products limiter is

$$R_k = AB \frac{\varepsilon}{\kappa} \left(\frac{\sum_P (i) Y_i}{\sum_P v''_{ki} Y_i}\right) \quad (3)$$

where P loops over all product components (mass fraction $Y_i$) in the elementary reaction k and $v''_{kl}$ is the stoichiometric coefficient for the product. The modeling constant default value is set to B=-1 in ANSYS CFX, which means that the products limiter is not used in the calculations. The product limiter is not suggested to be used in multi-step reaction schemes. This value is also used in their studies. In Ansys CFX, there is also a possibility to use the maximum flame temperature limiter. The UNSW group has used 3000 K to limit their maximum flame temperature. (Shen *et al*., 2008, 2009, 2009a, 2009b, 2009c, 2011, 2011b, 2012, 2012b, 2014, 2015, 2016)

Char oxidation and gasification have been modeled with the Gibb model in all of their models. There is very little information about the Gibb model outside of the Ansys CFX theory guide (ANSYS Inc., 2017b); the model was presented in a lecture by Gibb in 1985, and it is not published anywhere else to the best of my knowledge. Char oxidation to CO and $CO_2$ is solved as

$$\varphi C + O_2 \rightarrow 2(\varphi - 1)CO + (2 - \varphi)CO_2 \quad (4)$$

The parameter φ depends on the particle temperature $T_p$

$$\frac{2(\varphi-1)}{2-\varphi} = A_s \exp\left(-\frac{T_s}{T_p}\right) \quad (5)$$

The particle char mass reduction is calculated from equation

$$\frac{dm_c}{dt} = -\frac{3\varphi}{1-\varepsilon_{char}} \frac{M_c}{M_{O_2}} \frac{X_g}{\rho_c} (k_1^{-1} + (k_2 + k_3)^{-1})^{-1} m_c \quad (6)$$

where the char particle void fraction $\varepsilon_{char}$=0.5 and the Gibb constants are $A_s$=2500 and $T_s$=6240 K. $X_g$ is the mole fraction of the oxidizing species and $\rho_c$ is the density of char. $k_1$ is the rate of external diffusion

$$k_1 = \frac{D}{r_p^2} \quad (7)$$

where $r_p$ is the particle radius and D is the external diffusion coefficient of oxygen in the surrounding gas

$$D = \frac{D_{ref}}{\rho} \left(\frac{T_p + T_g}{2T_{ref}}\right)^{0.75} \quad (8)$$

where $D_{ref}$ is the dynamic diffusivity $1.8 \cdot 10^{-5}$ kg/(m·s), $T_g$ is the gas temperature, and $T_{ref}$ is the reference temperature 293 K. The surface reaction rate $k_2$ can be calculated using Eq. (9)

$$k_2 = (1 - \varepsilon_{char}) \frac{k_c}{r_p} \quad (9)$$

where $k_c$ is the carbon oxidation rate solved from the modified Arrhenius equation

$$k_c = A_c T_p \exp\left(-\frac{T_c}{T_p}\right) \quad (10)$$

Internal diffusion and surface reaction $k_3$ are solved from equation

$$k_3 = k_c(\beta coth\beta - 1)/(\beta^2 a) \quad (11)$$

where the particle volume/internal surface area ratio $a=5 \cdot 10^{-9}$, and β is calculated from

$$\beta = r_p \left(\frac{k}{D_p \varepsilon_{char} a}\right)^{0.5} \quad (12)$$

where the pore diffusivity $D_p$ is calculated as

$$D_p = 0.1D \quad (13)$$

$A_c$ and $T_c$ values vary with different reactions. For char oxidation, $A_c$=14 m/(s·K) and $T_c$=21580 K. For char gasification with $CO_2$, these values are $A_c$=20230 m/(s·K) and $T_c$=39743 K, and with $H_2O$, $A_c$=606.9 m/(s·K) and $T_c$=32406 K.

In the study, the coke bed in the full-scale simulations is modeled as a porous bed, where the momentum sink is calculated from the Ergun equation (Ergun, 1952). This is the most common way to solve the coke bed effect on velocity without actually modeling the coke particles. The source term $S_i$ for the momentum equation in the porous media is

$$S_i = -(R_v \mu u_i - 0.5 R_I \rho u_{mag} u_i) \tag{14}$$

where $u_i$ is the velocity in direction i and $u_{mag}$ is the velocity magnitude (m/s). Equations for the viscous resistance ($R_v$), which is the reciprocal of permeability and the inertial resistance ($R_I$), are derived from the Ergun equation and are given as

$$R_v = \frac{150*(1-\varepsilon_i)^2}{^2 d_{coke}^2 * \varepsilon_i^3} \tag{15}$$

where $\varepsilon_i$ is the porosity of zone I, $\psi$ is the sphericity of the coke particles, $d_c$ is the coke particle diameter (m), and

$$R_I = 3.5 \frac{1-\varepsilon_i}{*d_{coke} * \varepsilon_i^3} \tag{16}$$

The UNSW group has used the Field model for coke reactions in the porous coke bed. The reactions are modeled with a method that is presented by Shen *et al*. (2011). Coke reacts with $O_2$ and $CO_2$. $H_2O$ reactions are not added in this model. The reaction rate for coke with each species is calculated with the Field model (Field, Gill, Morgan, & Hawksley, 1967), which utilizes both diffusion and chemical reaction rates for the overall reaction rate

$$\frac{dm_{coke}}{dt} = \frac{\left(k_d^{-1} + k_c^{-1}\right)^{-1} X_g 4\pi r_{coke}^2 p}{p_A} \tag{17}$$

where $r_{coke}$ is the coke particle radius (m), $p_A$ is the atmospheric pressure (Pa) and diffusion of oxidizing species ($k_d$) on the coke surface is solved from the equation

$$k_d = \frac{\frac{D_{ref}}{r_{coke}} \left(\frac{T_{coke} + T_\infty}{^2 T_{ref}}\right)^{0.75} p_A}{p} \tag{18}$$

where $D_{ref}$ is the dynamic diffusivity ($1.8 \cdot 10^{-5}$ kg/(m·s)), $T_{coke}$ is the coke temperature (K), and $T_{ref}$ is the reference temperature (293 K). The chemical rate coefficient ($k_c$) is calculated from the following equation

$$k_c = A_c \exp\left(-\frac{T_c}{T_{coke}}\right) \quad (19)$$

where $A_c$ for $O_2$ is $3.2 \cdot 10^6$ kg/(m$^2$·s), and $T_c$ for $O_2$ is 10855 K. For $CO_2$, $A_c$ is $4.71 \cdot 10^9$ kg/(m$^2$·s) and $T_c$ is 29018 K. Other coke bed reactions are modeled as a heat sink

$$Q = -h_g A_{coke}(T_g - T_0), T_0 = max(0.75T_g, 1773[K]) \quad (20)$$

where $h_g$ is 128.2 W/(m$^2$·K), and $A_{coke}$ is 153 m$^2$ below the raceway and 141 m$^2$ in the rest of the coke bed.

The second most published group is the Department of Mechanical Engineering at Purdue University Calumet in the USA (Gu, Zhang, Selvarasu, Zhao, & Zhou, 2008; Gu *et al*., 2010; C. Zhou, 2008). They have been collaborating with United States Steel LLC and Mittal Steel, which is now ArcelorMittal. Their approach to CFD modeling is different from that of the UNSW group. Their model is composed from several parts. In the first step, they use ANSYS Fluent to model injection in the blowpipe, lance, and tuyere. In that model, the continuous phase is modeled with the Eulerian method and PC with the Lagrangian method. The flow properties of this tuyere model are used as an inlet condition for the second step, where they model the raceway formation. The phases are modeled with the Euler-Euler method, and individual particles are not studied. In these studies, a combined turbulent model for both phases is used, called $\kappa$-$\varepsilon$-$\kappa_p$, which uses the standard $\kappa$-$\varepsilon$ model together with a transport equation model for particle turbulent kinetic energy (L. Zhou & Huang, 1990). In this step, combustion is not modeled, but combustion models are added in the third step, where the raceway shape and size are constant. Radiation is modeled with the Discrete Ordinates (DO) method, which takes into account particles and gray gases as well as surface-to-surface radiation. Moisture evaporation is modeled in their studies with a diffusion model for a water droplet (C. Zhou, 2008). The coal devolatilization is modeled with the Kobayashi model. The gas phase combustion is modeled with the EBU/Arrhenius model, where the slower reaction rate is used. The rate of change in mass for each species is calculated as

$$\frac{dm_i}{dt} = A_i \rho^2 Y_F Y_{OX} \exp\left(-\frac{E_i}{RT}\right) \quad (21)$$

where $A_i$ and $E_i$ are reaction constants, R is the universal gas constant (R=8.314 J/(mol·K)), and T is the gas phase temperature (K). The oxidation of coal volatiles is described by a two-step model

$$C_dH_b + \frac{d}{2}O_2 \rightarrow dCO + \frac{b}{2}H_2 \quad (22)$$

$$2CO + O_2 \rightarrow 2CO_2 \quad (23)$$

$$2H_2 + O_2 \rightarrow 2H_2O \quad (24)$$

Char reactions are also modeled with the Arrhenius equation for $O_2$, $CO_2$, and $H_2O$. The $O_2$ reaction can lead to either $CO_2$ or CO. The change in the char mass is solved from

$$\frac{dm_c}{dt} = -\pi d_c^2 \rho Y_{OX} A_i \exp\left(-\frac{E_i}{RT_c}\right) \quad (25)$$

The coke bed is modeled as a porous momentum sink, where the momentum exchange rate between gas and solid phases is calculated with the Ergun equation. The Purdue group has been aiming towards a full blast furnace model, which can be used to virtualize the whole process. The later studies are moving away from the tuyere-raceway area and are not presented here. In Paper II, there is a review from the Purdue group's conference paper by Silaen *et al*. (2015).

The rest of the publications are singular. The first one is from Kawasaki Steel Corporation in Japan in collaboration with the Imperial College of Science from the UK (Takeda & Lockwood, 1997). They use the Euler method to model the continuous gas phase and the Lagrangian method to model the dispersed phase. The model itself is two-dimensional and applies the κ-$l_m$ turbulence model for the gas phase and stochastic tracking for the dispersed phase. There is no information in English available on the details of their turbulence model, which was created in 1996 by Takeda and Lockwood (Takeda & Lockwood, 1996a; Takeda & Lockwood, 1996b). The Ergun's equation is used to model the momentum sink caused by the coke bed. The PC devolatilization rate is modeled using the Arrhenius equation, and it employs a single kinetic rate. The gas phase combustion is modeled with the EDM. The combustion and gasification of the char and coke is modeled with the kinetic/diffusion-limited reaction model. Coke reacts with $O_2$, $CO_2$, and $H_2O$. The coke particle reaction temperature is 80% of the gas phase temperature. Finally, equilibrium calculations are done for $O_2$, CO, $CO_2$, $H_2$, and $H_2O$ species based on the local gas composition and temperature. (Takeda & Lockwood, 1997)

Christian Doppler Laboratory for Chemical Engineering at High Temperatures at the Vienna University of Technology in Austria has been working with CFD modeling of the BF tuyere-raceway area. They have worked together with the Voestalpine Stahl company (Andahazy *et al*., 2006). They have used the Euler method to model the continuous gas phase and the Lagrangian method to model the dispersed phase. The turbulence model used is Realizable κ-ε, which is

presented in equations (44)-(59) starting on page 64 in Section 4.2.1, and compressibility effects are taken into account. The dispersed phase turbulence is calculated with a stochastic tracking model (equations (64)-(69) starting on page 67 in Section 4.2.2). In the coke bed, the momentum sink is calculated from the Ergun equation, which is a similar approach to the other research groups mentioned earlier. The combustion model they used is called the Probability Density Function (PDF) model (Pope, 1985). It is used to model non-premixed combustion, where the thermochemistry is reduced to a single scalar, the mixture fraction. In the PDF combustion model, it is assumed that the chemistry is fast enough to reach chemical equilibrium, and combustion is considered to depend only on the mixing rate. Reactions take place in thin layers where the molecular transport and the chemical source term balance each other. To describe combustion, PDF is needed for the mixture fraction Z at point x and time t. The instantaneous averaged thermochemical state of the fluid depends on the local mixture fraction. The model includes eight main species, four radicals, and a solid carbon particle for soot modeling. Heavy oil vaporizes in the diffusion-limited model under the boiling point and utilizes the boiling model (equation 78 on page 71 in Section 4.2.2) when the boiling temperature is reached. The released vapor is calculated based on the ultimate analysis of heavy oil. Droplets are spherical and atomization is not modeled. The mean diameter, $d_p$=200μm, is calculated from an equation for heavy oil atomization in the BF tuyere-raceway area by Hakala & Paloposki (1996). The Rosin-Rammler size distribution is used to calculate 5 different size groups for droplets. The droplet diameter range is between 100 and 400 μm.

Natural Resources Canada's research center, CanmetENERGY, has been working in collaboration with U.S.Steel Canada to model tuyere behavior in PC and NG injections. They have used the Eulerian method to model the continuous phase and the Lagrangian method to model the PC. The turbulence model was a standard κ-ε model. Radiation is modeled with the Discrete Transfer method, which included the effects of gray gases and PC radiation. The coal devolatilization is modeled with a single rate Arrhenius equation. Char oxidation modeling is also a single Arrhenius rate between char and $O_2$. The gas-phase reaction rate is solved as a minimum between mixing-limited (EDM) and finite rate chemistry (Arrhenius). There is no raceway or coke bed in the model. (Majeski *et al*., 2015)

The Steel and Aluminum Research and Development Department of China Steel Corporation in Taiwan has been modeling the PC combustion in a BF tuyere. They used the Eulerian method to model the continuous phase and the Lagrangian method to model the PC. Turbulence was modeled with a standard κ-ε model.

Radiation was modeled as black body radiation, which included particle radiation. For the PC devolatilization the Kobayashi model was applied. Combustion was thought to be mixing-limited and the PDF model was used for the gas and solid phases. There is no raceway or coke bed in the model. (Du & Chen, 2006)

The Department of Engineering Science at the National Cheng Kung University in Taiwan has collaborated with China Steel Corporation to model the BF tuyere-raceway area (Yeh, Du, Tsai, & Yang, 2012). Also in this study, the continuous phase was modeled with the Euler method and the PC with the Lagrangian method. The turbulence model was a standard κ-ε model. No radiation model was used in the heat transfer. Coal devolatilization was modeled with the Kobayashi model using the Ubhayakar constants (Ubhayakar, Stickler, Von Rosenberg, & Gannon, 1977). Their combustion models for the gas and solid phase is a mixing-limited PDF model. A small coke bed surrounds the raceway, where the porous media momentum resistance is solved from the Ergun equation. The char combustion rate is solved with the kinetic/diffusion-limited model as follows

$$\frac{dm_c}{dt} = -\pi d_c^2 p_{ox} \frac{R_{diff} R_{kin}}{R_{diff} + R_{kin}} \tag{26}$$

$$R_{diff} = \frac{C_1}{d_c} \left( \frac{T_p + T_g}{2} \right)^{0.75} \tag{27}$$

where $p_{ox}$ is the partial pressure of oxygen, $C_1$ is the empirical constant for the diffusion-limited reaction rate (kg/s), $R_{diff}$, and the kinetic-limited reaction rate (kg/s), $R_{kin}$, is solved from Arrhenius equation. (Yeh *et al*., 2012)

Lumar Metals Research in Santana de Paraíso in Brazil (Almeida Santos *et al*., 2014) has modeled the tuyere-raceway area. Like most of the research, the continuous gas phase is modeled with the Euler method and the PC with the Lagrangian method. A standard κ-ε model is used to model turbulence. They mention radiation in the article, but no model is defined or shown in the heat transfer equation. Combustion models are copied from the article by Shen *et al*. (2009). No coke bed is added to the calculation.

## 3.2 Small-scale studies

Small-scale experimental rigs are used to validate CFD models used in the BF tuyere-raceway area modeling (Chui, 2005; Mathieson, Truelove, & Rogers, 2005; Nogami, Yamaoka, & Takatani, 2004). Three small-scale experimental rigs have been constructed and operated in the BHP Billitons Newcastle Laboratories. The first test rig was a hot raceway (with a small coke bed) model in 1981, which was

used to study the effect of coal particle size, coal volatile matter, blast temperature (950 °C) and the blast velocity on the gas temperature in the test rigs combustion section. No char or gas sampling technologies were used. The coal combustion was studied in the first part of the system, which is a 1 m long cylindrical reactor with an inner diameter of 0.05 m. Temperature measurements were done in 6 points along the reactor. (Mathieson *et al*., 2005)

The second test rig was used in 1983–1985. Its improvements over the first one include the test section expansion to 75 mm, an air blast temperature up to 1300 °C and a probe for the char and gas sampling. (Mathieson *et al*., 2005)

The newest test rig, which is closest to the actual blast furnace tuyere-raceway area, was planned to simulate expanding coal plume combustion. This test rig has been used to validate PC coal combustion models in the Lab for Simulation and Modeling of Particulate Systems at the University of New South Wales, Sydney, Australia. The geometry of the experimental rig is presented in Fig. 4. The lance outer diameter is 19.05 mm. The fuel injection rates in the test rig are between 2.1% and 4% of the actual blast furnace (B. Guo *et al*., 2005), and the reactions occur at atmospheric pressure, whereas the pressure in the Raahe's BF is about 3.6 bar. The experimental rig operates at atmospheric pressure, and velocity is about 60% of the actual BF, but temperature is 1473 K, which equals the real BF. Because of the lower fuel injection rate, the slip velocity between the air blast and PC is similar to the BF. The sizing of the tuyere and the raceway area is based on numerical modeling. (Mathieson *et al*., 2005)

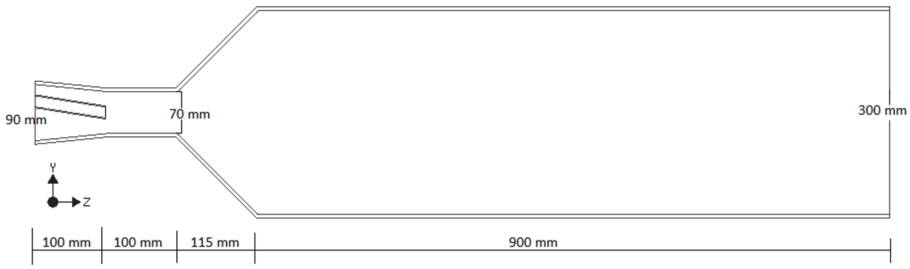


**Fig. 4. Geometry of the BF experimental rig (modified from B. Guo *et al.*, 2005).**

The experimental rig has been used to study seven different coals separately and mixtures of coals A–B, A-G, and A–D–E. Proximate and ultimate analyses of different coals are presented in Table 2. These coals range from semi-anthracite (coal D) to high volatile bituminous coals (coals B, C, E, and F). Variables in addition to coal in the experimental case studies include $O_2$ enrichment in the air blast and PC the injection rate. The $O_2$ volume fraction varies between 20.9% and 40%, and the injection rate varies from 22.9 to 46.7 kg/h. The lowest O/C ratio is 1.85. For complete carbon combustion the O/C ratio should be 2 if there were no volatiles in coal. In the BF process the amount of oxygen is typically presented with the O/C ratio, but stoichiometric combustion also requires enough oxygen for hydrogen and sulfur combustion. (B. Guo *et al.*, 2005; Y. S. Shen *et al.*, 2009; Y. S. Shen, Guo, Yu, & Zulli, 2009a; Y. S. Shen & Yu, 2016; Y. Shen *et al.*, 2008; Y. S. Shen *et al.*, 2009c)

**Table 2. Proximate and ultimate analyses of coals used in the experimental rig (modified from B. Guo *et al.*, 2005, Y. S. Shen *et al.*, 2009, Y. S. Shen *et al.*, 2009a, Y. S. Shen & Yu, 2016, Y. S. Shen *et al.*, 2008, Y. S. Shen *et al.*, 2009c).**

| Property | Coal A | Coal B | Coal C | Coal D | Coal E | Coal F | Coal G |
|---|---|---|---|---|---|---|---|
| Moisture w-% | 1.20 | 3.20 | 3.60 | 0.90 | 3.40 | 5.60 | 2.70 |
| Volatiles w-% | 20.00 | 32.50 | 35.10 | 12.40 | 32.60 | 39.10 | 26.85 |
| Ash w-% | 9.70 | 9.80 | 6.20 | 8.00 | 9.30 | 2.70 | 8.90 |
| Fixed carbon w-% | 69.10 | 54.50 | 55.10 | 78.70 | 54.80 | 52.60 | 61.55 |
| | | | | | | | |
| C | 89.10 | 83.50 | 82.60 | 91.30 | 84.70 | 79.40 | 85.15 |
| H | 4.70 | 5.30 | 5.44 | 4.00 | 5.60 | 5.60 | 5.05 |
| O | 4.10 | 8.60 | 9.50 | 2.30 | 7.00 | 12.90 | 7.77 |
| N | 1.70 | 1.95 | 2.15 | 1.90 | 2.10 | 1.50 | 1.70 |
| S | 0.37 | 0.60 | 0.30 | 0.50 | 0.70 | 0.60 | 0.34 |

The burnout (B) is used to measure the extent of the coal combustion. It is calculated using an ash balance

$$B = \left(1 - \frac{m_{a,0}}{m_a}\right) / (1 - m_{a,0}) \quad (28)$$

where $m_{a,0}$ is the initial ash content of the coal and the $m_a$ is the ash content of the burnt residual sampled.

Combustion efficiencies of different coals are compared between experimental and CFD results in Table 4. Cases 1-11 are results from Guo's article (B. Guo *et al*., 2005) and cases 12-16 are from Shen's article (Y. S. Shen *et al*., 2009). In cases 1-11, it can be seen that with Coal A the model underestimates burnout when the PC rate is higher, but when it gets lower the model overestimates the burnout. With Coal B, the behavior is similar to Coal A. In Coal C combustion, the O/C ratio has the smallest effect on the burnout. In cases 8 to 11, the lance coolant is methane. It can be seen that it has a very small effect on the PC burnout and the results remain practically unchanged. In cases 12-16, the combustion model was changed to add more species into volatiles and it proves to get better agreement with the experimental results with all other coals except the high volatile coal F, where the model overestimates the burnout. It should be noted that the $O_2$ boundary condition in the study is incorrect in all cases. The $O_2$ value is set to 20.9 wt-% instead of 23.3 wt-%, which is the atmospheric $O_2$ mass fraction. The error in the $O_2$ value is about 10%. This most likely leads to a case where the combustion rate is over-estimated. The only article where the correct value is used is Shen *et al*. (2009).

**Table 3. Experimental and CFD results from the BF test rig (modified from B. Guo *et al*., 2005; Y.S. Shen *et al*., 2009).**

| Case | Flow rate (kg/h) | VM (%) | Burnout experimental (%) | Burnout CFD (%) |
|---|---|---|---|---|
| 1 Coal A | 25.2 | 20.19 | 63.7 | 58.22 |
| 2 Coal A | 35.9 | 20.19 | 55.5 | 56.24 |
| 3 Coal B | 25.5 | 33.57 | 81.5 | 75.92 |
| 4 Coal B | 40.0 | 33.57 | 75.5 | 74.41 |
| 5 Coal B | 46.7 | 33.57 | 71.4 | 74.17 |
| 6 Coal C | 23.5 | 36.41 | 78.9 | 80.99 |
| 7 Coal C | 35.1 | 36.41 | 76.2 | 80.04 |
| 8 Coal A | 23.1 | 20.19 | 53.2 | 57.52 |
| 9 Coal A | 36.8 | 20.19 | 51.6 | 54.47 |
| 10 Coal B | 35.8 | 33.57 | 77.7 | 74.44 |
| 11 Coal C | 36.2 | 36.41 | 76.1 | 79.42 |
| 12 Coal A | 25.2 | 20.19 | 63.7 | 62.4-64.3 |
| 13 Coal D | 31.6 | 12.40 | 59.8 | 61.2-62.8 |
| 14 Coal E | 22.9 | 32.60 | 73.9 | 72.9-74.0 |
| 15 Coal E | 26.9 | 32.60 | 71.9 | 70.1-72.2 |
| 16 Coal F | 28.3 | 39.10 | 83.2 | 82.7-85.1 |

In the coal blend studies (Y. S. Shen, Guo, Yu, & Zulli, 2009a; Y. S. Shen & Yu, 2016), the results are average values between the blends. The results are obvious, because they are tracking PC types separately and the same boundary conditions are used for the blend and single coal types. The results are not presented here because they do not offer any new information.

The second test rig was also used in model validation studies (Y. Shen *et al*., 2008). In that case, the group used one medium volatile coal (VM=19.2%) and one high volatile coal (VM=39%). The samples of gas composition ($O_2$, $CO_2$, and CO) and burnout were taken at the distances of 0.33, 0.426, 0.626 and 1.03 m from the lance tip (Fig. 5). It can be seen in Fig. 5a, that $CO_2$ has the best agreement with data, but $O_2$ and CO have large differences between the measured and calculated results. This might be because of the relatively simple gas phase reaction model. There is also 8% of $O_2$ left in the last measurement point, which means that there is excess oxygen in the system. This is not optimal, because the group is validating a model, which should be able to take both combustion and gasification reactions into account.

From Fig. 5b, it can be seen that the calculated PC burnout matches well with the measured data. Most of the burnout consists of devolatilization of PC. The group used the constants for devolatilization from the article by Ubhayakar *et al*.

(1977), which were found to be a good match for the BF test rig data by Du & Chen (2006). Char combustion is mixing limited in the test rig conditions and the Gibb model with the standard κ-ε seems to behave well in this case. (Y. Shen *et al*., 2008)

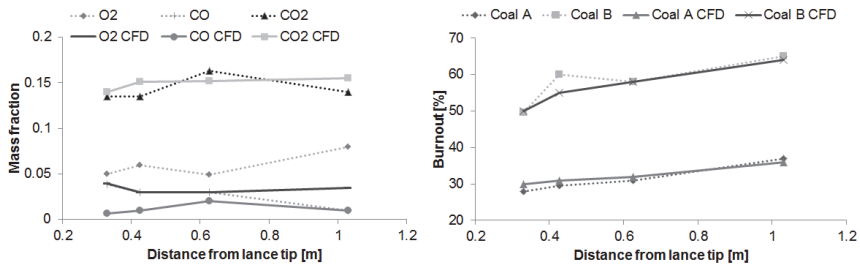


**Fig. 5. a) Gas compositions of O2, CO and CO2 from the lance tip, b) PC burnout from the lance tip (modified from Y. S. Shen *et al*., 2008).**

The results from the oldest BHP Billiton test rig was used to validate the devolatilization model (Kobayashi model with Ubhayakar constants) for BF CFD simulations (Du & Chen, 2006). Experimental results that were used to validate the model can be found from Mathieson *et al*., (2005). The results from those simulations can be seen in Fig. 6. It can be seen that the devolatilization can be divided into two stages. The first stage is where volatiles ignite and temperature is rapidly rising. In the second stage, the temperature increases slowly due to the char combustion. (Du & Chen, 2006)

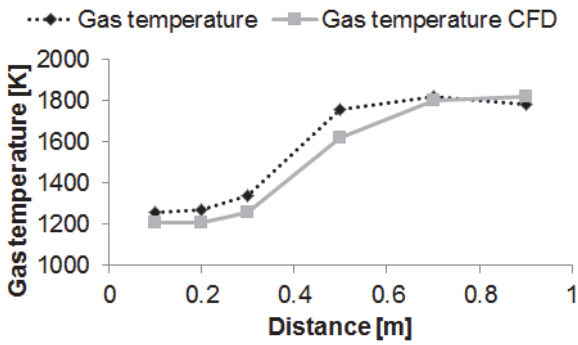


**Fig. 6. Gas temperature along the experimental rig (modified from Du & Chen, 2006).**

The CANMET Energy Technology Centre (CETC) has a small-scale test rig, which is used to test coal suitability for BF use. The test rig is a horizontal cylindrical reactor, which is 1 m in length and has an inner diameter of 0.03 m. Combustion air is pre-heated to 740 °C and the $O_2$ volume fraction at the inlet is 25%. There is a possibility for a combined PC and natural gas injection, but injection rates, air blast velocity, and fuel to air ratio are not public information in the study. Based on the measured data the stoichiometric ratio is much larger than 1, because the $O_2$ volume fraction after combustion is still about 13%. (Chui, 2005)

In the study by Majeski *et al*. (2015), the authors write that they have not validated their model, but Chui (2005) has done validation for his model based on the test rig. The group justifies the lack of validation with the fact that their CFD model was similar except for the treatment of radiation and the gas phase combustion model. It should have been validated, because radiation and gas phase combustion play a significant role in the PC combustion process. Chui (2005) used flamelet formulations for the premixed and non-premixed combustion, whereas Majeski *et al*. (2015) used the EDM/Arrhenius mechanism. Furthermore, the group used very high volatile coal (VM=55.6%) in the test rig, which makes gas phase reactions even more important. It is probably brown coal, which is typically not used in the BF process because of their low coke RR (Ishii, 2000).

Zhou (2008) used two different small-scale experimental rig results to validate her model. The first one was a raceway hot model at Sumimoto Metal Industries in Japan (Nogami *et al*., 2004). This experimental rig consists of a tuyere and a coke bed, where the blast temperature was between 800 and 1200 °C, the $O_2$ concentration was 10–22%, and the air flow rate was 375.32–700 $Nm^3/h$. The air blast pressure or PC size distribution are not given in the article. The tuyere

diameter is 65 mm, and the coke bed is 1200 mm deep, 1100 mm long and 500 mm wide. In this experimental rig raceway dimensions and shapes can be measured. Gas composition can be measured after the tuyere nose on the tuyere central axis. This data can be used to validate tuyere-raceway area combustion modeling. The second experimental rig was an entrained flow combustion reactor (Zhang, Wei, Zhou, & Sheng, 2005). In that system, the maximum velocities are in the range of 15 m/s and the combustion air temperatures are 250 and 350 °C for primary and secondary air, respectively. Conditions do not correspond well with the BF. The validation results for coke combustion are presented in Fig. 7a. The validation results for coal combustion are presented in Fig. 7Fig. 7b. It can be seen that combustion begins much slower in the CFD model and there are big differences in the near tuyere nose and burner regions. The combustion model, however, does not predict the ignition properly. Results look similar when the combustion is complete, because the gas phase has reached the balance.

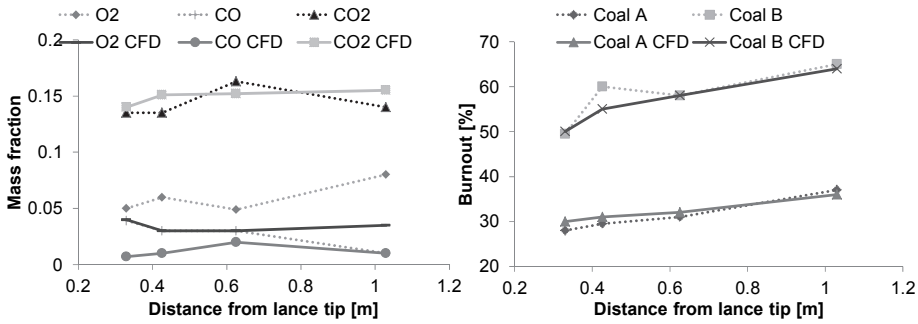


**Fig. 7. a) Gas composition for coke combustion validation (combined from (Nogami *et al.*, 2004; C. Zhou, 2008)), b) gas composition for coal combustion validation (combined from (Zhang *et al.*, 2005; C. Zhou, 2008)).**

## 3.3 Full-scale CFD models

Full-scale models also take into account the porous coke bed (Fig. 3), which has a great effect on the temperature and velocity of the flow in the BF. Most studies use heat sink and reactions in the coke bed to account for the iron oxide reduction and coke oxidation. The physical raceway area in the model creates recirculation of hot combustion gases, which heats the air blast but lowers the mole fraction of $O_2$. This changes the combustion chemistry more to the gasification side, which is not taken

into account in most studies where combustion is modeled with a simple one-step or two-step combustion model.

Almost all of the studies concern coal combustion, which is the most commonly used auxiliary fuel in BF. Other studied fuels are heavy oil (Andahazy *et al*., 2006), natural gas (NG) (Majeski *et al*., 2015), coke oven gas (COG) and basic oxygen furnace gas (BOFG) (Hellberg, Jonsson, & Jönsson, 2005), and plastic (Harasek *et al*., 2007).

Shen *et al*. (2011) published a study about the PC injection model creation for the BF tuyere-raceway area. The most important finding was that the recirculation region is important to include in the model to obtain more realistic CO levels compared to the older studies.

Shen *et al*. (2012a) reported a parametric study on the effects of operating conditions on the PC burnout. The parameters for the CFD model are presented in Table 4. The volume flow rate and the air blast pressure are kept constant, i.e., 5000 $Nm^3$/min and 461 kPa, respectively. Blast temperature, $O_2$ enrichment, PC rate, and different cooling gases are the variables chosen for the parameter study. The results indicate that the blast temperature increases from 1273 to 1673 K, affects the devolatilization rate, and the PC burnout increases by 6%. The $O_2$ enrichment from 23% to 35% causes the particle temperature to rise from about 2600 to 2900 K, boosting the PC burnout by 7%. According to Shen *et al*. (2012a), the cooling gas has a small effect on the PC burnout. There is no difference in the PC burnout between air and pure $O_2$, but $CH_4$ lowers the burnout by 2%, even though it initially increases the particle temperature. The $CH_4$ combustion consumes a part of the available $O_2$, leading to a lower burnout. The PC flow rate change from 583.33 to 1387.13 kg/min decreases the burnout by about 30%.

**Table 4. Parameters and results from the PC injection study (modified from Y. S. Shen *et al*., 2012).**

| Case | Blast temperature (K) | O2 (wt-%) | Coal rate (kg/min) | Conveying gas flow (Nm3/min) | Cooling gas (Nm3/min) | Burnout (%) |
|---|---|---|---|---|---|---|
| Base | 1473 | 22.9 | 583.33 | 21.95 | 83.33/100% O2 | 83.4 |
| 2 | 1273 | 22.9 | 583.33 | 21.95 | 83.33/100% O2 | 80.5 |
| 3 | 1673 | 22.9 | 583.33 | 21.95 | 83.33/100% O2 | 85.3 |
| 4 | 1473 | 30.0 | 583.33 | 21.95 | 83.33/100% O2 | 87.5 |
| 5 | 1473 | 35.0 | 583.33 | 21.95 | 83.33/100% O2 | 89.0 |
| 6 | 1473 | 22.9 | 916.47 | 21.95 | 83.33/100% O2 | 64.5 |
| 7 | 1473 | 22.9 | 1168.49 | 21.95 | 83.33/100% O2 | 72.5 |
| 8 | 1473 | 22.9 | 1387.13 | 21.95 | 83.33/100% O2 | 59.0 |
| 9 | 1473 | 22.9 | 583.33 | 21.95 | 83.33/Air | 83.2 |
| 10 | 1473 | 22.9 | 583.33 | 21.95 | 83.33/CH4 | 81.5 |

Shen *et al*. (2012b) made a parameter study on the effect of coke bed porosity on flows and PC combustion in the tuyere-raceway area. They varied porosities of the coke bed in the deadman zone and the dripping zone as well as the PC injection rate. The PC particle burnout and the parameters used in the CFD are shown in Table 5. It can be seen that the deadman zone porosity affects the burnout. As porosity decreases from 0.25 to 0.15, the burnout lowers by 3%. This is caused by the increased recirculation of combustion gases inside the raceway area. The dripping zone has a similar effect on the PC burnout. Higher porosity leads to better combustion. When the porosity is raised from 0.4 to 0.6, the burnout rises from 81.5 to 84.0%. The coal rate increase decreases the particle burnout. The results are almost the same when compared to their previous study (Shen *et al*., 2012a), where the coke bed was treated as a uniform porosity zone.

**Table 5. Parameters and results from the PC injection study (modified from Y. Shen, Yu, Austin, & Zulli, 2012).**

| Case | Porosity of deadman zone | Porosity of dripping zone | Coal rate (kg/min) | Burnout CFD (%) |
|---|---|---|---|---|
| Base | 0.25 | 0.5 | 583.33 | 83.4 |
| 2 | 0.15 | 0.5 | 583.33 | 80.9 |
| 3 | 0.25 | 0.6 | 583.33 | 84.0 |
| 4 | 0.25 | 0.4 | 583.33 | 81.5 |
| 5 | 0.25 | 0.5 | 916.47 | 82.2 |
| 6 | 0.25 | 0.5 | 1168.49 | 70.2 |
| 7 | 0.25 | 0.5 | 1387.13 | 59.0 |

Shen *et al*. (2014) made an investigation on the effects of bird's nest on the transport phenomena in the BF tuyere-raceway area. Fine char from unburnt PC and fine coke may accumulate in the boundary at the end of the raceway at the tuyere level. It forms a low-permeability region called a bird's nest. The group compared the case without a bird's nest to the other case where it was included. The bird's nest has a clear effect on the fluid flow in the raceway area. It impacts the length of the air blast penetration into the raceway area because of the increased pressure loss at the end of the raceway. The bird's nest does not affect the PC burnout at the endpoint of the raceway, but it lowers the burnout over the raceway surface by 17%. They conclude that the possible effects of a bird's nest should be taken into account.

Zhou (2008) reported the largest single study on PC combustion in BF and raceway formation. The study also covered fouling effects of PC volatiles on the inner surface of the injection lance and co-injection of NG and PC. In this thesis, the interest lies in the PC injection and that part is covered below. Different cases of the study are presented in Table 6. In the parameter study, the blast temperature, $O_2$ enrichment, coal mass flow rate, and tuyere diameter were varied. In the study, a remarkable increase in the devolatilization rate was found when the temperature was increased by 166 K. The increase was from 0.004 kg/s to 0.045 kg/s, resulting in a burnout growth from 81.5% to 84%. A larger tuyere diameter lowers the velocity of the air blast, increasing the residence time of PC in the tuyere. This improves devolatilization in the tuyere area, therefore leading to higher combustion efficiency, i.e., from 87.5% to 92.5%. The $O_2$ enrichment was found to have a significant effect on the devolatilization of PC as well. When the $O_2$ level is increased from 25% to 29%, the devolatilization rate increases from 0.0093 kg/s to 0.013 kg/s. A higher PC injection rate decreases the temperature, which causes a lower burnout. With the PC injection rate of 0.3565 kg/s, the burnout is about 82% but drops to 75.8% when the injection rate is 0.458 kg/s.

**Table 6. Parameters and results from the PC injection study. (C. Zhou, 2008)**

| Case | Blast temperature (K) | Volume flow ($Nm^3/min$) | Pressure (atm) | $O_2$ (wt-%) | Moisture ($g/Nm^3$) | Coal rate (kg/s) | Tuyere diameter (m) |
|---|---|---|---|---|---|---|---|
| 1 | 1338.6 | 160.6 | 3.313 | 25.02 | 14.483 | 0.357 | 0.1651 |
| 2 | 1283.0 | 160.6 | 3.313 | 25.02 | 14.483 | 0.357 | 0.1651 |
| 3 | 1394.1 | 160.6 | 3.313 | 25.02 | 14.483 | 0.357 | 0.1651 |
| 4 | 1449.6 | 160.6 | 3.313 | 25.02 | 14.483 | 0.357 | 0.1651 |
| 5 | 1338.6 | 160.6 | 3.313 | 25.02 | 14.483 | 0.357 | 0.1397 |
| 6 | 1338.6 | 160.6 | 3.313 | 26.02 | 14.483 | 0.357 | 0.1651 |
| 7 | 1338.6 | 160.6 | 3.313 | 27.02 | 14.483 | 0.357 | 0.1651 |
| 8 | 1338.6 | 160.6 | 3.313 | 29.02 | 14.483 | 0.357 | 0.1651 |
| 9 | 1338.6 | 160.6 | 3.313 | 25.02 | 14.483 | 0.408 | 0.1651 |
| 10 | 1338.6 | 160.6 | 3.313 | 25.02 | 14.483 | 0.458 | 0.1651 |

Gu *et al*. (2008) studied the effect of the tuyere diameter on the PC combustion efficiency. They used two different tuyere diameters, i.e. 0.165 m and 0.146 m. Ignition takes place inside the 0.165 m tuyere, but in the 0.146 m tuyere it does not happen. It takes about 0.9 m longer for PC particles to ignite in the 0.146 m tuyere case. The difference in tuyere diameter between the two cases leads to a large difference in the particle burnout, which is 85.3% when the tuyere diameter is 0.165 m and 60.6% in the 0.146 m case. Velocity is about 28% higher in the 0.146 m tuyere, which comes directly from the difference in the cross-sectional area. In their calculation, thermal expansion of gases is not taken into account, because it would have an effect on the velocity. The combustion efficiency can be seen in the maximum temperature as well. Maximum temperatures are 3075 K and 2893 K in the 0.165 m and 0.146 m tuyeres, respectively. The combustion chemistry is probably oversimplified, because the maximum temperature increases at an extremely high level. The differences between these cases seem large compared to the change in the tuyere diameter.

Gu *et al*. (2010) reported a study on the effect of PC particle size (particle sizes 30, 60 and 90 μm), PC type (volatile matter 34.32% and 19.95%), and injection angle (angle 10.8 ° and 0 ° to the tuyere center line and 4.0 ° and 0 ° to the right) on combustion efficiency. The geometry considered only the tuyere area. They found out that all of these parameters affected combustion and the coal volatile matter content has the biggest influence on combustion efficiency. When the volatile matter is lowered from 34.32% to 19.95%, the PC burnout decreases from 46.04% to 35.02%. Particle size also has a notable effect. When the particle size is increased from 30 to 90 μm the burnout decreases from 51.03 to 44.21%. The

injection angle has a small effect on the particle burnout. The lance with an injection angle gets about 3% higher combustion compared to the case without an injection angle.

Li *et al*. (2014) reported a parametric study with CFD of the blast furnace raceway and tuyere areas. The gas phase combustion model in the study was the EBU-Arrhenius model. They evaluated the burnout rate of PC and optimized seven parameters by orthogonal experiments (Table 7). The parameter sequence is when the combustion efficiency is considered from the most effective to the least effective. The parameters were the PC type (F) (low volatile anthracite coal (CA), high volatile bituminous coal (CB) and 1:1 mixture of these coals (CC)), the PC injection ratio (B), the blast $O_2$ enrichment (E), the blast temperature (D), the lance type (G) (single lance (SG), double lance (DG), and the oxygen lance (OG)), the blast volume flow rate (C), and the lance angle (A) (0° and 11°) with respect to the tuyere centerline. Their results indicate that the most effective parameter on the combustion efficiency is the type of the PC. In the standard case (A=11°, B=100 kg/thm, C=2050 $Nm^3$/min, D=1423 K, E=1.5%, F=CA and G=SG) the combustion efficiency was 43.37%. After optimization (A=11°, B=100 kg/thm, C=1950 $Nm^3$/min, D=1523 K, E=5.0%, F=CB and G=DG) the combustion efficiency increased to 91.43%, which is about 111% higher than the standard case.

**Table 7. Parameters and results from the parametric study. (Li, Zhang, Zhang, Zhou, & Yan, 2014)**

| Case | A (°) | B (kg/thm) | C ($Nm^3$/min) | D (K) | E (%) | F | G | Burnout (%) |
|---|---|---|---|---|---|---|---|---|
| 1 | 11 | 100 | 1950 | 1423 | 1.5 | CA | SG | 46.02 |
| 2 | 11 | 100 | 2050 | 1473 | 3.0 | CC | OG | 88.12 |
| 3 | 11 | 100 | 2150 | 1523 | 5.0 | CB | DG | 88.12 |
| 4 | 11 | 125 | 1950 | 1423 | 3.0 | CC | DG | 69.06 |
| 5 | 11 | 125 | 2050 | 1473 | 5.0 | CB | SG | 81.68 |
| 6 | 11 | 125 | 2150 | 1523 | 1.5 | CA | OG | 44.52 |
| 7 | 11 | 150 | 1950 | 1473 | 1.5 | CB | OG | 74.34 |
| 8 | 11 | 150 | 2050 | 1523 | 3.0 | CA | DG | 46.21 |
| 9 | 11 | 150 | 2150 | 1423 | 5.0 | CC | SG | 66.10 |
| 10 | 0 | 100 | 1950 | 1523 | 5.0 | CC | OG | 79.02 |
| 11 | 0 | 100 | 2050 | 1423 | 1.5 | CB | DG | 81.43 |
| 12 | 0 | 100 | 2150 | 1473 | 3.0 | CA | SG | 46.32 |
| 13 | 0 | 125 | 1950 | 1473 | 5.0 | CA | DG | 53.19 |
| 14 | 0 | 125 | 2050 | 1523 | 1.5 | CC | SG | 67.13 |
| 15 | 0 | 125 | 2150 | 1423 | 3.0 | CB | OG | 77.62 |
| 16 | 0 | 150 | 1950 | 1523 | 3.0 | CB | SG | 78.33 |
| 17 | 0 | 150 | 2050 | 1423 | 5.0 | CA | OG | 40.67 |
| 18 | 0 | 150 | 2150 | 1473 | 1.5 | CC | DG | 64.46 |

Takeda and Lockwood (1997) made a two-dimensional study on the PC combustion in the BF tuyere-raceway area. They modeled different types of oxygen supply methods for combustion. In the first type, $O_2$ was added uniformly in the air blast. In the second type, $O_2$ was added through the oxy-coal lance, and in the third type the $O_2$ is supplied through a separate $O_2$ lance after the PC injection. The third option produced the most effective combustion. The difference from the first type was about 5% and from the second type about 9%. Another case that the group studied was the effect of lance design on the combustion efficiency. The first lance was a straight pipe, the second was a straight pipe with a swirl, the third one was a thicker pipe with double the diameter (4 cm) of other lances (2 cm), and the fourth one used an artificial radial velocity to potentially increase mixing. Different lance positions behaved very similarly when compared to each other (burnout about 0.44%), but the thicker pipe provided 20% higher burnout than the other methods (burnout about 55%). The mixing is improved significantly with an increased lance diameter, which is important to the actual process design.

# 4 CFD modeling of auxiliary fuel injection

CFD is used to analyze systems involving fluid flow and all the important phenomena relating to it, e.g., heat and mass transfer and chemical reactions. Today, CFD is commonly used to solve problems in academia as well as in different fields of industry to aid in research and development. With CFD, it is possible to try several different configurations and boundary conditions in modeling and to reduce the need for experimental work. This lowers the costs in development of new processes or products. CFD is based on solving conservation equations for mass, momentum and energy. (Versteeg & Malalasekera, 2007)

In CFD, the model geometry is divided into discrete computational cells called the mesh. All the governing equations are solved in the computational nodal point in each of the cell centers. The time needed for the solution increases with an increasing mesh size. In addition, all the values that are needed for the calculation are stored in each nodal point, which leads to an increase in the file size and memory use as the mesh size increases. This creates limitations for the feasible mesh size. Nevertheless, the mesh density has to be high enough to capture important phenomena. (Versteeg & Malalasekera, 2007)

Several methods have been used to discretize the Navier-Stokes equations, which include finite difference, finite element, spectral element, and finite volume methods. The finite volume method (FVM) is commonly used for discretizing CFD equations, and the other methods are not discussed here. FVM is used to solve partial differential equations in the algebraic equation form. The governing conservation equations are integrated over each computational cell. (Marshall & Bakker, 2004)

## 4.1 Conservation equations

The fundamental conservation equations solved for mass, momentum, energy, and chemical species, which are necessary for the tuyere-raceway CFD modeling, are presented here. The conservation laws of physics are as follows: (1) The mass of a fluid and chemical species are conserved; (2) the rate of change of momentum equals the sum of the forces on a fluid particle (Newton's second law); and (3) the rate of change of energy is equal to the sum of heat addition to and the rate of work done on a fluid particle (first law of thermodynamics). (Peters, 2000; Versteeg & Malalasekera, 2007)

### 4.1.1 Mass conservation

The continuity equation for the compressible fluid flow is written in the form of mass conservation

$$\frac{\partial \rho}{\partial t} + \nabla \cdot (\rho \vec{v}) = S_m \tag{29}$$

where ρ is the fluid density (kg/m$^3$), t is time (s), $\vec{v}$ is the velocity vector (m/s), and $S_m$ is the source term for mass addition (kg/(m$^3$s)) to the continuous phase from the dispersed phase. In this case, it is the mass of fuel vapor from heavy oil droplets and moisture or volatiles from PC. The rate of change of the fluid density is described with the first term in the left-hand side (LHS) and the second term is the convective net flux of mass. (ANSYS Inc., 2017a; Versteeg & Malalasekera, 2007)

The continuous phase is modeled as a compressible ideal gas. The density value is solved from the following equation

$$\rho = \frac{p_{op} + p_s}{\frac{R}{M_w} T} \tag{30}$$

where $p_s$ is the calculated local static pressure relative to the operating pressure (Pa) and $p_{op}$ is the operating pressure (Pa), R is the universal gas constant (8.3145 kg·m$^2$/(s$^2$·K·mol)), $M_w$ is the molecular weight (g/mol), and T is temperature (K). (ANSYS Inc., 2017a)

### 4.1.2 Momentum conservation

The suffix notation has been used in the momentum equation. The convention in this notation is that i or j = 1 corresponds to the x-direction, i or j = 2 the y-direction and i or j = 3 the z-direction (Versteeg & Malalasekera, 2007). The Reynolds-averaged Navier-Stokes momentum equation in Cartesian tensor form is written as

$$\frac{\partial}{\partial t}(\rho u_i) + \frac{\partial}{\partial x_j}\left(\rho u_i u_j\right) = -\frac{\partial p_s}{\partial x_j} + \frac{\partial}{\partial x_j}(2\mu S_{ji} - \rho\overline{u_i' u_j'}) + \rho g_i \tag{31}$$

where $x_j$ is the position vector (m), μ is the dynamic viscosity (kg/(m·s)), $S_{ji}$ is called the mean strain rate tensor (equation (53) on page 65 in Section 4.2.1) and $\overline{u_i'}$ and $\overline{u_j'}$ are the temporal averages of the fluctuating velocity (m/s). The first term in the LHS is the local change of momentum and the second term is the rate of change of momentum by convection. On the right-hand side (RHS) the first term is the pressure gradient, the second term represents the molecular transfer due to viscosity, and the third term is called the Reynolds stress tensor, which represents

the turbulent fluctuations of the flow. The Reynolds stress tensor is modeled with the Buossinesq hypothesis in the κ-ε turbulence model, which is used in this thesis (Peters, 2000; Versteeg & Malalasekera, 2007)

$$-\rho\overline{u_i'u_j'} = \mu_t\left(\frac{\partial u_i}{\partial x_j}+\frac{\partial u_j}{\partial x_i}\right)-\frac{2}{3}\left(\rho\kappa+\mu_t\frac{\partial u_k}{\partial x_k}\right)\delta_{ij} \quad (32)$$

where $\mu_t$ is the turbulent viscosity (kg/(m·s)), κ is the turbulent kinetic energy, and $\delta_{ij}$ is the Kronecker delta ($\delta_{ij} = 1$ if $i = j$ and $\delta_{ij} = 0$ if $i \neq j$).

### 4.1.3 Energy conservation

Energy conservation has to be taken into account in combustion modeling. In combustion, heat is released when the chemical bonds of the fuel molecules are breaking (Peters, 2000). The energy conservation equation can be described as follows (ANSYS Inc., 2017a):

$$\frac{\partial}{\partial t}(\rho E)+\nabla\cdot\left(\vec{v}(\rho E+p)\right)=\nabla\cdot\left(k_{eff}\nabla T-\sum_i h_i\vec{J}_i+(\bar{\bar{\tau}}_{eff}\cdot\vec{v})\right)+S_h \quad (33)$$

where $k_{eff}$ is the effective conductivity (W/(m·K)) $k+k_t$ (where k is thermal conductivity and $k_t$ is the turbulent thermal conductivity). $S_h$ includes chemical reactions, heat sources and sinks, and radiation heat sources. In the LHS, the first term is the rate of change of energy and the second term is the heat transfer by convection. In the RHS, the first term is the heat conduction, the second term is the species diffusion, and the third term is the viscous dissipation of energy, which is important in compressible flows. (ANSYS Inc., 2017a; Peters, 2000; Versteeg & Malalasekera, 2007) The species' diffusion flux in turbulent flows is solved by

$$\vec{J}_i=-\left(\rho D_{i,m}+\frac{\mu_t}{Sc_t}\right)\nabla Y_i-D_{T,i}\frac{\nabla T}{T} \quad (34)$$

where $D_{i,m}$ is the mass diffusion coefficient ($m^2/s$) for species i in the mixture, $Y_i$ is the mass fraction of species i, $D_{T,i}$ is the thermal diffusion coefficient ($m^2/s$) for species i, and $Sc_t$ is the turbulent Schmidt number

$$\mathrm{Sc_t}=\frac{\mu_t}{\rho D_t} \quad (35)$$

where $D_t$ is the turbulent diffusivity ($m^2/s$). Laminar diffusion is generally much slower in turbulent flows than the turbulent diffusion, and the laminar diffusion coefficient can be kept constant for all species. The effective viscous stress tensor $\bar{\bar{\tau}}_{eff}$ is calculated from

$$\bar{\bar{\tau}}_{eff} = \mu_{eff}\left[(\nabla\vec{v} + \nabla\vec{v}^T) - \frac{2}{3}\nabla\cdot\vec{v}I\right] \quad (36)$$

where $\mu_{eff}$ is the effective viscosity (kg/(m·s)) $\mu+\mu_t$ (where $\mu_t$ is the turbulent viscosity), and I is the unit tensor. E is the energy, which is calculated by

$$E = h - \frac{p}{\rho} + \frac{v^2}{2} \quad (37)$$

where sensible enthalpy h (J/kg) in the case of ideal gas is

$$h = \sum_i Y_i h_i \quad (38)$$

$Y_i$ is the mass fraction of species i. Enthalpy for the individual species i is calculated from

$$h_i = \int_{T_{ref}}^{T} c_{p,i} dT \quad (39)$$

For the pressure-based solver, the reference temperature $T_{ref}$ = 298.15 K.

### *Heat radiation modeling*

Thermal heat radiation is energy transfer in the form of electromagnetic radiation. It is the exchange of heat between surfaces or between a surface and its surroundings through absorbing/emitting gases. Radiation heat transfer becomes stronger with an increasing temperature difference between the radiation sources to the fourth power. There are high temperatures with large differences (maximum 2440 K) in the tuyere-raceway area, which makes the radiation heat transfer important. Due to the high air blast velocity of more than 200 m/s, forced convection is the dominating heat transfer phenomenon in the raceway area. The forced convection is weaker in the upper parts of the raceway and in the coke bed. Furthermore, combustion modeling without radiative heat transfer produces highly inaccurate results because combustion occurs as a balance in small volumes (finite-volume framework) and the radiative heat transfer involves the long distance interaction. (Bejan & Kraus, 2003; Gonçalves dos Santos *et al*., 2008)

Discrete Ordinates (DO) is chosen as the radiation heat transfer method. The model includes the effect of the gray gases, such as $CO_2$, $H_2O$ and hydrocarbons, and it can be used to model radiation in porous areas. Droplets, walls, and the coke bed are assumed to be black bodies. The particle scattering factor is set to $\sigma_p$=0.9, which is the recommended value for the coal combustion modeling (Lockwood, Rizvi, & Shah, 1986). In the ANSYS Fluent, the droplet radiation interaction results

in scattering of the continuous phase being ignored. The radiation heat transfer by the DO method with the droplet interaction is modeled with the following equation

$$\nabla \cdot (I\vec{s}) + \left(a + a_p + \sigma_p\right) I(\vec{r}, \vec{s}) = an^2 \frac{\sigma T^4}{\pi} + E_p + \frac{\sigma_p}{4\pi} \int_0^{4\pi} I(\vec{r}, \vec{s}') \, \Phi(\vec{s} \cdot \vec{s}') d\Omega' \quad (40)$$

where I is the intensity (W/m$^2$), $\vec{s}$ is the direction (m), a is the gas absorption coefficient, $a_p$ is the equivalent absorption coefficient, $\sigma_p$ is the equivalent particle scattering factor, $\vec{r}$ is the position (m), n is the refractive index, σ is the Stefan-Boltzmann constant ($5.67 \cdot 10^{-8}$ W/(m$^2$K$^4$)), $E_p$ is the equivalent emission (W/m$^3$), $\vec{s}'$ is the scattering direction vector, $\Phi$is the phase function, and $\Omega'$ is the solid angle.

The weighted sum of the gray gases model (WGSSM) is used for absorption modeling of gray gases. The equation for the total emissivity over length s is

$$\epsilon = \sum_{i=0}^{I} a_{\epsilon,i}(T)(1 - e^{-\kappa_i p_x s}) \quad (41)$$

where $a_{□,i}$ is the emissivity weighting factor for the *i*th gray gas, $\kappa_i$ is the absorption coefficient of the *i*th gray gas, and $p_x$ is the sum of the partial pressures of all absorbing gases.

### *4.1.4 Chemical species conservation*

Mass transfer is the motion of chemical species with diffusion or convective transport. For multicomponent systems, the local mass fraction of each species is calculated with a convection-diffusion equation for the species i (ANSYS Inc., 2017a; Peters, 2000; Versteeg & Malalasekera, 2007):

$$\frac{\partial}{\partial t}(\rho Y_i) + \nabla \cdot (\rho \vec{v} Y_i) = -\nabla \cdot \vec{J}_i + R_i + S_d \quad (42)$$

where $\vec{J}_i$ is the species' diffusion flux in turbulent flows (equation (34)), $R_i$ is the net rate of production of species i by chemical reaction (kg/(m$^3$s)), and $S_d$ is the rate of creation by addition from the dispersed phase (kg/(m$^3$s)). The first term in the LHS is the local change of species i and the second term is the rate of change of species i by convection. On the RHS, the first term is the diffusion of species i.

## 4.2 Eulerian-Lagrangian modeling

In the Eulerian-Lagrangian approach, the continuous phase is modeled with the Eulerian method and particles (solid particles, droplets) are modeled as a dispersed

Lagrangian phase. In this thesis, the gas phase (continuum) is always modeled with the Eulerian method, and heavy oil or PC is modeled with the Lagrangian method.

In the Lagrangian method, each fluid particle is tracked and its current state is known in each time step. All the particle properties such as location, velocity, direction, temperature, diameter, and volatile fraction are known and can be followed individually, which is very important when the heavy oil droplet or the PC particle fates are studied. (Martin & Williams, 2009)

In the Eulerian modeling, the flow is divided into control volumes, where individual fluid particles are not tracked. Fluid flow properties, such as velocity, temperature, or pressure are expressed as fields inside these control volumes. Therefore, in the Eulerian method, all the fluid particles in the same control volume have the same properties as a function of space and time, and the individual behavior is not tracked. This is a useful quality in fluid dynamics because fluid flow is a continuum and tracking each fluid particle separately is unnecessary. (Martin & Williams, 2009)

### *4.2.1 Turbulence modeling*

Fluid flow behavior is divided into laminar and turbulent flows. Flow characterization is done by using the Reynolds number

$$Re = \frac{\rho v l}{\mu} \tag{43}$$

where l is the characteristic length scale of the system, e.g., the pipe diameter. When the Reynolds number is below the critical value $Re_{crit}$, the flow is laminar and becomes fully turbulent after $Re_t$. The transition from laminar to turbulent flow occurs between $Re_{crit}$ and $Re_t$. In a pipe, flow transition occurs between $Re_{crit}$ = 2000 and $Re_t = 10^5$. In a laminar flow, fluid layers slide over each other in an orderly fashion, and these layers interchange momentum only on a molecular level. Viscous shear forces are high enough to damp instabilities and turbulence in flows. When the flow starts the transition from laminar to turbulent flow, it has qualities of both laminar and turbulent flows. In a turbulent flow, velocity and other flow properties vary in a random and chaotic way. The turbulent fluctuations have rotational flow structures called turbulent eddies. The eddy cascade hypothesis forms the basis for closure of turbulence models. Large eddies break up into smaller eddies, which in turn break up into even smaller ones, until the smallest eddies disappear due to viscous forces. This leads to scale invariance of energy transfer in the inertial

subrange of turbulence in sufficiently large Reynolds numbers. All the classical turbulence models include this feature, and they satisfy the requirement of Reynolds number independence. (Peters, 2000; Versteeg & Malalasekera, 2007)

Combustion takes place in the turbulent flow field in most technical processes, because turbulence enhances the mixing of fuel and oxidizer. Furthermore, the combustion itself generates turbulence because it releases heat, which causes buoyancy and gas expansion. In a tuyere-raceway area, flow is highly turbulent, which makes the turbulence modeling important. A classical approach to model turbulent flows is to use single-point averages of the Navier-Stokes equations. These types of models are called the Reynolds-averaged Navier-Stokes (RANS) models. This approach is often used in industrial modeling of flows and is considered to be the best compromise. The most commonly used RANS model is the κ-ε model. In the κ-ε model, it is assumed that the turbulent eddy viscosity is isotropic, which means that the ratio between the Reynolds stresses and the mean rate of deformations is uniform in all directions. RANS are typically used in steady-state simulations when the detailed structure of turbulent eddies is not the area of interest. (Peters, 2000)

In the thesis, turbulence is simulated with the Realizable κ-ε model (Shih, Liou, Shabbir, Yang, & Zhu, 1994). It is a two-equation model that is based on the modeled equations for the turbulence kinetic energy (κ) and its dissipation rate (ε). Realizability ensures the positivity of turbulent normal stresses and Schwartz' inequality between any of the fluctuating quantities. It prevents a turbulence model from producing unphysical results and works properly in the turbulent transition region, where the κ value is typically small. The transport equation for turbulent kinetic energy is (Shih *et al*., 1994)

$$\frac{\partial}{\partial t}(\rho\kappa) + \frac{\partial}{\partial x_j}(\rho\kappa u_j) = \frac{\partial}{\partial x_j}\left[\left(\mu + \frac{\mu_t}{\sigma_k}\right)\frac{\partial \kappa}{\partial x_j}\right] + G_\kappa + G_b - \rho\varepsilon - Y_M \quad (44)$$

where the production of turbulent kinetic energy $G_\kappa$ is calculated from

$$G_\kappa = -\rho\overline{u_i' u_j'}\frac{\partial u_j}{\partial x_i} \quad (45)$$

Buoyancy effects on the production of turbulent kinetic energy $G_b$ in ideal gas conditions is solved from the equation

$$G_b = -g_i \frac{\mu_t}{\rho \mathrm{Pr}_t}\frac{\partial \rho}{\partial x_i} \quad (46)$$

Fluctuating dilatation in the compressible turbulence to the overall dissipation rate is calculated as

$$Y_M = 2\rho\varepsilon M_t^2 \tag{47}$$

where $M_t$ is the turbulent Mach number defined as

$$M_t = \sqrt{\frac{k}{v_s^2}} \tag{48}$$

where $v_s$ is the speed of sound ($v_s \equiv \sqrt{\gamma RT}$, where γ is the isentropic expansion factor).

The turbulent dissipation rate ε is based on the dynamic equation of the mean-square vorticity fluctuation. The buoyancy effects are not included in the turbulent dissipation rate, therefore $G_b$ is 0 in the ε equation, which removes the last term in the RHS (Shih *et al*., 1994)

$$\frac{\partial}{\partial t}(\rho\varepsilon) + \frac{\partial}{\partial x_j}(\rho\varepsilon u_j) = \frac{\partial}{\partial x_j}\left[\left(\mu + \frac{\mu_t}{\sigma_\varepsilon}\right)\frac{\partial \varepsilon}{\partial x_j}\right] + \rho C_1 S\varepsilon - \rho C_2 \frac{\varepsilon^2}{\kappa + \sqrt{v\varepsilon}} + C_{1\varepsilon}\frac{\varepsilon}{\kappa}C_{3\varepsilon}G_b \tag{49}$$

where

$$C_1 = max\left[0.43, \frac{\eta}{\eta+5}\right] \tag{50}$$

$$\eta = S\frac{\kappa}{\varepsilon} \tag{51}$$

$$S = \sqrt{2S_{ij}S_{ij}} \tag{52}$$

$$S_{ij} = \frac{1}{2}\left(\frac{\partial u_j}{\partial x_i} + \frac{\partial u_i}{\partial x_j}\right) \tag{53}$$

where η is the time scale ratio of the turbulence to the mean strain, and S is the modulus of the mean rate of strain tensor $S_{ij}$. Turbulent viscosity is calculated in the Realizable κ-ε model from

$$\mu_t = \rho C_\mu \frac{\kappa^2}{\varepsilon} \tag{54}$$

where $C_\mu$ is not constant, but computed from

$$C_\mu = \frac{1}{A_0 + A_s\frac{\kappa U^*}{\varepsilon}} \tag{55}$$

where

$$U^* = \sqrt{S_{ij}S_{ij} + \widetilde{\Omega}_{ij}\widetilde{\Omega}_{ij}} \tag{56}$$

and $A_0 = 4.04$,

$$A_s = \sqrt{6}\left(\cos\left(\frac{1}{3}\arccos\left(\sqrt{6} * \frac{S_{ij}S_{ji}S_{ki}}{(S_{ij}S_{ij})^{\frac{3}{2}}}\right)\right)\right) \tag{57}$$

$$\widetilde{\Omega}_{ij} = \Omega_{ij} - 2\varepsilon_{ijk}\omega_k \quad (58)$$

$$\Omega_{ij} = \overline{\Omega}_{ij} - \varepsilon_{ijk}\omega_k \quad (59)$$

where $\Omega_{ij}$ is the rotation rate viewed from the absolute frame of reference, and $\overline{\Omega}_{ij}$ is the mean rotation rate viewed in a rotating reference frame. $\omega_k$ is the angular velocity and $\varepsilon_{ijk}$ is the Levi-Civita permutation symbol. In Ansys Fluent, by default, the extra rotation term $\widetilde{\Omega}_{ij} = \Omega_{ij}$. Because the model can calculate the mean rotation rate of turbulence, it is useful in the BF simulations (Shih *et al*., 1994). The Realizable κ-ε converged well, and the model was applied in the simulations.

### *4.2.2 Discrete phase modeling*

Discrete phase in this thesis consists of either extra heavy oil or pulverized coal. Gasification and combustion of different types of auxiliary fuels involves complex physical and chemical phenomena. These include turbulence, droplet atomization, heat and mass transfer and chemical reactions. The models describing the combustion of these two fuels are different from each other. EHO combustion and gasification can be divided into three stages: vaporization, gas phase combustion, and cenosphere combustion. Cenosphere mass is about 8% of the total droplet mass. In this study, cenospheres are not included in the computation. This can be done because the cenosphere mass fraction is so low that the sufficient combustion efficiency can be determined from the droplet vaporization. To achieve a high surface area for effective combustion, the injection temperature is about 200 °C, which lowers the viscosity of EHO, leading to smaller droplets via better atomization.

The combustion model for PC can be divided into five steps: heating, drying, devolatilization, char combustion and gas phase combustion. Heating and drying models are the same for both fuels. All the necessary models for both EHO and PC are covered in this section.

In the ANSYS Fluent, the Lagrangian method is called the Discrete Phase Model (DPM). The particle force balance between inertia and forces acting on the particle is solved from the equation (ANSYS Inc., 2017a)

$$\frac{d\vec{u}_p}{dt} = F_D\left(\vec{u} - \vec{u}_p\right) + \frac{\vec{g}(\rho_p - \rho)}{\rho_p} + \vec{F} \quad (60)$$

where $\vec{v}_p$ is the particle velocity (m/s), $\vec{v}$ is the continuous phase velocity (m/s), $\rho_p$ is the particle density (kg/m$^3$), $\vec{F}$ is an additional acceleration (m/s$^2$) and the drag force ($F_D$) is calculated from the equation:

$$F_D = \frac{3\mu C_D Re_d}{4\rho_p d_p^2} \tag{61}$$

where $C_D$ is the drag coefficient

$$C_D = \begin{cases} 0.424, Re > 1000 \\ \frac{24}{Re}\left(1 + \frac{1}{6}Re^{\frac{2}{3}}\right), Re \leq 1000 \end{cases} \tag{62}$$

and $Re_d$ is the droplets' relative Reynolds number

$$Re_d \equiv \frac{\rho d_p |\vec{u}_p - \vec{u}|}{\mu} \tag{63}$$

### *Discrete random walk*

A popular method to model the turbulence effect on particle trajectory is the Discrete Random Walk (DRW) model. This method applies a stochastic method to determine the instantaneous gas velocity. When the trajectory for the droplet or particle is calculated, instantaneous fluid velocity $u = \overline{u} + u'$ is used to predict turbulent dispersion, where $\overline{u}$ is the mean fluid phase velocity and u' is the velocity fluctuation. To model the particle dispersion, integral time scale (T) is used. It describes the time that a particle spends in turbulent motion along the particle path (ds) (ANSYS Inc., 2017a)

$$T = \int_0^\infty \frac{u_p'(t) u_p'(t-\tau)}{\overline{u_p'^2}} ds \tag{64}$$

Larger values of T indicate a more turbulent flow. In addition, this model requires the Lagrangian integral time scale

$$\tau_L = \frac{C_L \kappa}{\varepsilon} \tag{65}$$

in which κ and ε are solved from turbulence models and $C_L$ is 0.15 in the κ-ε-model. This represents the life time of small eddies in the range of a turbulent microscale. The characteristic life time $\tau_e$ for turbulent eddies is calculated either from equation

$$\tau_e = 2\tau_L \tag{66}$$

or by the stochastic approach

$$\tau_e = \tau_L \log(r) \tag{67}$$

with the random number $0 \leq r \leq 1$. The second time scale is the particle eddy crossing time

$$\tau_{cross} = -\tau_p \ln\left[1 - \left(\frac{L_e}{\tau_{p|\vec{v}-\vec{v}_p|}}\right)\right] \quad (68)$$

where $L_e$ is the turbulent eddy length scale

$$L_e = \sqrt{c_\mu}\frac{\kappa^{3/2}}{\varepsilon} \quad (69)$$

### *Droplet atomization*

The secondary atomization is an important multiphase phenomenon in combustion applications. Atomization of the liquid fuel into a large number of small droplets increases its surface area and leads to higher heat and mass transfer between dispersed and continuous phases. Droplet atomization occurs when aerodynamic forces are greater than the forces that are resisting the deformation and fragmentation. Surface tension forces try to restore a droplet's spherical shape, and viscosity slows down the deformation and dissipates energy from aerodynamic forces. Dimensionless numbers are used to evaluate the secondary atomization of the droplet. The most important dimensionless numbers are listed in Table 8. (Guildenbecher, López-Rivera, & Sojka, 2009; Reitz, 1987)

**Table 8. Dimensionless numbers in droplet atomization.**

| Dimensionless number | Equation |
|---|---|
| Weber number (We) | $\frac{\rho_g * u_g^2 * d_l}{\mu_g}$ |
| Ohnesorge number (Oh) | $\frac{\mu_l}{\sqrt{d_l * \rho_l \sigma_l}}$ |
| Reynolds number (Re) | $\frac{\rho_g * u_g * l}{\mu_g}$ |
| Mach number (Ma) | $\frac{u_g}{c}$ |
| Density ratio ($\rho^*$) | $\frac{\rho_l}{\rho_g}$ |
| Viscosity ratio ($\mu^*$) | $\frac{\mu_l}{\mu_g}$ |

The Weber number (We) is typically used to evaluate the type of atomization. Droplet atomization is divided into five types: vibrational breakup, bag breakup, multimode breakup, sheet thinning breakup, and catastrophic breakup. These atomization types are presented in Fig. 8. In BF conditions, the initial breakup type is catastrophic breakup (We > 350) because the We number can be up to 10,000.

Other types of breakups can occur when the slip velocity becomes lower as the droplets accelerate or break up into smaller fragments. (Guildenbecher *et al*., 2009)

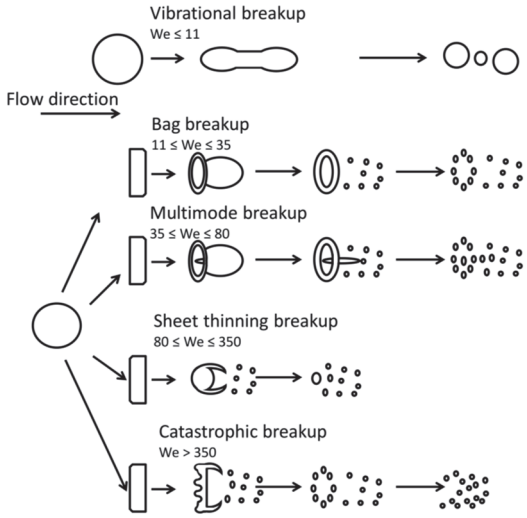


**Fig. 8. Droplet atomization (modified from Guildenbecher *et al*., 2009).**

Catastrophic breakup occurs, when waves start to form on the droplet surface. These large amplitude and long wavelength waves penetrate the droplet and create a small number of large fragments, which in turn breaks up into a large number of small fragments. Wave growth in the catastrophic breakup can be described with the Rayleigh-Taylor (R-T) or the Kelvin-Helmholz (K-H) instabilities. Other droplet atomization types are not discussed in detail, because the breakup model is used. If the liquid phase was modeled with the Eulerian method, then the breakup types could be seen with an extremely fine mesh. (Guildenbecher *et al*., 2009; Reitz, 1987, Reitz & Beale, 1999)

The droplet atomization is modeled with the Wave breakup model (Reitz, 1987). In high Weber number atomization (We > 100), the Kelvin-Helmholz instabilities are considered to dominate the droplet breakup (ANSYS Inc., 2017a). In the Wave Breakup Model, the maximum growth rate, Ω, and its corresponding wavelength, Λ, are calculated from (Reitz, 1987)

$$\Omega\left(\frac{\rho_1 r_d^3}{\sigma}\right) = \frac{(0.34+0.38We^{1.8})}{(1+Oh)(1+1.4Ta^{0.6})} \tag{70}$$

and

$$\frac{\Lambda}{r_d} = 9.02 \frac{(1+0.45Oh^{0.5})(1+0.4Ta^{0.7})}{(1+0.87We^{1.67})^{0.6}} \quad (71)$$

where Ta is the Taylor number $Ta = Oh\sqrt{We}$. New droplets of diameter $d_{st}$ are formed

$$d_{st} = 2B_0\Lambda \quad (72)$$

where $B_0$ is the droplet size constant, which is set to the value of 0.54 (default in Fluent is 0.61). The rate of change in droplet diameter for the parent droplet is calculated as follows

$$\frac{dd}{dt} = -\frac{(d-d_{st})}{\tau}, d_{st} \leq d \quad (73)$$

where the breakup time, τ, is calculated from the equation

$$\tau = \frac{3.726B_1 r_0}{\Lambda\Omega} \quad (74)$$

where $B_1$ is the breakup time constant, which is set to 1 (varies between 1 and 60). Droplet diameters are presented as Volume Median Diameter (VMD), which can be solved from the equation

$$\int_{D_{min}}^{D_{V,0.5}} V(D)dD = 0.5 \quad (75)$$

Droplet diameters smaller than VMD represent 50 % of the total volume of the liquid phase.

### *Droplet vaporization*

Liquid fuels vaporize to a gas phase when they are heated up and their temperature increases above the vaporization temperature $T_p > T_{vap}$. Below that temperature, the droplets are only heated up without any mass transfer to the bulk phase. It is also applicable to the PC drying. Vaporization is slow in the beginning of heating; but when the particle reaches its boiling point, gas bubbles start to form inside the droplet leading to vigorous vaporization. The phase change requires lots of energy, and the vaporization process is typically considered to be limited by heat transfer in turbulent spray combustion. (Bartok & Sarofim, 1991)

The droplet vaporization is modeled with a convection and diffusion controlled model, which is meant for high Re flows when convection is important. PC drying is also modeled with the same model. (Sazhin, 2006)

$$\frac{dm_p}{dt} = k_c A_p \rho_\infty \ln(1 + B_m) \quad (76)$$

where $m_p$ is the droplet mass (kg), $k_c$ is the mass transfer coefficient (m/s), $A_p$ is the droplet surface area ($m^2$), $\rho_\infty$ is the density of bulk gas ($kg/m^3$), and $B_m$ is the Spalding mass number:

$$B_m = \frac{Y_{i,s} - Y_{i,\infty}}{1 - Y_{i,s}} \tag{77}$$

where $Y_{i,s}$ is the vapor mass fraction at the surface and $Y_{i,\infty}$ is the vapor mass fraction in the bulk gas.

When the temperature reaches the boiling point of the droplet the vaporization equation changes to

$$\frac{d(d_p)}{dt} = \frac{2}{\rho_p h_{fg}} \left[ \frac{2k_\infty \left[1 + 0.23\sqrt{Re_d}\right]}{d_p} \left(T_\infty - T_p\right) + \varepsilon_p \sigma \left(\theta_R^4 - T_p^4\right) \right] \tag{78}$$

Droplet or PC temperature is calculated as a heat balance that relates the sensible heat change in the droplet to the convective and latent heat transfer between the droplet and the continuous phase

$$m_p c_p \frac{dT_p}{dt} = hA_p \left(T_\infty - T_p\right) - \frac{dm_p}{dt} h_{fg} + A_p \varepsilon_p \sigma \left(\theta_R^4 - T_p^4\right) \tag{79}$$

$C_p$ is the droplet heat capacity (J/(kg·K)), $T_p$ is the droplet temperature (K), $T_\infty$ is the temperature of the continuous phase (K), $h_{fg}$ is the latent heat of vaporization (J/kg), $\varepsilon_p$ is the particle emissivity and the convective heat transfer coefficient h is calculated from

$$\frac{h d_p}{k_\infty} = \frac{\ln(1 + B_T)}{B_T} \left(2 + 0.6 Re_d^{0.5} Pr^{1/3}\right) \tag{80}$$

where $d_p$ is the particle diameter (m), $k_\infty$ is the thermal conductivity of the continuous phase (W/(m·K)), $Re_d$ is the droplet Reynolds number, and Pr is the Prandtl number of the continuous phase ($c_p \mu / k_\infty$) and $B_T = B_m$. (ANSYS Inc., 2017a; Sazhin, 2006)

### *Pulverized coal devolatilization*

Volatile matter is released from the coal particle when it is heated. The weight loss during devolatilization depends on the volatile matter content in the fuel. In a complete devolatilization, a coal particle leaves solid residue called char, which contains mostly carbon and ash-forming elements. This residual particle is often larger than the original coal particle because of the swelling caused by escaping gases. (Bartok & Sarofim, 1991)

The model for devolatilization is based on two competing reactions (Kobayashi *et al*., 1977), where reaction rate constants are defined for low and high temperature reactions. The devolatilization reactions consume coal and produces char and volatiles. The model parameters are taken from the article by Du & Chen (2006). The experimental data had a good fit to the model with these parameters. Devolatilizing species are calculated from the coal proximate and ultimate analysis (Table 2). To simplify the reaction model, sulfur and nitrogen are not taken into consideration in the calculations, whereas they are modified to be presented as $C_xH_yO_z$. Low temperature devolatilization is represented as

$$Coal \overset{R_1}{\rightarrow} Char\ (1-\alpha_1) + Volatile\alpha_1 \tag{81}$$

where $\alpha_1$ is the volatile yield. High temperature devolatilization is calculated similarly, but $\alpha_2$ is 1.5*$\alpha_1$ (Ubhayakar *et al*., 1977)

$$Coal \overset{R_2}{\rightarrow} Char(1-\alpha_2) + Volatile\alpha_2 \tag{82}$$

The overall devolatilization rate is determined by

$$\frac{dm_v}{dt} = \left(m_{p,0} - m_a\right)(\alpha_1 R_1 + \alpha_2 R_2)\exp(-\int_0^t (R_1 + R_2)dt) \tag{83}$$

The reaction rates ($R_1$ and $R_2$) for the devolatilization are calculated from the Arrhenius equation, where $A_1$, $E_1$, $A_2$ and $E_2$ are $3.7 \cdot 10^5$, $7.4 \cdot 10^7$ J/kmol, $1.46 \cdot 10^{13}$, and $2.51 \cdot 10^8$ J/kmol, respectively. (Du & Chen, 2006; Ubhayakar *et al*., 1977)

### 4.3 Gas phase combustion and gasification

In the blast furnace raceway, the maximum temperatures are around 2800 K, and the equivalence ratios are from 0.5 to 0.8, which means that gasification reactions are important and reactions occur through radical reactions (Ishii, 2000; Peters, 2000). In modeling, the gasification and radical reactions finite rate combustion model is needed and the Eddy Dissipation Concept (EDC) is chosen (Magnussen, 1981). The volatile combustion model is based on GRI-MECH 1.2, which contains 22 species and 104 reactions (Frenklach *et al*., 1995; Frenklach *et al*., 2016). The CHEMKIN-CFD solver is used to calculate the chemical reactions.

In EDC, it is assumed that most of the reactions take place in the smallest scales of the turbulence, which are called the fine structures. These fine structures are treated as well-stirred reactors. In EDC, each computational cell is treated as a constant pressure reactor, with initial conditions taken as the current species and

temperature. The equation for the length fraction of the fine structures is (Magnussen, 1981)

$$\xi^* = C_\xi \left(\frac{\nu\varepsilon}{\kappa^2}\right)^{1/4} \tag{84}$$

where * indicates the fine structure quantities, $C_\xi$ is the volume fraction constant (2.1377), and ν is the kinematic viscosity ($m^2/s$). Reactions occur in the fine structures over a time scale

$$\tau^* = C_\tau \left(\frac{\nu}{\varepsilon}\right)^{1/2} \tag{85}$$

where $C_\tau$ is the time scale constant (0.4082). The source term in the conservation equation (equation 42) for chemical species i is modeled as

$$R_i = \frac{\rho(\xi^*)^2}{\tau^*[1-(\xi^*)^3]}(Y_i^* - Y_i) \tag{86}$$

where $Y_i^*$ is the fine structure species mass fraction after reacting over time $\tau^*$.

Heavy oil combustion requires vaporizing species and to adjust the correct ratio (H/C = 1.49) between carbon and hydrogen, $C_{37}H_{55}$ was added to the reactions to represent heavy oil volatiles. The volatiles' cracking method into smaller components is presented as

$$C_{37}H_{55} \rightarrow 18.5C_2H_2 + 9H_2, \Delta H° = 5217\ J/kmol \tag{87}$$

The activation energy ($E_a$) for cracking is $2.027 \cdot 10^8$ J/kmol and the pre-exponential factor A = $2.119 \cdot 10^{11}$, which are taken from the ANSYS Fluent coal calculator kinetics for two-step coal combustion. Volatile cracking is expected to be similar to that of coal.

Similarly, devolatilizing species were added for the PC types A, B and C (Table 2). The volatile species are $C_{21}H_{91}O_5$, $C_{14}H_{39}O_4$, and $C_{29}H_{82}O_9$, respectively. The volatiles' cracking method into smaller components is presented in equation

$$C_xH_yO_z \rightarrow \frac{x-z}{2}C_2H_4 + \frac{y-2(x-z)}{2}H_2 + zCO \tag{88}$$

Reaction for the Coal A volatile cracking is

$$C_{21}H_{91}O_5 \rightarrow 8C_2H_4 + 29.5H_2 + 5CO, \Delta H° = 6255\ J/kmol \tag{89}$$

Reaction for the Coal B volatile cracking is

$$C_{14}H_{39}O_4 \rightarrow 5C_2H_4 + 9.5H_2 + 4CO, \Delta H° = 4341\ J/kmol \tag{90}$$

Reaction for the Coal C volatile cracking is

$$C_{29}H_{82}O_9 \rightarrow 10C_2H_4 + 21H_2 + 9CO, \Delta H° = 8523\, J/kmol \quad (91)$$

The Arrhenius parameters for the cracking are as follows: A is $2.119 \cdot 10^{11}$ and $E_a$ is $2.027 \cdot 10^8$ J/kmol, which are taken from the Fluent coal calculator kinetics for two-step coal combustion. (ANSYS Inc., 2017a)

The temperature from the probability density function (PDF) combustion model is compared with the EDC combustion model to assess its behavior (Paper II). The chemical equilibrium combustion model assumes that the chemistry is fast enough to reach chemical equilibrium, and combustion is considered to depend only on the mixing rate. The instantaneous averaged thermochemical state of the fluid depends on the local mixture fraction. PDF models give a very general description of turbulent reacting flows, which makes them applicable to premixed, non-premixed, and partially premixed combustion. The used model contains 22 species. (ANSYS Inc., 2017a; Peters, 2000)

The probability density function p(f), can be used to solve temporal fluctuations of f in the turbulent flow. In adiabatic systems, the mass fractions of the density-weighted mean species and the temperature for a single mixture fraction system (heavy oil) can be solved as

$$\overline{\emptyset}_i = \int_0^1 p(f)\emptyset_i(f)df \quad (92)$$

The mean time-averaged fluid density $\bar{\rho}$ can be solved from

$$\frac{1}{\bar{\rho}} = \int_0^1 \frac{p(f)}{\rho(f)}df \quad (93)$$

where ρ(f) is solved from the ideal gas law equation using the instantaneous density and species mass fractions. In the single mixture fraction cases, the shape of the assumed PDF is described using the β-function

$$p(f) = \frac{f^{\alpha-1}(1-f)^{\beta-1}}{\int f^{\alpha-1}(1-f)^{\beta-1}df} \quad (94)$$

where

$$\alpha = \bar{f}\left[\frac{\bar{f}(1-\bar{f})}{\overline{f'^2}} - 1\right] \quad (95)$$

and

$$\beta = (1-\bar{f})\left[\frac{\bar{f}(1-\bar{f})}{\overline{f'^2}} - 1\right] \quad (96)$$

The PDF shape is a function of the mean mixture fraction $\bar{f}$ and the mixture fraction variance $\overline{f'^2}$. The density-averaged transport equation for the mixture fraction is

$$\frac{\partial}{\partial t}\left(\rho\bar{f}\right) + \nabla\cdot\left(\rho\vec{v}\bar{f}\right) = \nabla\cdot\left[\left(\frac{\mathrm{k}}{C_p} + \frac{\mu_t}{Pr}\right)\nabla\bar{f}\right] + S_m \quad (97)$$

where k is the laminar conductivity of the mixture, $C_p$ is the mixture specific heat, and $S_m$ is the source term from the dispersed phase. The droplet vaporization is added as a source term to the mixture fraction transport equation, and in the areas with a high vaporization rate the mixture fraction variance is increased. The density-averaged conservation equation for the mixture fraction variance can be solved from

$$\frac{\partial}{\partial t}\left(\rho\overline{f'^2}.\right) + \nabla\cdot\left(\rho\vec{v}\overline{f'^2}.\right) = \nabla\cdot\left[\left(\frac{\mathrm{k}}{C_p} + \frac{\mu_t}{Pr}\right)\nabla\overline{f'^2}\right] + C_g\mu_t\cdot\left(\nabla\bar{f}\right)^2 - \frac{C_d\rho\varepsilon}{k}\overline{f'^2} \quad (98)$$

where the default values for constants Pr, $C_g$, and $C_d$ are 0.85, 2.86, and 2.0, respectively. (Versteeg & Malalasekera, 2007)

### 4.4 Solid phase combustion and gasification

Char oxidation is a very significant part of the coal reaction process. When considering coal combustion, it is the most time-consuming part. It is known that the low-rank coal chars are more reactive than the high-rank coal chars and thus a single model cannot explain all of the coal types accurately (Bartok & Sarofim, 1991). However, in this model, the approximation is based on the data collected from coals similar to the experimental coal in Guo *et al*. (2005). Char reactions occur between solid carbon and gas phase species. In this case, the species are $O_2$, $CO_2$, and $H_2O$. During combustion, the particle diameter remains constant, but density lowers when the combustion degree progresses.

The exothermic partial oxidation of char with $O_2$ is presented in equation (99). Gasification equations (100) and (101) are endothermic and therefore require heat, and they occur more easily when the temperature increases.

$$2C + O_2 \xrightarrow{k_3} 2CO \quad (99)$$

$$C + CO_2 \xrightarrow{k_4} 2CO \quad (100)$$

$$C + H_2O \xrightarrow{k_5} CO + H_2 \quad (101)$$

The Arrhenius parameters $A_3$, $E_3$, $A_4$, $E_4$, $A_5$, and $E_5$ for equations 10–12 are 2.013, $7.9818\cdot10^7$ J/kmol, 3.1, $1.31\cdot10^8$ J/kmol, 1.33, and $1.15\cdot10^8$ J/kmol, respectively. (Bartok & Sarofim, 1991)

Coke reactions take place in the porous coke bed where coke reacts with $O_2$, $CO_2$ and $H_2O$. The reaction rate for coke with each species is calculated with the

Field model (Field *et al*., 1967), which utilizes both diffusion and the chemical reaction rate for the overall reaction rate. The model is described in equations (17)-(19). $A_c$ for $O_2$ is $3.2 \cdot 10^6$ kg/($m^2$·s) and $T_c$ for $O_2$ is 10855 K. $A_c$ and $T_c$ for $CO_2$ and $H_2O$ are expected to be equal. The value for $A_c$ is $4.71 \cdot 10^9$ kg/($m^2$·s), and the value for $T_c$ is 29018 K. Other coke bed reactions are modeled as a heat sink in the same way as in equation (20), and the same values are used as Y.S Shen, Guo, Yu, Austin & Zulli (2011). The value of $h_g$ is 128.2 W/($m^2$·K) and $A_{coke}$ is 153 $m^2$ below the raceway and 141 $m^2$ in the rest part of the coke bed. (Y. S. Shen, Guo, Yu, Austin, & Zulli, 2011)

# 5 Materials and methods

## 5.1 Extra heavy oil atomization and mixing

### *5.1.1 Experimental setup*

CFD model geometry for the extra heavy oil atomization is based on the experimental setup of Hakala & Paloposki (1996). The experimental setup is a small-scale physical model of the blowpipe-tuyere-raceway region of the blast furnace at the SSAB Raahe steel mill. The size of the experimental setup is approximately 2/3 of the actual blast furnace. Air is at atmospheric pressure and temperature is the ambient temperature. Extra heavy oil is substituted with mixtures of water, glycerol, and ethanol. Experimental studies of droplet atomization were done at Helsinki University of Technology during the years 1994-1996 (Hakala & Paloposki, 1996). A Malvern Particle Sizer was used to measure the droplet size distributions of the spray. Droplet sizes are given as Volume Median Diameter (VMD). Fig. 9 describes the experimental setup with instrumentation of the droplet atomization study.

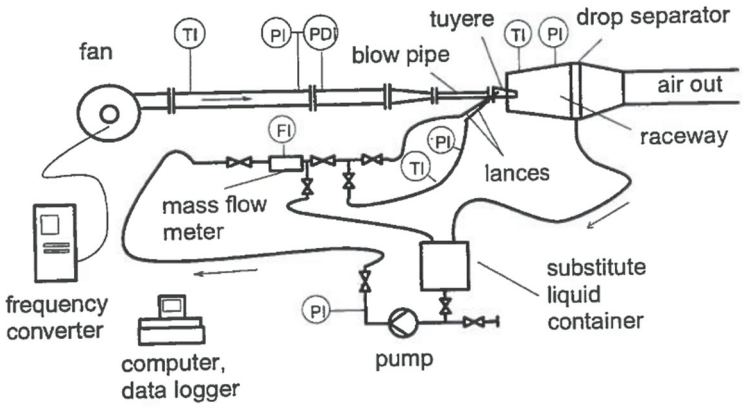


**Fig. 9. Experimental setup. (Hakala & Paloposki, 1996)**

The experimental setup was designed based on the dynamic similarity between the experimental setup and the actual blast furnace. Dimensionless variables have good agreement between the experimental setup and the blast furnace (Table 9). All of these dimensionless variables are important and generally used in the droplet

atomization studies. The only compromise was done with surface tension. It should have been 4.6 $mN \cdot m^{-1}$ for the Ohnesorge number to match the BF value. Using mixtures of water, ethanol and glycerol instead of heavy oil was a reasonable choice for Hakala and Paloposki (1996) for laboratory experiments at room temperature.

The initial droplet velocity is only 8 m/s, which means that the oil flows as a single stream from the lance and atomization starts in the air blast. Therefore, the initial droplet size is the diameter of the lance tip.

**Table 9. Dimensionless variables in the experimental model and the blast furnace.**

| Dimensionless variable | Experimental model | Blast furnace |
|---|---|---|
| Air flow | | |
| Reynolds number (Re) | 509000 | 430000 |
| Mach number (Ma) | 0.291 | 0.291 |
| Oil flow | | |
| Reynolds number (Re) | 634 | 643 |
| Ohnesorge number (Oh) | 0.0264 | 0.102 |
| Air and oil flow | | |
| Density ratio ($\rho^*$) | 987 | 1009 |
| Viscosity ratio ($\mu^*$) | 889 | 774 |

Operating conditions of the experiments and the actual blast furnace are presented in Table 10. These operating conditions are also used as the boundary conditions for the CFD modeling.

**Table 10. Operation conditions in the experimental model and the blast furnace.**

| Variable | Experimental model | Blast furnace |
|---|---|---|
| Air flow | | |
| Diameter for tuyere tip (mm) | 77 | 115 |
| Air flow rate (kg/s) | 0.55 | 2.1 |
| Air temperature (K) | 293 | 1363 |
| Air pressure (kPa) | 101.3 | 360 |
| Air Velocity (m/s) | 100 | 215 |
| Oil flow | | |
| Diameter of lance tip (mm) | 4.6 | 7 |
| Oil flow rate (kg/s) | 0.0367 | 0.145 |
| Oil temperature (K) | 293 | 483 |
| Oil viscosity (mPas) | 16 | 41 |
| Oil density (kg/m3) | 1175 | 1000 |
| Oil surface tension (mN/m) | 55 | 25 |

### *5.1.2 Model geometry*

Geometry for the CFD modeling consists of a blast pipe, a tuyere, an oil lance and a space roughly describing the raceway volume. The inlet boundary for the air blast is marked in Fig. 10 as the inlet, which is set in the beginning of the blast pipe. The inlet for oil injection is set in the end of the oil lance. The outlet is in the end of the box, which illustrates the raceway. Similar geometry (but with different dimensions) was used for the experimental setup and full-scale modeling.

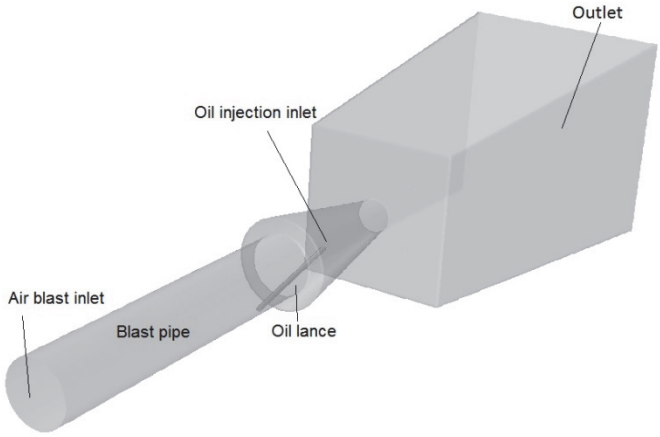


**Fig. 10. Geometry of the CFD model (modified from Paper I, published with permission of Steel Research International).**

For the CFD model, the geometry and meshing (Fig. 11) were done with Gambit 2.4.6. The mesh consists of 521,000 hexahedral and tetrahedral computational cells. The mesh is denser in the tuyere area and is designed to keep wall $y^+$ values under 300 so that the wall functions behave properly.

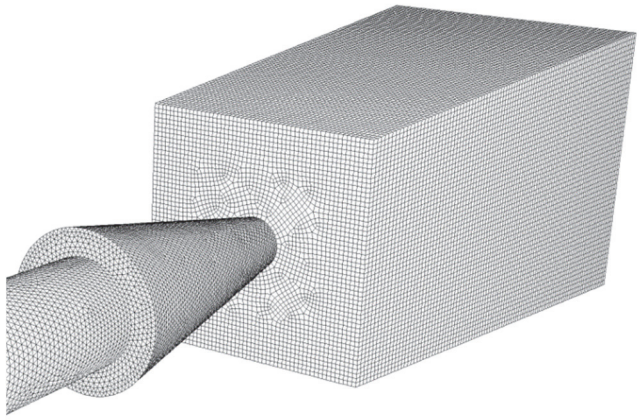

**Fig. 11. Mesh of the CFD model (Paper I, published with permission of Steel Research International).**

## 5.2 Heavy oil combustion in the tuyere-raceway area

Lance position is an important variable in auxiliary fuel combustion. Its position affects the residence time, vaporization, mixing and ignition, which influences the overall combustion in the tuyere-raceway area. The geometry for the lance position study with the CFD model consists of a tuyere, a raceway, and part of the coke bed (Fig. 12a). In the heavy oil combustion, lance positions (Fig. 12b) in different cases are $y_{tuy}$=0 cm (Case 1), $y_{tuy}$=10 cm (Case 2), and $y_{tuy}$=20 cm (Case 3) from the tuyere-raceway intersection towards the beginning of the tuyere.

The inlet boundary for the air blast is set at the inlet of the tuyere and the outlet is in the upper part of the coke bed (Fig. 12a). Oil injection is set as injection points in the front of the oil lance, which represents holes in the nozzle. The geometry is presented in Fig. 12c; it is based on the results in Paper I. Other boundaries are considered as adiabatic no-slip walls. The porosities in the deadman and the rest of the coke bed are based on the core-drill measurements in the Raahe blast furnace. The porosity in the deadman is $\varepsilon_1$=0.35, and in the rest of the coke bed it is $\varepsilon_2$=0.4. In Fig. 12a, a plane illustrates the boundary between the deadman and the rest of the coke bed. To simplify the model, porosity in the raceway area is set to $\varepsilon_3$=1, which is also the porosity in the tuyere area.

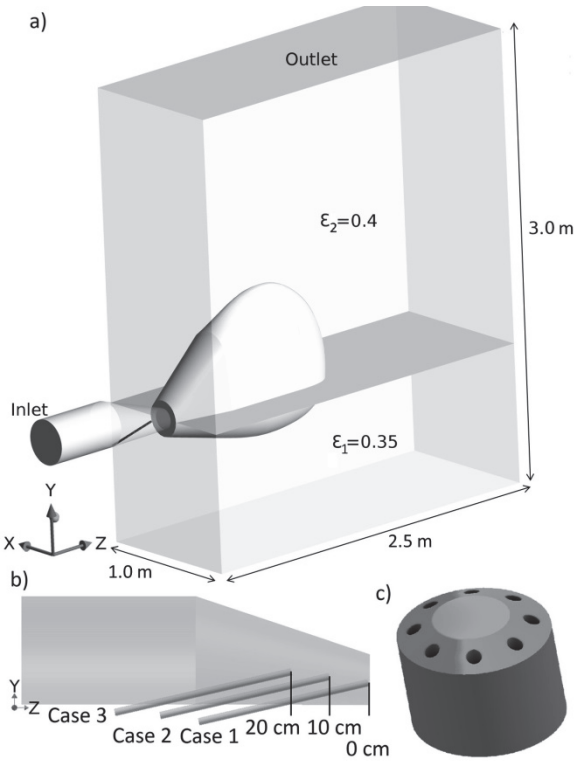


**Fig. 12. Conceptual drawing of the computational geometry and the coke bed porosities (a), lance positions in tuyere in different cases (b), and nozzle geometry (c) (Paper II, published with permission of ISIJ International).**

There are several different methods for calculating the raceway dimensions, but according to Liaos's (1998) licentitate thesis, Nomura's (1986) correlation creates similar dimensions to Raahe's blast furnace. Based on the discussions with SSAB Europe Oy, the estimated depth of the raceway is $d_R$=1.5 m. The estimated depth is used to calculate the other dimensions of the raceway; therefore equation (102) is not needed and other dimensions can be calculated easily when the tuyere diameter is known. In Nomura's correlation, the raceway size and form are calculated with the following equations:

$$\frac{d_R}{d_T} = 0.315 \left[ \rho_{g0} \left( \frac{V_g}{A_T} \right)^2 \left( \frac{p_A}{p_g} \right) \left( \frac{T_g}{298} \right) \left( \frac{1}{g d_{coke} \rho_{coke}} \right) \right]^{0.567} \quad (102)$$

where $d_R$ is the raceway depth (m), $d_T$ is the tuyere diameter (m), $\rho_{g0}$ is the gas density under standard conditions (kg/m$^3$), $V_g$ is the volume flow of the air blast

($m^3/s$), $A_T$ is the area of the tuyere nose ($m^2$), $p_A$ is the atmospheric pressure (Pa), $p_g$ is the air blast pressure (Pa), $T_g$ is the air blast temperature (K), g is the gravity constant, $d_{coke}$ is the coke particle diameter (m), and $\rho_{coke}$ is the coke particle density ($kg/m^3$). (Liao, 1998; Nomura, 1986)

The raceway width ($w_R$) is calculated by

$$\frac{w_R}{d_T} = 2.631 \left(\frac{d_R}{d_T}\right)^{0.331} \tag{103}$$

The raceway height ($h_R$) is calculated from

$$\frac{(4h_R^2+d_R^2)w_R}{(h_R d_T^2)} = 23.1 \left(\frac{d_R}{d_T}\right)^{1.052} \tag{104}$$

When the tuyere diameter ($d_T$) is 0.14 m, the calculated raceway dimensions are: depth ($d_{R)}$ = 1.5 m, width ($w_{R)}$ = 0.44 m and height ($h_{R)}$ = 0.85 m.

The boundary conditions and oil parameters, including the ultimate analysis for the simulations are presented in Table 11. The values are based on the blast furnace in Raahe. The oil injection level of 0.344 kg/s is equivalent to 100 kg/thm. The heavy oil is simplified to contain only carbon and hydrogen because other elements are present in small quantities and are not in the scope of the study.

**Table 11. Boundary conditions and oil parameters.**

| Variable | Quantity | Element | Extra heavy oil [wt-%] |
|---|---|---|---|
| Air blast flow rate | 2.4 kg/s | C | 86.6 |
| Air blast $O_2$ | 28.0 vol-% | H | 10.8 |
| Air blast temperature | 1423 K | O | 0.7 |
| Outlet pressure | 342 kPa | N | 0.3 |
| Oil mass flow rate | 0.344 kg/s | S | 1.6 |
| Oil temperature | 473 K | | |
| Oil density | 1020 kg/m3 | | |
| Oil viscosity | 31.5 mPas | | |
| Oil surface tension | 25 mN/m | | |

## 5.3 Pulverized coal combustion in a BF test rig

The combustion model for the PC is made and validated in a geometry (Fig. 13) that is based on the BHP Billington-BlueScope Steel test rig (Mathieson *et al*., 2005). The model is created with the Ansys DesignModeler 16.0. It contains a blast pipe, a tuyere, a lance, and a cylinder that illustrates the raceway area. The inlet is placed in the beginning of the blast pipe, and the outlet is in the end of the raceway.

Inlets for the coal-nitrogen mixture (inner white circle) and cooling gas (outer white circle) are in the lance tip.

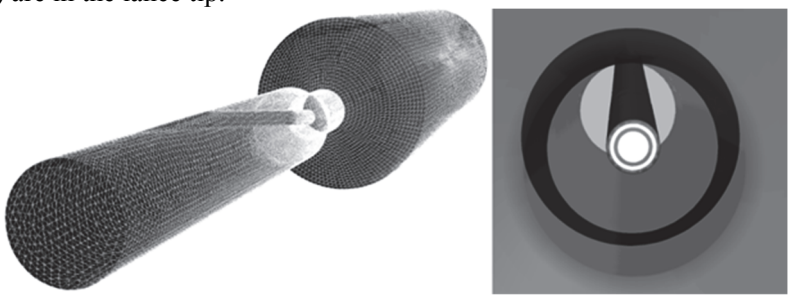

**Fig. 13. Geometry and the mesh of the CFD model (Paper III, published with permission of Industrial Combustion).**

The diameters of the parts, in the geometry, are as follows: the blast pipe is 110 mm long; the tuyere tip diameter is 70 mm; the lance diameter is 12.7 mm with the outer wall thickness of 1.6 mm; the cooling shroud diameter is 19.05 mm with the outer wall thickness of 1.6 mm; and the raceway diameter is 300 mm. The tuyere tip diameter is about 140 mm in the Raahe BF; therefore the difference from the real case is 50%. The lance is similar to the actual blast furnace.

Meshing for the CFD model has been done with ANSYS Meshing 16.0. The mesh consists of about 713,000 hexahedral and tetrahedral computational cells. The mesh is dense in the tuyere area, where small surfaces are used as inlets for the cooling gas and PC carrier gas, and the velocity of the air blast is highest. On the tuyere walls, the cell height is 1 mm to keep the $y^+$ values between 30 and 300.

Operating conditions from experimental studies for the simulation are presented in Table 12. These conditions are based on the study by Guo *et al*. (2005). Boundary conditions other than the type and amount of coal are kept the same in all of the simulations.

**Table 12. Boundary conditions and coal parameters. (B. Guo *et al.*, 2005)**

| Variable | Quantity |
|---|---|
| Air blast flow rate | 300 $Nm^3/h$ |
| Outlet pressure | 1 atm |
| Temperature | 1473 K |
| Coal temperature | 323 K |
| Air blast $O_2$ | 21 vol-% |
| Cooling gas flowrate | 3.2 $Nm^3/h$ |
| Conveying gas flowrate | 2.0 $Nm^3/h$ |
| Cooling gas temperature | 600 K |
| Conveying gas temperature | 323 K |

Proximate and ultimate analyses of the pulverized coals (coals A, B, and C) used in the simulation are given in Table 2. All of the coals are bituminous, but A is a medium volatile coal, and coals B and C are high volatile coals. (Carpenter & IEA Coal Research, 1988; B. Guo *et al.*, 2005)

The cumulative volume distribution of coal particles is presented in Fig. 14. The mean particle size in cases A, B, and C are 30 µm, 40 µm, and 40 µm, respectively. Particle sizes from 1 to 200 µm are used in the CFD model, and they are divided into 12 groups. These distributions are approximated from Fig. 1 from B. Guo *et al.*, (2005), using the Weibull cumulative distribution function. Shape and scale parameters for coals A, B, and C are 1, 43 µm, 1.1, 60 µm and 1.2, 56 µm, respectively. Injections are released from the coal lance surface at the same angle as the coal lance outlet is.

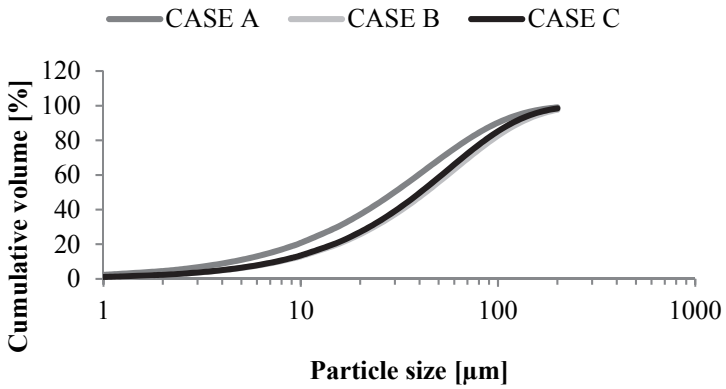


**Fig. 14. Cumulative volume distribution of coal particles (Paper III, published with permission of Industrial Combustion).**

## 5.4 Pulverized coal combustion in the BF tuyere-raceway area with the double lance injection system

The pulverized coal double lance position affects the combustion and flow-related phenomena in the tuyere-raceway area. It affects the PC ignition, temperatures, and pressure drop, as well as combustion efficiency. All of these are important factors in the blast furnace operation and have an effect on the lifetime of injection lances and tuyere walls. Furthermore, PC causes clogging inside the tuyere (Fig. 15), which creates uneven flow in the BF and increased pressure losses. CFD modeling is used to study the PC lance position's effect on these variables and to evaluate the PC combustion efficiency in different cases.

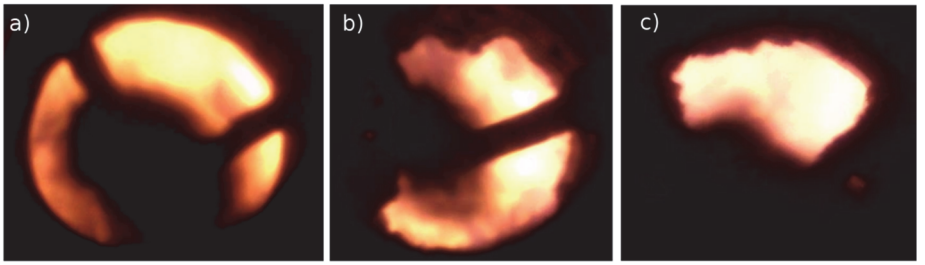


**Fig. 15. Fouling of tuyere walls during 1 month of injection, a) at the beginning of injection, b) after the first week, and c) after one month.**

The geometry used is otherwise the same in each case, but the lance position is varied. The geometry for case 4 CFD model is presented in Fig. 16a. Lance positions are varied in relation to the tuyere nose in different cases. In cases 1, 2, 3, and 4, the lance positions are 25, 30, 40, and 45 cm from the tuyere nose (Fig. 16b), respectively. It includes part of the blowpipe, tuyere, raceway and part of the coke bed. The dimensions for the tuyere and raceway are equal to the heavy oil study. The inlet is placed in the beginning of the blowpipe and the outlet is in the top part of the coke bed. The symmetry boundary condition is used on the sides of the coke bed.

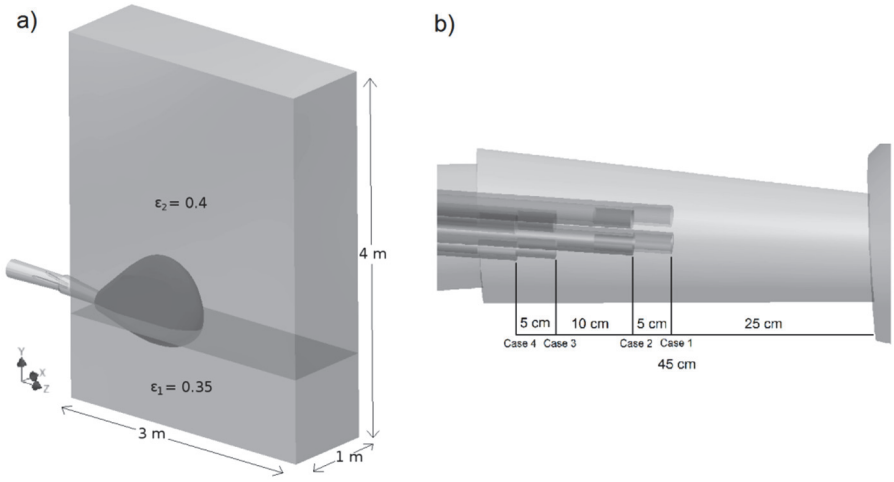


**Fig. 16. Geometry of the CFD model in case 4 (a) and lance positions in cases 1 to 4 (b).**

The mesh in all cases consists of about 1.4 million hexahedral and tetrahedral cells. The cell height on the tuyere walls is 0.8 mm to keep the $y^+$ values between 30 and 300. The mesh is densest in the tuyere area and in the beginning of the raceway area to capture the important phenomena.

The cumulative volume distribution of coal particles is presented in Fig. 17. Particle sizes from 1 to 200 μm are used in the CFD model, and they are divided into 12 groups. The distribution used in the CFD model is approximated with the measured data from SSAB Raahe, using the Weibull cumulative distribution function. The shape and scale parameters are 0.63 and 54 μm, respectively. Injections are released from the coal lances. The combustion model is the same as for Coal A in Paper III.

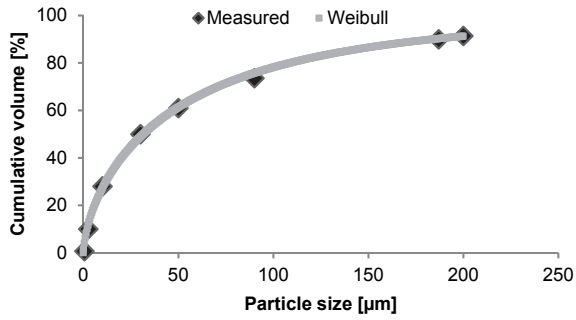


**Fig. 17. Cumulative volume distribution of coal particles.**

The boundary conditions for the simulations are presented in Table 13. Values are based on the blast furnace at SSAB Raahe. The PC injection level of 0.4 kg/s is equivalent to 160 kg/thm.

**Table 13. Boundary conditions for the PC injection CFD modeling.**

| Variable | Quantity |
|---|---|
| Air blast flow rate | 2.58 kg/s |
| Air blast $O_2$ | 28.0 vol-% |
| Air blast temperature | 1423 K |
| Outlet pressure | 340 kPa |
| PC mass flow rate | 0.4 kg/s |
| PC temperature | 348.15 K |
| Conveying gas flowrate | 0.052 kg/s |
| Conveying gas pressure | 400 kPa |
| Conveying gas temperature | 348.15 K |

# 6 Results and discussion

## 6.1 Atomization of extra heavy oil (Paper I)

Fig. 18 shows the comparison between the droplet size VMD in experiments by Hakala and Paloposki (1996) and CFD modeling as a function of velocity. The sampling plane is a cross section 350 mm downstream from the tip of the injection lance, where the atomization of the oil droplets has ended. The droplets' velocity does not increase after the first 300 mm, and after that the secondary atomization does not take place in the center of the flow. In the small-scale CFD model and the corresponding experimental setup the velocity of the air varies from 75 to 120 m/s. In all of these cases other variables are kept constant.

Trend lines between the experimental values and the small-scale CFD modeling results are consistent, and the Root Mean Square (RMS) between the experimental results and the small-scale CFD model is 1.45 μm. The CFD model gives 1 μm smaller VMD than the experimental results at the base level velocity (100 m/s). It can be seen that the droplet size VMD decreases quickly as the velocity of the air increases, but the effect gets weaker as the velocity increases.

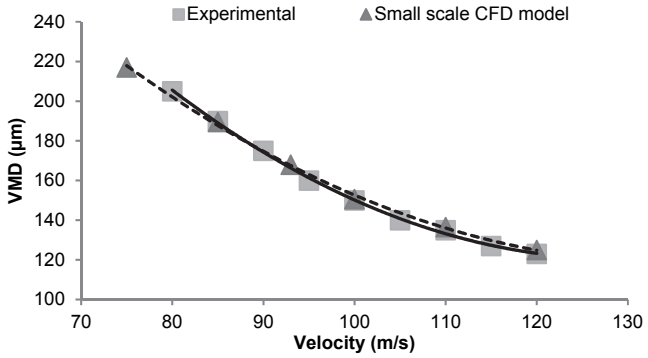


**Fig. 18. Droplet size VMD as a function of air velocity (modified from Paper I, published with permission of Steel Research International).**

The validated atomization model is applied to the actual blast furnace operating conditions to evaluate its suitability for the simulations. The dimensionless velocity is used to compare the droplet size results between the experimental rig, the small-scale CFD model, and the large-scale CFD model. The dimensionless velocity is set to be one in the base level of the blast furnace. The base level equals to 100 m/s in the experimental rig and 215 m/s in the actual blast furnace CFD model. The

results for the droplet size VMD as a function of dimensionless velocity are shown in Fig. 19. It can be seen that the wave breakup model behaves similarly in small-scale and large-scale models. Both CFD models produce droplets that are consistent with the experimental results in the given velocity range. And therefore, choices in dynamic similarity with the experimental setup describing the actual blast furnace conditions are reasonable. The RMS between the experimental values and the actual blast furnace CFD model is 3.47 μm. It seems that the deviation in the Ohnesorge number is not dominating compared to the Weber number and therefore not to the Taylor number.

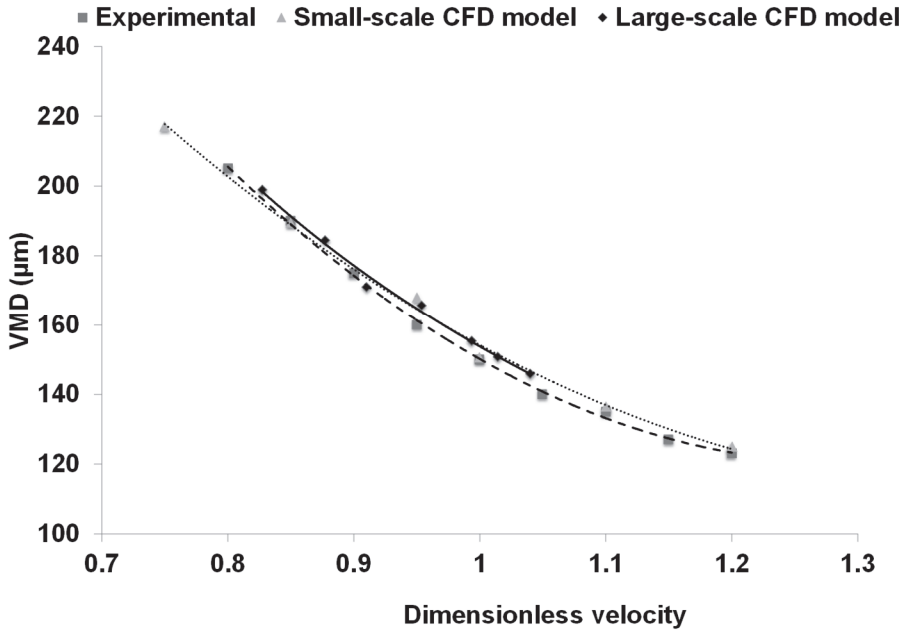


**Fig. 19. Droplet size VMD as a function of dimensionless velocity (modified from Paper I, published with permission of Steel Research International).**

### *6.1.1 Mixing between heavy oil and air blast (Paper I)*

Fluid mixing in the tuyere of the experimental setup (Hakala & Paloposki, 1996) and the CFD model are compared with an image from a video recording. The comparison is presented in Fig. 20. It is evident that most of the droplets are in a

small radial area of the air blast in both cases. Mixing is minimal, and there will not be enough oxygen inside the spray for efficient combustion. The air blast is very close to the plug flow, and therefore mixing has to be done with improved injection methods.

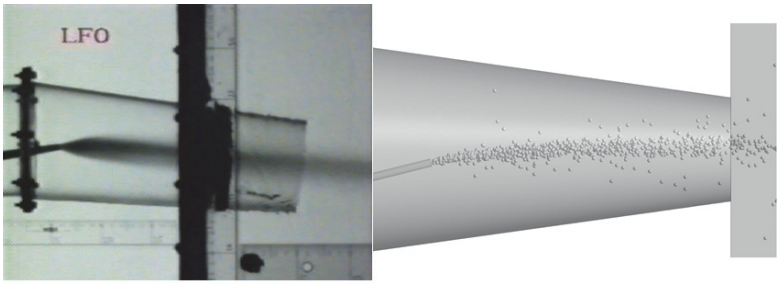


**Fig. 20. Droplet distribution in the tuyere-raceway area. Comparison between an image of a video recording and CFD (Paper I, published with permission of Steel Research International).**

The axial velocity of the air blast for small-scale and full-scale CFD models is presented in Figs. 21 and 22, respectively. According to Fig. 21 and Fig. 22, velocity decreases drastically in the center of the air blast, because most of the oil is concentrated in a narrow area of the flow field. In the small-scale CFD model, most of the oil is concentrated in the flow center, which diameter is 3 cm. In the actual blast furnace CFD model, the problem is even worse because the tuyere outlet is larger, but the area where oil is dispersed is about the same. Most of the oil is concentrated in the flow area, which has a diameter of only about 3 cm.

In the small-scale CFD model (Fig. 21), the maximum velocity in the air blast is from 75 to 118 m/s, but in the center it is from 60 to 88 m/s. The retarding effect on the air blast velocity caused by the injected oil is significant. With increasing air blast velocity, the retarding effect of the oil injection increases.

The retarding of the air blast velocity by the oil injection is also observed in the actual blast furnace CFD model (Fig. 22). With the average velocity of 230 m/s of the air blast, the minimum velocity in the middle is about 140 m/s and the maximum velocity at the edge 228 m/s. With the average air blast velocity of 170 m/s, the velocity in the middle is 107 m/s and at the edge it is 169 m/s. The amount of injected oil is 0.145 kg/s in all of the cases, but the air velocity varies in the tuyere nose between 170 and 230 m/s.

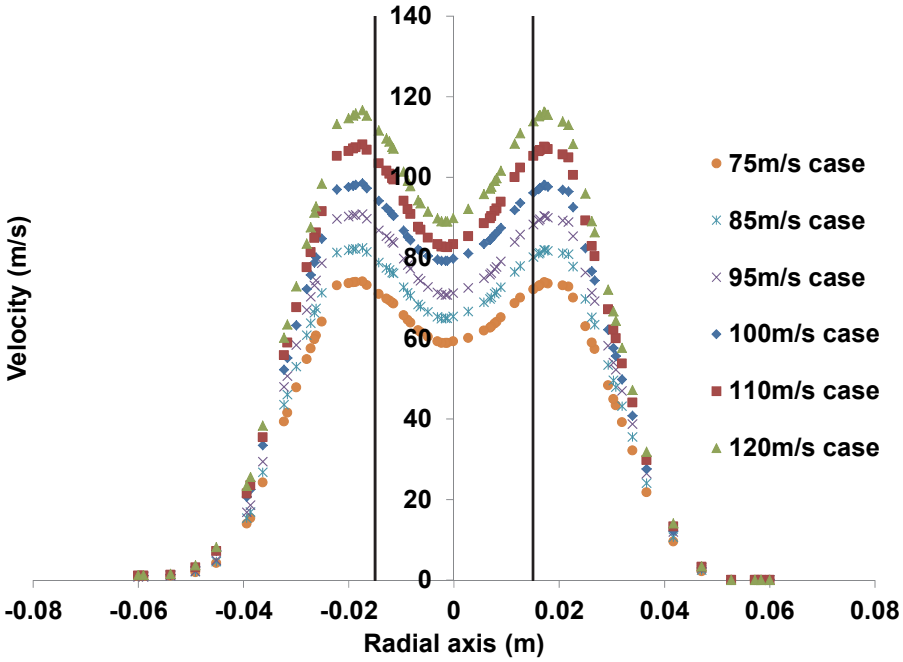


**Fig. 21. Axial velocity of the air flow on radial axis in the small-scale model (modified from Paper I, published with permission of Steel Research International).**

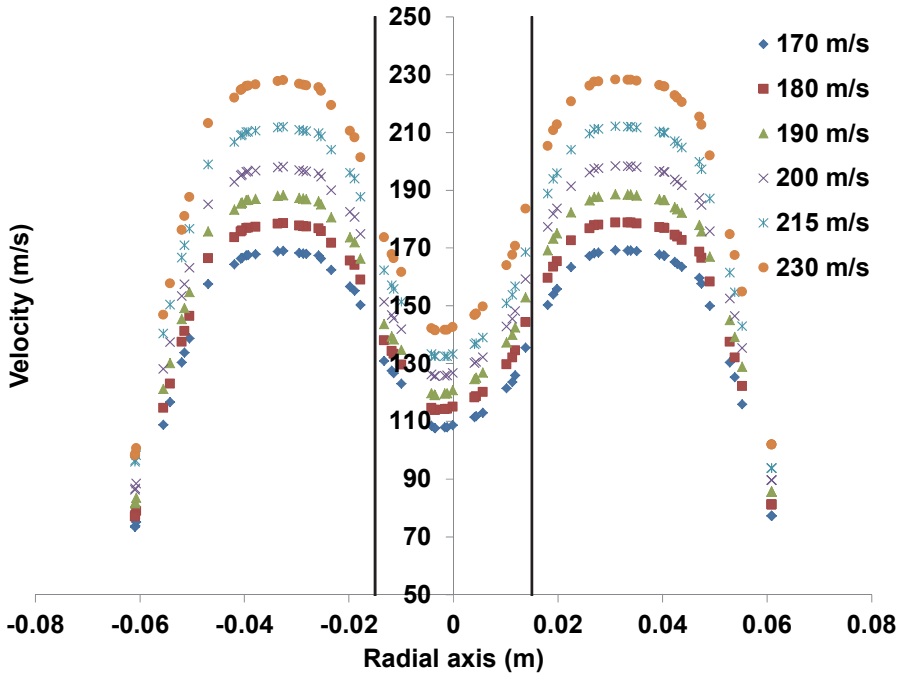


**Fig. 22. Axial velocity of the air flow on radial axis in the actual blast furnace CFD model (modified from Paper I, published with permission of Steel Research International).**

Good mixing is essential for efficient combustion. To enhance the mixing, different nozzle variations are modeled. The eight-holed nozzle (hole diameter 2 mm) with a 30° angle from the lance centerline was proven to be the best. It produced proper mixing, and oil did not hit the tuyere walls as it did with the 45 degree 8-holed nozzle. The 4- and 5- hole nozzles did not produce as good of a mixing as the 8-holed nozzle did, and the droplets also hit the tuyere walls. In the 5-hole nozzle, one of the holes was in the center of the nozzle. The stream originating from that center hole united with the stream above it. Fig. 23 shows the difference between velocities with the 8-hole 30° angle nozzle and the simple lance without any nozzle. The difference between mixing is clear in the velocity field of the air blast, where a simple lance results in a velocity drop in the middle of the flow, but the 8-hole nozzle results in only a slight drop of the velocity in the air blast edges. The nozzled flow also leads to about a 10% smaller final VMD.

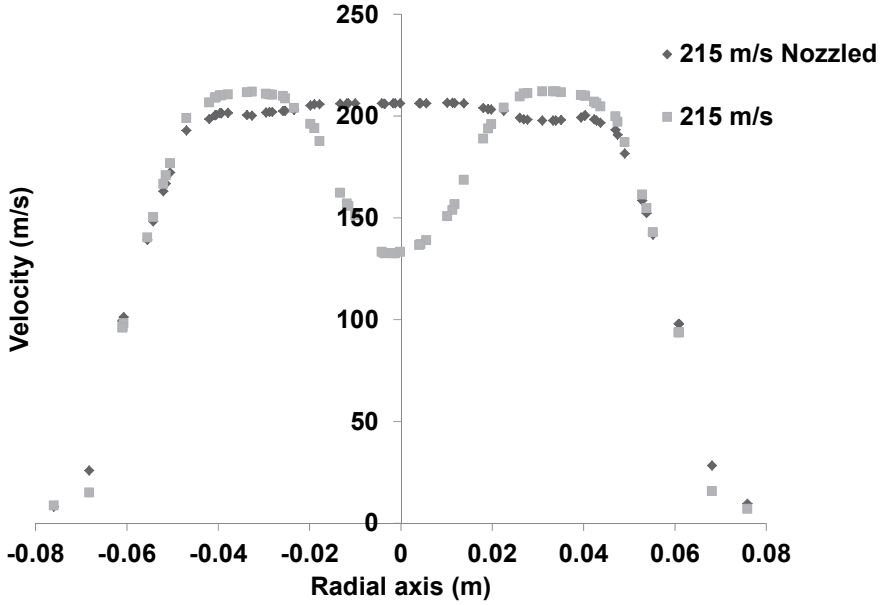


**Fig. 23. Axial velocity of the air flow on the radial axis in the actual blast furnace CFD model (modified from Paper I, published with permission of Steel Research International).**

Good mixing of the heavy oil is very important, because heat transfer to the accelerating droplet is the fastest when the difference between the carrying gas and the liquid droplet is the highest. Vaporization of the droplet is strongly dependent on the droplet diameter. Therefore, it would be beneficial to produce small droplets using optimized lance-nozzle configurations. Improved combustion and gasification of the heavy oil would make it possible to increase the injection rates and to replace expensive coke. Furthermore, soot and cenosphere resulting from the insufficient combustion result in clogging of the coke bed, lowering the permeability of the gases in the coke bed. This increases the pressure losses of the coke bed and causes instability problems in the blast furnace operation.

## 6.2 Heavy oil combustion and lance positioning (Paper II)

### *6.2.1 Grid independency*

The grid independency is studied with three different meshes based on configuration in case 2, which is presented in Section 5.2. The mesh in the area of interest (i.e., the tuyere-raceway area) was changed. In the coarse mesh, the cell size is 10 mm in the tuyere area and 15 mm in the raceway area. In the medium mesh, the cell size is 9 mm in the tuyere area and 13.5 mm in the raceway area. In the fine mesh, the cell size is 8 mm in the tuyere area and 12 mm in the raceway area. By each change, the total number of cells is increased about 50%. In each case, the mesh size near the walls remains the same to keep the $y^+$ value at the desired level. On the tuyere walls and the lance wall the first cell is 0.8 mm, which results in $y^+$ values less than 300 but above 30. The coarse mesh has 668,842 cells, the medium mesh has 1,079,563 cells, and the fine mesh has 1,554,277 cells.

Grid independency is studied by comparing the pressure, velocity, temperature, droplet penetration, and $O_2$ mole fractions with the difference tool in CFD-Post. The results for the pressure at the inlet, the maximum temperature, the velocity at the tuyere nose, and the particle penetration are presented in Table 14. There are differences between the droplet penetration, temperature, and $O_2$ mole fractions between the coarse and medium meshes, but the differences are very small between the fine and medium mesh cases. Therefore the medium mesh is chosen for the calculations.

**Table 14. Results from the grid independency study.**

| Mesh | Pressure (Pa) | Temperature (K) | Velocity (m/s) | Particle penetration (m) |
|---|---|---|---|---|
| Coarse | 364,316 | 2930 | 204 | 1.48 |
| Medium | 366,225 | 2922 | 230 | 1.62 |
| Fine | 365,858 | 2921 | 229 | 1.60 |

### *6.2.2 Comparison between combustion models*

To investigate the reliability of the combustion model, the EDC (case a) and the PDF (case b) combustion models are compared to each other in the case 2 setup, which was introduced in Section 5.2 (Fig. 12). The coke bed reactions are not included in the combustion model comparison cases to clarify the difference between two combustion models. Temperature contours of case a and case b are

shown in Fig. 24. It can be seen that combustion begins already in the tuyere in case b and also combustion occurs inside the heavy oil spray. A photo of oil injection in the blast furnace tuyere is shown in Fig. 25. It can be seen that combustion begins after the tuyere nose, and combustion does not occur in the heavy oil spray, which is opposite to the results from the PDF model. In the EDC case, combustion begins after the tuyere and combustion takes place on the spray surface, which appears to be more realistic than the PDF model. The highest temperature in case a is 2973 K and in case b it is 2910 K.

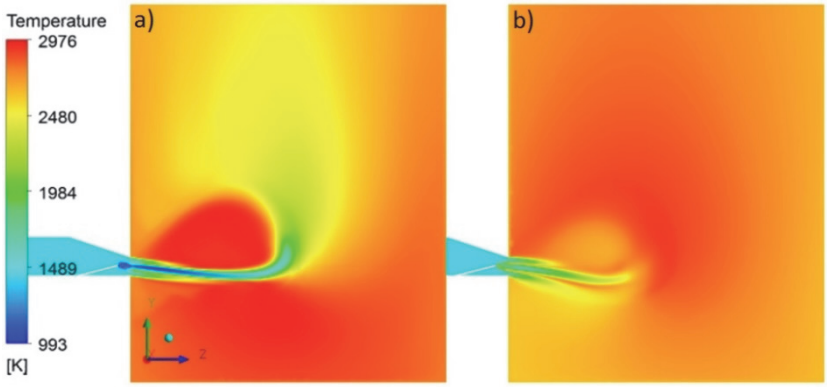


**Fig. 24. Temperature field in cases a and b (modified from Paper II, published with permission of ISIJ International).**

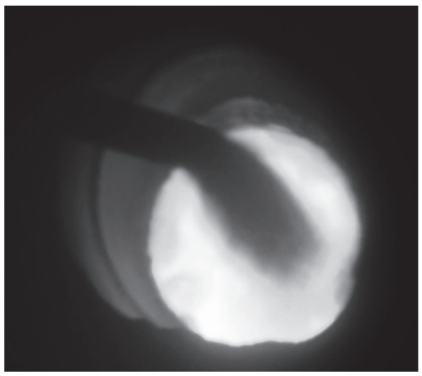

**Fig. 25. Photo of oil injection through the tuyere viewing window (Paper II, published with permission of ISIJ International).**

Adiabatic flame temperature ($T_{ad}$) is calculated with Cantera 2.2.1 to evaluate, if the maximum temperature levels obtained by the CFD combustion model are

realistic. The initial temperature in the adiabatic flame temperature calculation is 1423 K, which is the air blast inlet temperature. The results for $T_{ad}$ as a function of the equivalence ratio with the initial hydrocarbon, oxygen volume fraction, and pressure are given in Fig. 26. A stoichiometric mixture is presented with the cut line where the equivalence ratio is 1. The well-known phenomenon of, the maximum value of $T_{ad}$ being on the rich side of the fuel equivalence ratio in the mixtures of hydrocarbon and air can be seen in Fig. 26. (Law, Makino, & Lu, 2006). It can also be seen that the pressure hinders dissociation, which moves the peak temperature closer to the stoichiometric ratio. The maximum $T_{ad}$ in the blast furnace initial conditions (1423 K, 3.6 bar, 28% $O_2$) is 2981 K, which is 8 K higher than the results from the CFD model, which seems reasonable when considering that the oxidizer stream heats further in the blast furnace tuyere-raceway area.

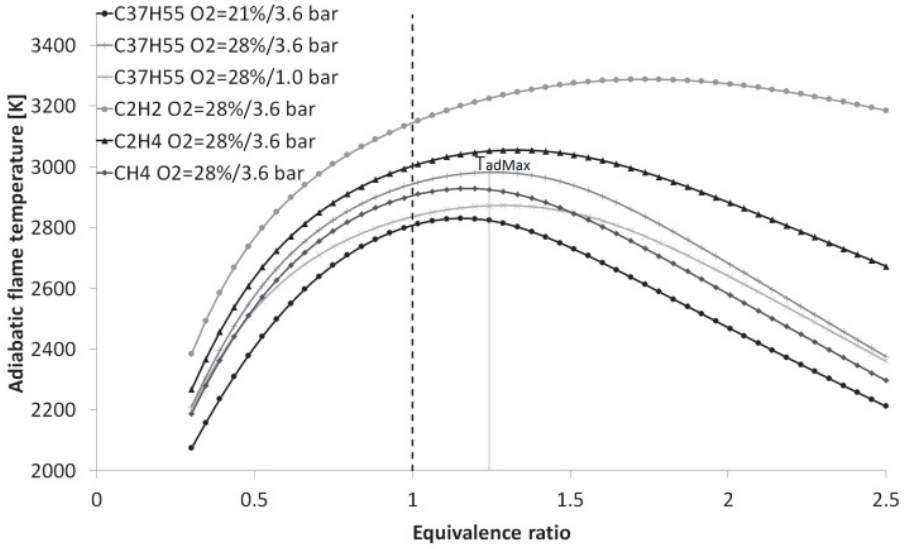


**Fig. 26. Adiabatic flame temperature of different hydrocarbons as a function of equivalence ratio (Paper II, published with permission of ISIJ International).**

### *6.2.3 Effect of lance position*

Fig. 27 presents the contours of the velocity with different lance positions. The lance positions in different cases are presented on page 77 in Section 5.2. According to the results, the air blast velocity increases when the injection lance is drawn inside the tuyere. The lowest maximum velocity (212 m/s) is in the case 1, and the

highest velocity (252 m/s) in the case 3. The difference in the maximum velocity of the air blast inside the raceway is about 16% between cases 1 and 3. In the case 2, the maximum velocity is 230 m/s. The high vaporization rate of the heavy oil and gas phase combustion increase the pressure drop in the tuyere in case 3, which results in an increased velocity in the tuyere-raceway area, because the air blast mass flow rate is kept constant throughout the calculation.

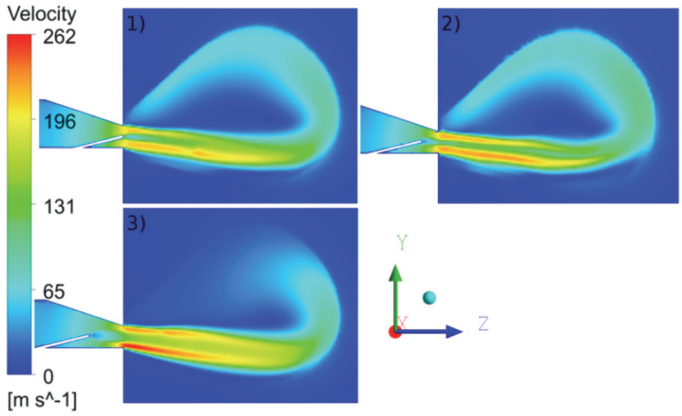


**Fig. 27. Velocity contours in the tuyere-raceway area in cases 1, 2 and 3 (Paper II, published with permission of ISIJ International).**

The air blast velocity affects both the droplet residence time in the raceway and the mixing phenomena. After the 10 cm flight in each case, the heavy oil is concentrated in an area with diameters of 3.5 cm, 4 cm, and 6 cm in cases 1, 2, and 3, respectively. This is reasonable because the air velocity is also lower in the beginning of the tuyere, so the heavy oil is spread over a larger area.

The heavy oil tracking is presented in Fig. 28. The maximum droplet penetration range is 1.60 m in case 1, 1.62 m in case 2, and 0.45 m in case 3. The droplet penetration increases drastically when the injection lance is closer to the tuyere nose. The reason for this behavior is most likely that the heavy oil mixes well with the air blast in case 3, which leads to a higher surface area and faster vaporization rate. In cases 1 and 2, the aerodynamic forces are higher than in case 3, which reduces the mixing between the blast and extra heavy oil, leading to a slower vaporization rate.

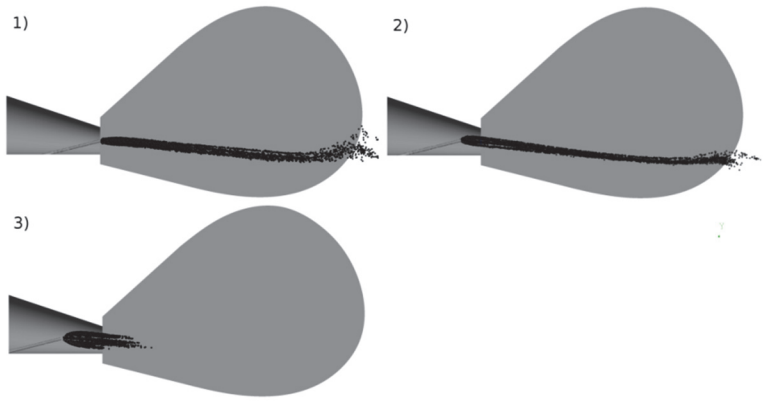


**Fig. 28. Heavy oil tracking in the tuyere-raceway area in cases 1, 2 and 3 (Paper II, published with permission of ISIJ International).**

Temperature contours are shown in Fig. 29. It can be seen that the temperature fields vary for the investigated cases and the maximum temperatures are located in different areas. In case 1, the temperature is the highest under the heavy oil spray. Mixing is poorest in this case and the most of the combustion occurs on the spray surface and only moderately in the upper part of the raceway. In case 2, the highest temperature is located on the surface of the spray, but a high temperature also exists in the upper part of the raceway. In case 3, the temperature field is the most uniform on the spray surface and the mixing is the best of these three cases. In case 3, combustion begins already in the tuyere, which might cause wear and ablation in the tuyere walls. Combustion does not occur in the heavy oil stream because vaporization and heating of the droplets use the excess heat.

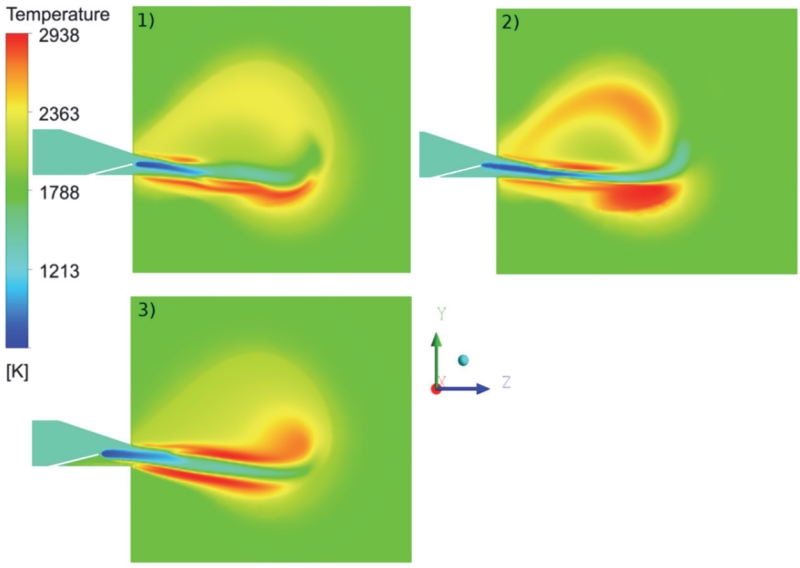


**Fig. 29. Contours of temperature in cases 1, 2, and 3 (Paper II, published with permission of ISIJ International).**

The pressure level of the domain outlet is fixed at 342 kPa, but because of the pressure drop in the coke bed, the inlet pressure adjusts to the level of 360 kPa with the mass flow of 2.56 kg/s and no injection. The air blast pressure cannot be increased above 400 kPa with the existing system, so it is important to study the pressure losses in different cases. The inlet pressure varies within each case because heavy oil vaporization and combustion increase the pressure drop. In addition, the lance position has some effect on the pressure, since the cross-sectional area varies in different parts of the tuyere. Fig. 30 shows the change in the inlet pressure. The zero point is 366 kPa, which is the inlet pressure in case 1. The pressure increases slightly, when the lance is moved 10 cm back from the tuyere tip, but increases drastically when the lance is moved 20 cm from the tuyere tip. The lowest pressure drop is observed in case 1, where vaporization takes place completely in the raceway area. According to the experimental results of the former Koverhar blast furnace by Helle and Saxen (Helle & Saxen, 2002), the blast furnace pressure loss increases when the heavy oil lance is pulled back from the tuyere tip, which is consistent with the modeled results. The increase in the pressure drop, which was observed in case 3, might cause problems in the actual blast furnace, where 21 tuyeres are used instead of only one.

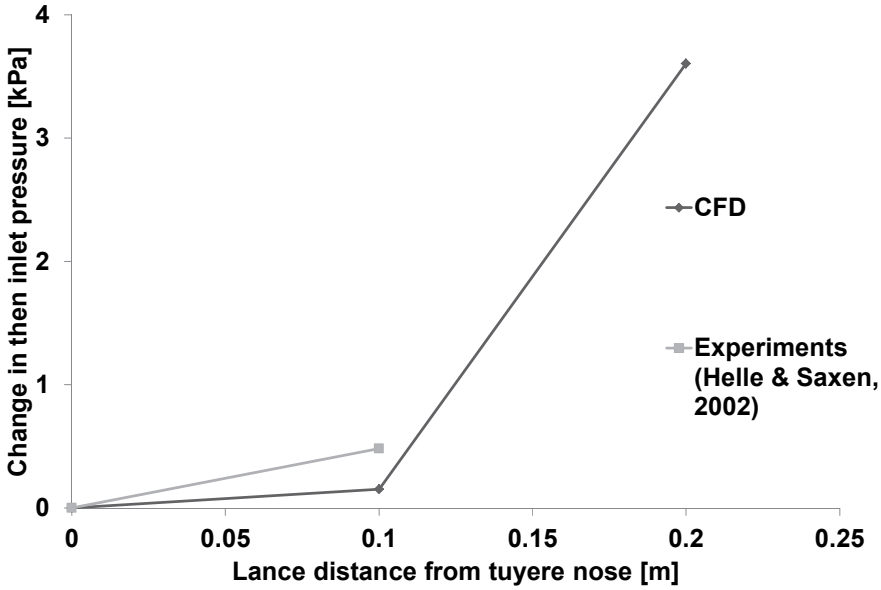


**Fig. 30. Change in the inlet pressure with different lance positions (modified from Paper II, published with permission of ISIJ International).**

The mole fractions of $O_2$, CO, $CO_2$, $H_2$, and $H_2O$ are presented in Fig. 31. It can be seen that the gasification gases move towards the tuyere nose, when the lance is moved 20 cm away from the tuyere tip. Mixing is best in case 3 when the lance is moved back, indicating that more oxygen is reacting and gasification starts earlier. Gasification takes place in the areas with low oxygen content and high temperatures. Gasification reactions are endothermic, and it can be seen that the areas with high CO and $H_2$ levels also have lower temperatures (Fig. 29) and no oxygen.

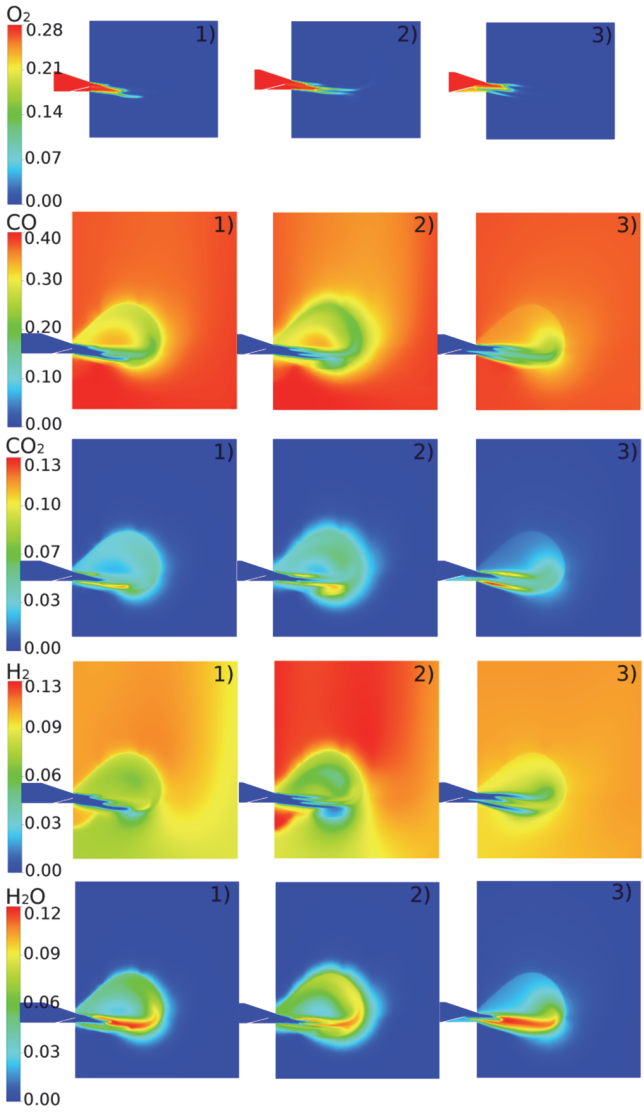


**Fig. 31. Mole fractions of $O_2$, CO, $CO_2$, $H_2$ and $H_2O$ in cases 1, 2, and 3 (Paper II, published with permission of ISIJ International).**

Based on these results, the most effective lance position is 10 cm inside the tuyere (case 2). Even though the combustion is best in case 3, the problem is that combustion begins inside the tuyere, which might lead to wearing and ablation of the tuyere walls. Furthermore, blast velocities higher than 230 m/s (case 3) cause

high degradation of coke (Iwanga & Takatan, 1989), producing fine coke dust and thus lowering the permeability in the deadman. The lance at the tuyere raceway connection (case 1) is the best solution from the point of view of pressure drop because there will be no combustion inside the tuyere. The mixing in that case is the poorest, and the coke bed might be reacting more than in the other two cases. This might result in incomplete combustion and the accumulation of fine particles in the coke bed. The 10 cm case (case 2), is a compromise between the two cases, but an optimized position of the lance would need more simulations around the suggested lance position.

Based on the discussions with SSAB Raahe and also the tuyere videos (Fig. 25), the model produces results similar to those seen in the SSAB Raahe process. There is no visible flame when the lance is 10 cm inside the tuyere. It should also be noted that increasing the heavy oil injection rate above 100 kg/thm, with the current settings leads to unburned fuel, which causes clogging of the coke bed, leading to an unstable process. The same phenomena occur both in the actual blast furnace and the CFD model with the same injection level, which is important when considering the reliability of the model.

### 6.3 Pulverized coal combustion model (Paper III)

The observation plane for the PC particle combustion sampling is the cross section 1 m downstream from the tip of the injection lance. The measurements (B. Guo *et al*., 2005) of the burnout degree in the test rig were done at the same spot. The results of the burnout degree from the CFD calculations are compared to the experimental results from the literature (B. Guo *et al*., 2005) in Table 15. It can be seen that the burnout degree matches well with the experimental results. The results vary a little with different coal types. When the modeling is done with the A1 setup, the burnout degree is 64.8%, which overestimates the combustion degree by 1.7%. With the B1 setup, the CFD produces a result that underestimates the burnout degree by about 5.3%. In the C1 setup, the results differ from the experimental results by only 4.1%. The B3 setup produced the most accurate results. The results from the experimental rig and CFD modeling do not differ from each other in the first decimal. In this case, the injection level was the highest, which is most important when considering the actual blast furnace case. The lowest correspondence between the results is in case A2, where the difference is 7.3%.
The stoichiometric ratio has a strong effect on the PC burnout. The results in Table 15 show that cases with fuel-lean combustion conditions lead to a higher burnout

of the PC than in the fuel-rich conditions. The probability of collision and reaction between the oxygen and fuel molecules increases with the increasing stoichiometric ratio.

The model overestimates the particle combustion with oxygen in the case with medium volatile matter coal (Coal A) and underestimates the reaction rate in lower rank coals (Coals B and C). Due to the time dependency of the model mixing varies a little during the calculation. This might lead to the deviation from the experimental measurements. Changes in mixing are minimized with long sampling times and large sampling sizes over 20,000 particles.

**Table 15. Calculated and experimental burnout of coal particles (modified from Paper III, published with permission of Industrial Combustion).**

| Case | Flowrate [kg/h] | VM [%] | Stoichiometric ratio | Burnout experimental [%] | Burnout CFD [%] | Accuracy [%] |
|---|---|---|---|---|---|---|
| Coal A1 | 25.2 | 20.19 | 1.20 | 63.7 | 64.8 | 1.70 |
| Coal A2 | 35.9 | 20.19 | 0.84 | 55.5 | 59.9 | 7.35 |
| Coal B1 | 25.5 | 33.57 | 1.25 | 81.5 | 77.2 | -5.57 |
| Coal B2 | 40.0 | 33.57 | 0.80 | 75.5 | 74.8 | -0.94 |
| Coal B3 | 46.7 | 33.57 | 0.68 | 71.4 | 71.4 | 0.00 |
| Coal C1 | 23.5 | 36.41 | 1.37 | 78.9 | 75.7 | -4.23 |
| Coal C2 | 35.1 | 36.41 | 0.92 | 76.2 | 71.5 | -6.57 |

The PC burnout as a function of particle size is presented in Fig. 32. It can be seen that the particle size has a strong effect on the burnout. Almost all of the particles below 40 μm have enough time to burn during the 1 m flight. The biggest particles (200 μm) in cases Coal A1, B3, and C1 had burnout degrees of about 31.3%, 42.7%, and 45.2%, respectively. The burnout degree increases as the level of volatile matter gets higher, since the devolatilization is faster than the char combustion.

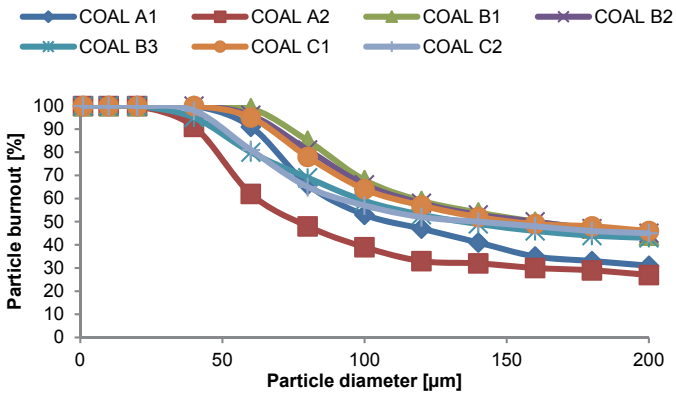


**Fig. 32. Effect of particle size on burnout degree (Paper III, published with permission of Industrial Combustion).**

The CFD results estimate that the maximum drying time of PC particles is 3 ms because the moisture fraction in a particle is small. The devolatilization time of PC (Coal B) is presented in Fig. 33. Particle sizes are based on the groups that are set as a boundary value. Devolatilization time increases linearly with the particle diameter. Small particles lose their volatile matter quickly; but for the larger particles, complete devolatilization takes about 0.035 seconds. Therefore particle devolatilization takes about ten times longer than particle drying.

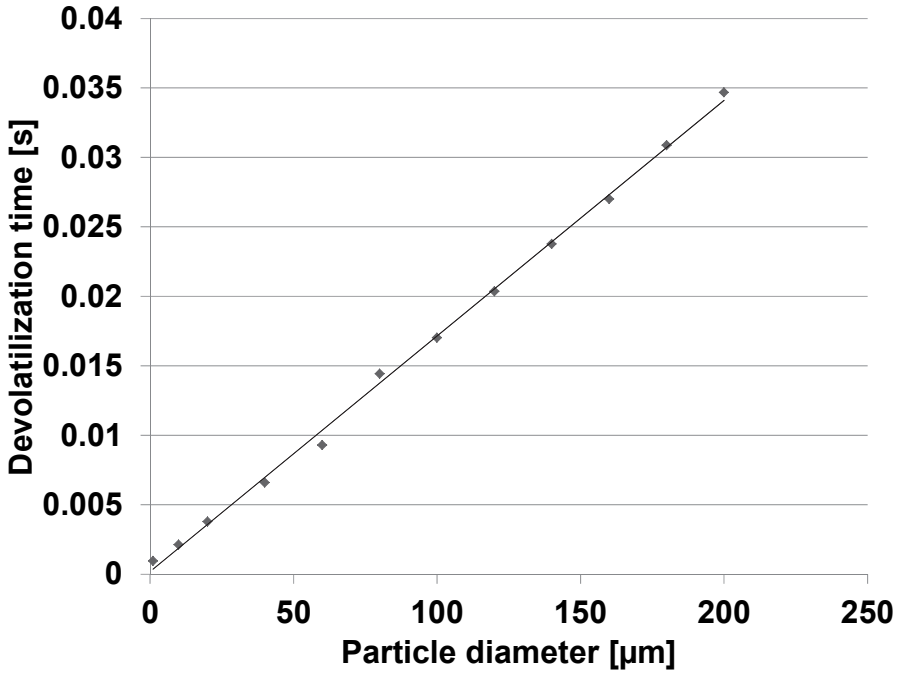


**Fig. 33. Particle devolatilization time (Paper III, published with permission of Industrial Combustion).**

Residence time is an important quantity in combustion processes. In the test rig, the PC particle size affects the overall residence time, because larger particles accelerate slower than the small ones. Results from the CFD modeling indicate that, an average particle spends from 0.03 to 0.06 seconds in the test rig, which is a very short time when considering PC combustion. Due to the short residence time, the mixing between PC and air blast should be optimized to increase the PC burnout.

The velocity magnitude along the z-axis is presented in Fig. 34. The velocity magnitude at the tuyere nose 3 cm up and down from the center is about 128 m/s, which is consistent with the CFD results from the same geometry in Y. S. Shen *et al*., (2009a). The PC lance (z-axis 0.53 m) creates an obstacle to the center of the tuyere, which decreases the cross-sectional area of the tuyere and leads to an increased velocity at the tuyere exit. At the center, the velocity is also lower because of the retarding effect of the PC on the air blast. This is a result of the poor mixing, which is a well-known problem in PC injection systems (Ishii, 2000).

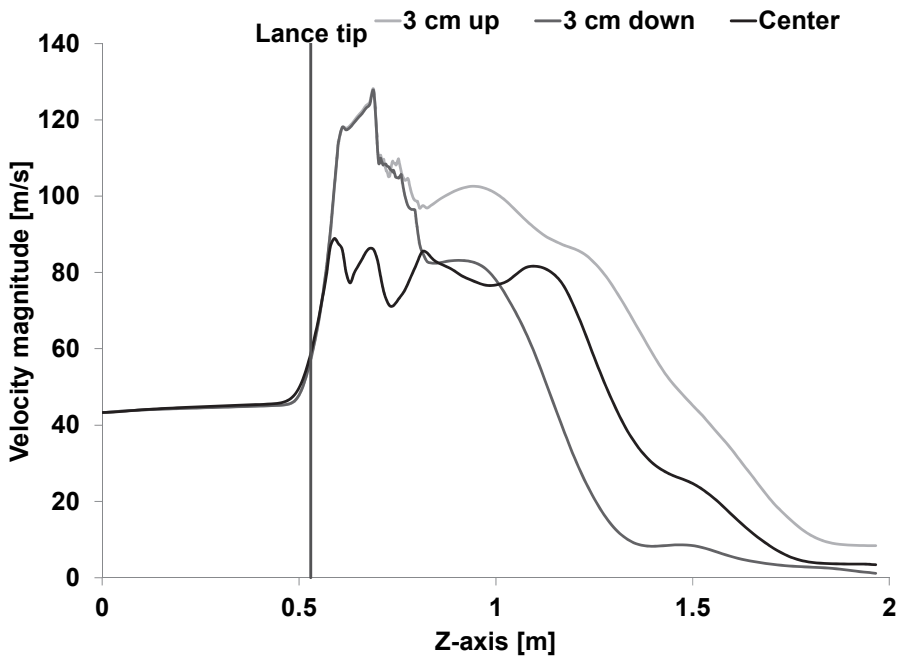


**Fig. 34. Air blast velocity along the z-axis (Paper III, published with permission of Industrial Combustion).**

The gas phase temperature along the z-axis is shown in Fig. 35. Particles with a diameter is less than 10 μm, release their volatile matter quickly, and combustion starts only 4 cm from the lance tip (z-axis 0.53 m), which consumes all the available oxygen from the PC dust cloud. Maximum temperature is about 2800 K in the gas phase. Combustion occurs at the surface of the PC dust cloud. Since there is no oxygen in the center of the flow, only devolatilization occurs there. Mixing dilutes the PC cloud enough to ignite the mixture in the center line about 60 cm from the lance tip and the temperature reaches 2500 K, but the hottest temperatures are located 80 cm from the lance tip.

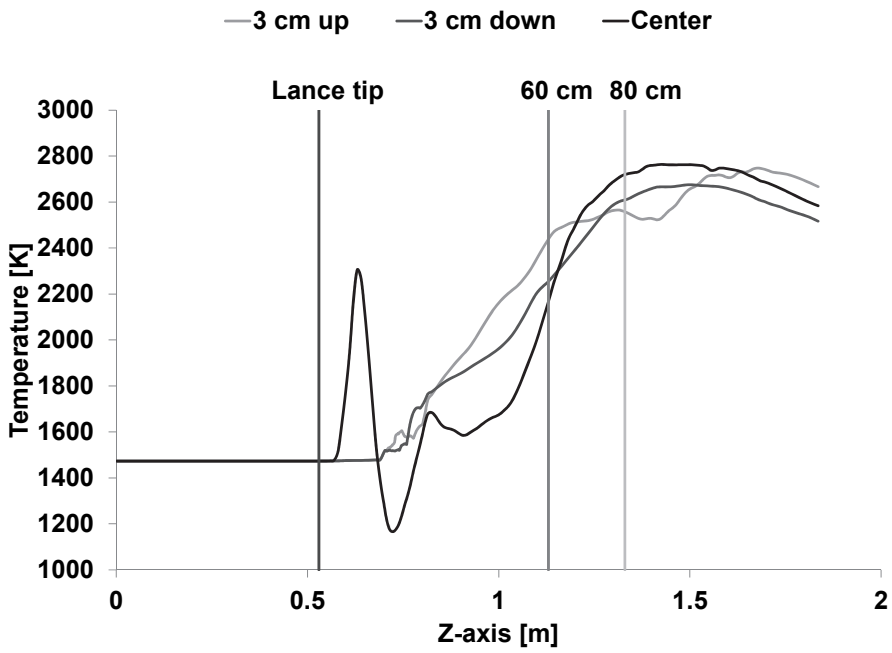


**Fig. 35. Gas temperature along the z-axis (Paper III, published with permission of Industrial Combustion).**

The experimental rig is not a perfect match for the actual blast furnace, and it is mainly used to evaluate combustion of different types of coals and their suitability as an injection material. The velocity difference and temperature between the air blast and PC after injection is on the same level in the test rig and the blast furnace. The pressure difference between Raahe's blast furnace and the test rig is about 2.56 atm. Increased pressure (increased density of the air blast) leads to higher reaction rates and creates uncertainty in the combustion model. Another cause for possible errors is that there is no gas-phase measurement data available, and thus the gas phase model cannot be validated. The model predicted that the PC particles with a diameter less than 10 μm release their volatiles quickly after the injection and ignite close to the lance tip. This behavior should be modeled and validated in an actual blast furnace.

## 6.4 Double lance position in a tuyere (Paper IV)

The observation plane for sampling in pulverized coal particle combustion is the raceway surface, which can be seen in Fig. 16a. The results indicate that most of the particles have a straight flight path and do not recirculate in the raceway area. The results of the particle burnout and the average residence time results for the different cases are presented in Table 16. The lance position has only a small effect on combustion efficiency. The difference in the PC burnout is about 1 percentage point between cases 1 and 4, which are presented in Table 12.Fig. 16b. The particle burnout is about 80% in all cases. The results are similar to the study by Nozawa *et al*. (2011), where they noticed that moving the lance away from the tuyere nose stops having an effect on achieved combustibility when the lance is about 25 cm from the tuyere nose. After that point, the achieved combustibility is almost constant. CFD results indicate that the particles below 80 μm have enough residence time to be completely combusted before the raceway boundary in all lance positions. Particles below 80 μm make up about 66% of the total PC mass (Fig. 17). The result is positive when considering the optimum place for the lance position. It is important to minimize the thermal load on the tuyere walls. The average residence time increases when the lance is moved further inside the tuyere. The residence time in case 4 is about 24% longer than in case 1.

**Table 16. Burnout and average residence time of PC with different lace positions.**

| Case | Burnout (%) | Average residence time (ms) |
|---|---|---|
| Case 1 | 79.60 | 29.51 |
| Case 2 | 79.41 | 29.67 |
| Case 3 | 79.87 | 33.14 |
| Case 4 | 80.07 | 36.65 |

Fig. 36 presents the contours of velocity with different lance positions. It can be seen that the maximum air blast velocity is about 210 m/s in cases 1 and 4. In cases 2 and 3, the maximum velocity is about 200 m/s. In all cases the velocity is below 230 m/s, which is the limit for the high degradation of the coke bed in the raceway (Iwanga & Takatan, 1989). Therefore air blast velocity does not create a limit for the lance position.

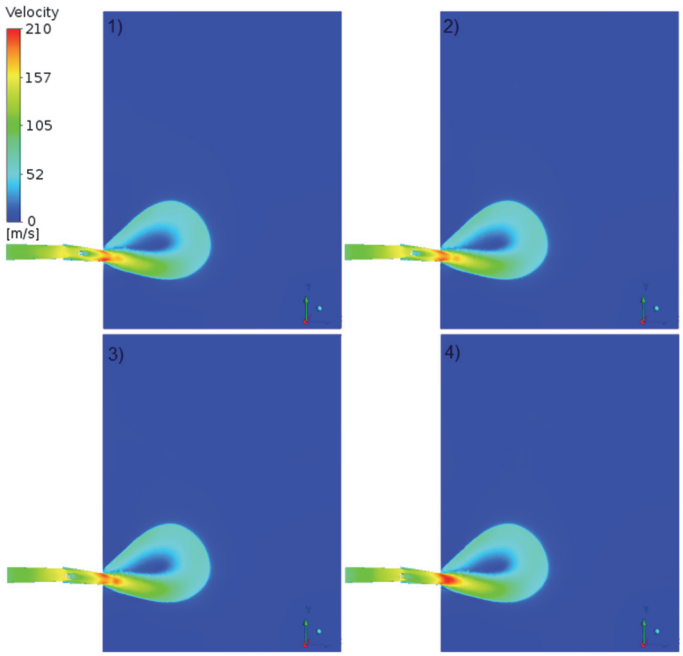


**Fig. 36. Contours of velocity with different lance positions.**

The PC tracking results for all the lance positions are presented in Fig. 37. The particle track remains stable until the end of the raceway. The lightest 1 µm particles, which have only ash left, recirculate in the raceway, but larger and heavier particles exit the raceway without recirculation. It can be seen that the particles travel in a downwards trajectory towards the center of the BF and particles slow down in the coke bed and start to move towards the outlet. The coke bed behavior of the PC varies between cases, but it does not affect the burnout results because it is taken from the raceway boundary.

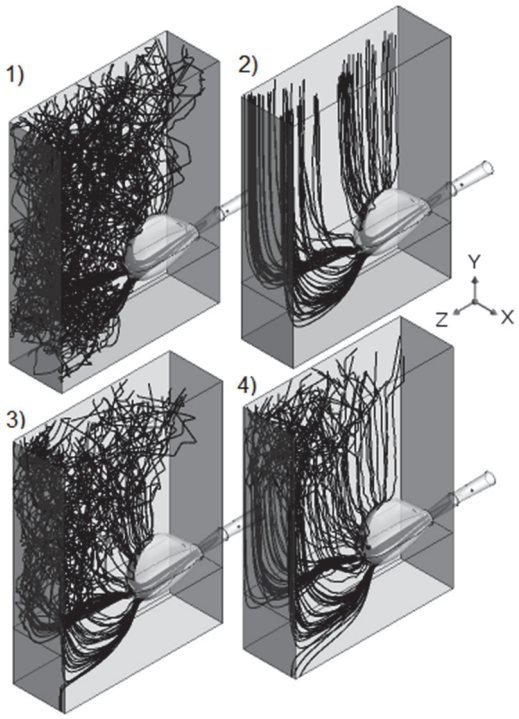


**Fig. 37. PC tracking in the tuyere-raceway area in cases 1, 2, 3 and 4.**

Contours of the temperature for each case are presented in Fig. 38. It can be seen that the maximum temperatures are the same (about 2800 K) in all cases. The lance position affects the ignition point. In case 4, combustion inside the tuyere is strong enough to increase the temperature above 2000 K. In other cases, the temperature does not rise above the initial air blast temperature, which is 1423 K. The increased temperature inside the tuyere may lead to ablation and wear of the tuyere walls, leading to the need for the tuyere replacement, which eventually increases the costs of the ironmaking.

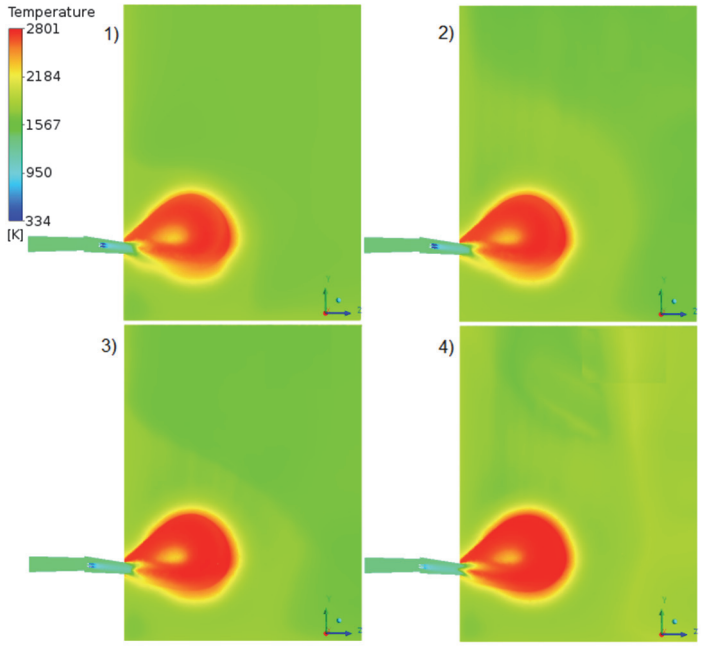


**Fig. 38. Contours of temperature with different lance positions.**

The mole fractions of $O_2$, $H_2O$, $H_2$, $CO_2$, and CO are shown in Fig. 39. It can be seen that the $CO_2$ and $H_2O$ gases move towards the tuyere nose when the lance is moved further inside the tuyere. This indicates that the combustion starts earlier. $H_2O$ is also released from particle drying, which occurs almost immediately after the injection. Gasification reactions increase the CO and $H_2$ contents in the areas with a low oxygen content and high temperature. Most of the gasification takes place in the center of the raceway, where gas velocity is low and all of the oxygen is depleted. In can be seen from Fig. 38 that gasification reactions use a lot of heat and the temperature is about 600 K lower than that of the surrounding area. In addition, $O_2$ that does not react with PC in the blast furnace tuyere-raceway area will react with coke, leading to increased fuel costs.

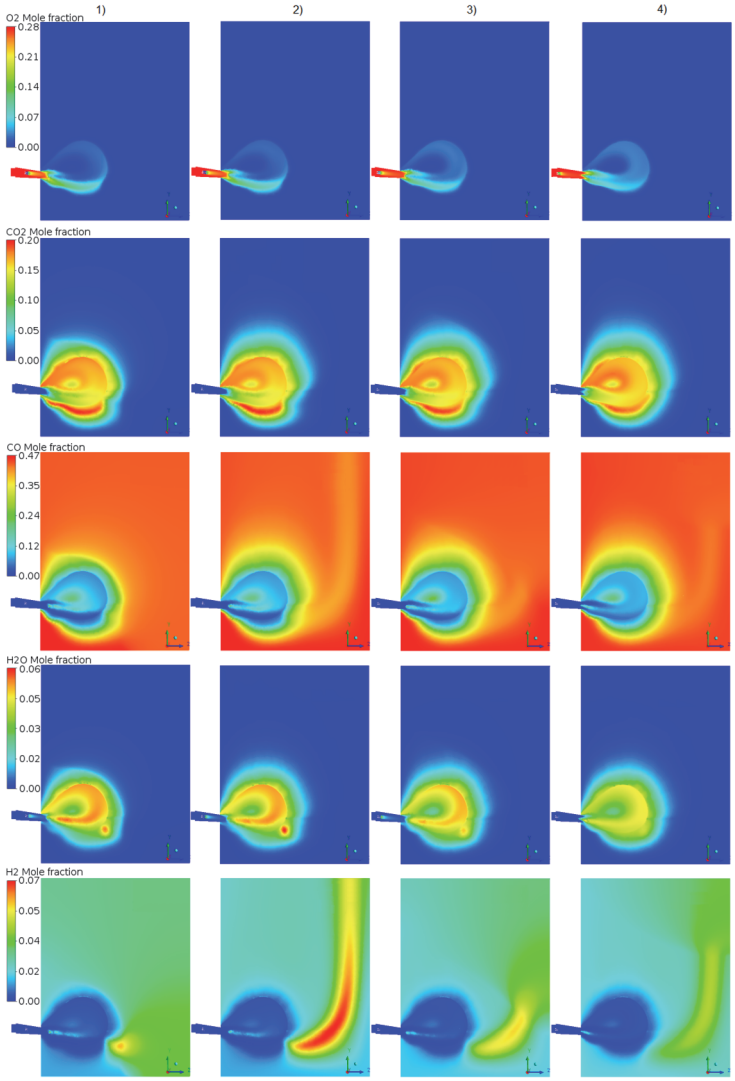


**Fig. 39. Contours of O2, CO2, CO, H2O and H2 mole fractions in cases 1 to 4.**

The domain outlet pressure level is fixed at 342 kPa. The pressure drop in the coke bed causes the inlet pressure to adjust to the level of 360 kPa when there is no injection. The maximum air blast pressure with the existing system is 400 kPa. Therefore, it is important to study the pressure losses with different lance positions. Pressure losses increase when the lance is moved farther from the tuyere nose. The

inlet pressure is 362.4, 362.3, 362.5, and 365 kPa, in cases 1 to 4, respectively. Cases 1 and 2 have less than a 100 Pa difference and the pressure is lower in case 2 than case 1. In case 4, the pressure loss increases, because of the thermal expansion of gases caused by combustion inside the tuyere.

According to the results, the most effective lance position is 40 cm inside the tuyere, i.e., in case 4. Even though the combustion is the most effective in case 4, the case is problematic since combustion starts inside the tuyere. It might lead to fouling and ablation of the tuyere walls. Blast velocities are not above 230 m/s in any of the lance positions and do not contribute to the high degradation of coke (Iwanga & Takatan, 1989). The difference in pressure losses is small in cases 1, 2, and 3 and increases in case 4. Increased pressure losses might create problems for the pump's ability to provide a sufficient air blast mass flow, which in turn would lower the combustion efficiency in an actual blast furnace process. In addition, pumping costs would rise.

# 7 Industrial relevance and future interests

This thesis has a direct connection to the blast furnace ironmaking process. The main advantage of CFD is that it can be applied to systems that are difficult to measure or where experimental costs are high. Typically, industrial experiments are very expensive and possess a risk for production stability. In the blast furnace tuyere-raceway area, CFD can be used to study different tuyere and lance configurations, different auxiliary fuels, and the overall behavior of the injection process. It is hard to evaluate the monetary value of the new knowledge related to the process, but the improvements in auxiliary fuel injections can be quantified in euros.

Market prices for Pulverized Coal Injection (PCI) coal, thermal coal, and metallurgical coke are shown in Fig. 40. The metallurgical coke has a very volatile market price (average price in March/April 2017 was 249.50 €/t) and it is about 138 €/t more expensive than the coal for the PC injection (average price in March/April 2017 was 111.10 €/t) (KPMG, 2017; Platts, 2015). The coke use in the SSAB Raahe's BF process is 900,000 t/a, which means that each percent that can be replaced with coal saves about 1.24 M€/a. Therefore, coke replacement does not have to be big to make significant savings. Coal also has a higher H/C ratio than that of coke, which leads to decreased $CO_2$ emissions. With stoichiometric combustion of Coal A, the $CO_2$ emissions are 2.95 t/t of coal and 3.22 tons for a ton of coke. The savings depend on the $CO_2$ emission allowance price, which is expected to increase in the future. At the moment (1.9.2017), the price is 5.88 €/t $CO_2$ (Markets Insider, 2017). If one percent of coke is replaced with coal, the savings from the emission allowance are 14,574 €. With the current $CO_2$ emission allowance price, the difference is small.

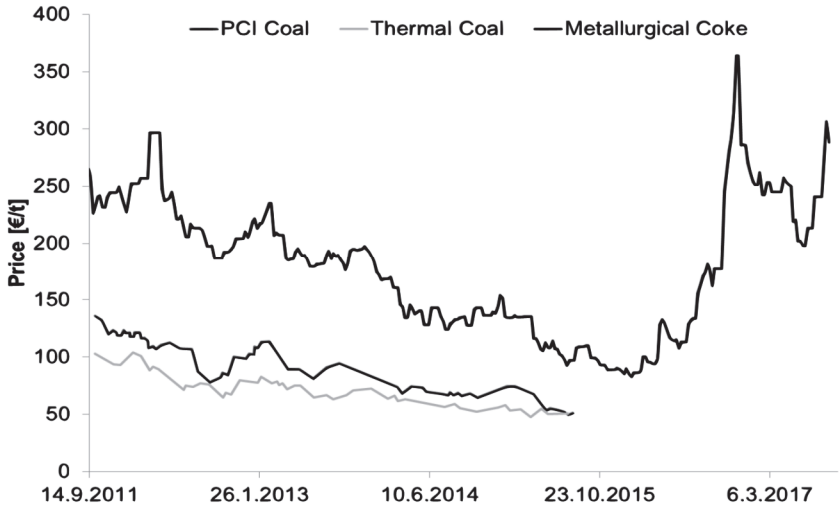


**Fig. 40. Market price of PCI coal, thermal coal and metallurgical coke as a function of time. (KPMG, 2017; Platts, 2015)**

The most easily identified advantage of this work is the study of the different heavy oil nozzle configurations. The results of the industrial experiments were similar to the CFD and the nozzle was selected for industrial use.

In the PC injection, the difference in combustion efficiency is small with the modeled four lance positions and other variables might be more important when making the final design. This is important, because the lance position affects the probability of particle wall contact. When the lance was 45 cm inside the tuyere there was considerable clogging near the tuyere nose in the actual BF. With the double lance PC injection, there is still a lot to study because the tuyere model requires the cooling of the tuyere to be taken into account to solve the thermal load on the tuyere walls. The industrial experiments are starting, and they will offer new information on the subject.

In future studies, OpenFOAM is going to be used to solve the cases. Increasing license prices drive the change from commercial ANSYS Fluent to open source solvers. Most of the required models can be found in OpenFOAM but the gasification and combustion reaction models of PC particles have to be added to the program. It has already been implemented and verified, but the actual simulations will be made later. The EDC combustion solver with the ISAT chemistry tabulation was added to OpenFOAM 5, which decreases the simulation

time drastically. The interesting subjects are related to charcoal injection and injection of dusts containing iron oxides. Charcoal injection reduces the environmental effect of the ironmaking by reducing the $CO_2$ emissions. According to Mathieson *et al*. (2012), it is more reactive than the PC, and it shows promising results when it is mixed with PC. Dusts that contain iron oxides exist in high quantities in the steel mills. It might be possible to inject this dust with PC to improve its use on-site. In addition, coking plant dusts are mixed with PC to improve material efficiency. The PC injection model can be used as a basis for all of these cases. Furthermore, the combustion models can be used in all kinds of burners or gasification units that use heavy oil or PC as a fuel.

CFD-DEM (Discrete Element Method) modeling could provide a better understanding about coke degradation during high velocity air blast flows. This would make the model more realistic with a dynamic coke bed and the possibility to model the bird's nest phenomena beyond the raceway boundary. An improved reduction reaction model for iron oxides should be created and to add a phase change model for all other burden materials except for coke. This kind of model could estimate the shape and size of the raceway with different injection levels and could solve the location of the cohesive zone. These aspects affect the BF operation greatly and thus they would improve the understanding of the process.

# 8 Summary and conclusions

The auxiliary fuels (pulverized coal (PC), natural gas, extra heavy oil, tar, etc.) are injected into the BF through the tuyeres to reduce consumption of expensive coke, to decrease carbon dioxide ($CO_2$) emissions (higher H/C ratio), to stabilize the process and to increase productivity. The fuels can replace coke in two ways, i.e. as a source of reducing agents for iron oxides (CO, $H_2$), and as a provider of energy for the blast furnace operation.

This thesis aims to increase the auxiliary fuel injection rate to replace coke in the blast furnace. Coke is an expensive fuel, which is mainly composed of carbon; therefore its combustion product is mainly $CO_2$. Coke can be replaced only partially, because it remains solid at high temperatures and acts as a support material in the BF creating a porous bed, and allows gases to flow upwards. In this thesis, the atomization model for the heavy oil was selected and results from literature were used to find out constants that fit the BF tuyere-raceway area (Paper I). CFD modeling was used to improve mixing of the air blast and the heavy oil by choosing the most efficient nozzle geometry (Paper I). Furthermore, the goal was to study the effect of heavy oil lance positioning in tuyere, to improve combustion efficiency (Paper II). In addition to heavy oil combustion also pulverized coal was studied. Combustion model for the PC was created and it was validated using results from the literature (Paper III). The combustion model for PC was applied to study the effect of lance position on the combustion efficiency of PC in the tuyere-raceway area (Paper IV).

In the blast furnace tuyere-raceway area, the heavy oil atomization is not instant, but occurs during the first 350 mm of the droplets flight. Big droplets atomize into a large number of small droplets, which increases the surface area and boosts the vaporization rate, leading to faster combustion. Results from the atomization test rig based on the SSAB Raahe blast furnace tuyere-raceway area are reported in the literature. A CFD model was created based on the test rig and the results were used to adjust constants for the Wave breakup atomization model. The model produced a good fit with the experimental results.

CFD modeling was used to evaluate performance of different nozzles for the heavy oil atomization and mixing in the BF tuyere-raceway area. Nozzles improved mixing greatly and it was found out that there should not be a hole in the center of the nozzle, because the stream that originates from that hole unites with the stream above it. The angle between the centerline of the lance and the holes in the nozzle

should be 30° to avoid droplets from hitting the tuyere wall. An 8 holed nozzle was found to be the most effective nozzle type in mixing.

A heavy oil atomization model and the nozzle geometry were applied in the study regarding the heavy oil lance position and its effect on the combustion efficiency. The combustion model was created for the heavy oil. Because of the lack of good validation material for heavy oil combustion, the reliability of model was evaluated in alternative ways. The adiabatic flame temperature was calculated for the heavy oil vapor combustion with different pressures and $O_2$ fractions in the combustion air. Other hydrocarbons were compared to set levels for realistic temperature ranges. The combustion model was compared with the equilibrium model as well, which in turn were compared with the video material from the tuyere viewing window. It was found out that the developed model behaved more realistically than the equilibrium model, when compared to the video material. The equilibrium combustion model estimated the combustion to take place in the fuel stream, which did not occur in the video. The developed model showed a cool area in the middle of the fuel stream resulting from the vaporization and boiling of heavy oil. The change in the inlet pressure was also compared to the literature data. It was found out that the lance position shows a similar trend with the experimental results. The results of the lance positioning showed that the case where the lance is 20 cm from the tuyere nose results in the most efficient combustion. The problem with that position is that combustion begins already inside the tuyere, which may lead to ablation of tuyere walls, and further increased maintenance costs. In addition, the velocity increases above 230 m/s in the tuyere due to the phase change from liquid to gas and thermal expansion of gases. In the literature it can be found that, increased velocity causes high degradation of coke, which leads to lower gas permeability in the coke bed. This increases the pressure losses in the blast furnace. The case where the lance was 10 cm inside the tuyere was proved to be the best solution of the three studied cases. The pressure loss in the system was only slightly higher than in the case where the lance is at the tuyere nose.

The combustion model was created for the pulverized coal injection in the blast furnace. The model was validated with data from the literature. The results from the combustion CFD modeling had a good fit to the experimental results. It was found out that with a medium volatile coal, the combustion model slightly overestimates the combustion. On the other hand, the combustion model slightly underestimates combustion with high volatile coals. The explanation for this behavior could be that the high volatile coals have more reactive char than the medium volatile coals. No temperature measurements were done in the

experimental rig in the literature and the temperature from the combustion modeling was compared to the results from the equilibrium combustion model. The maximum temperature was found to be similar in the studied models.

The pulverized coal combustion model was added to the blast furnace tuyere-raceway model to simulate the effect of different double lance positions on the combustion efficiency. Simulations showed that, when the lances are 45 cm from the tuyere nose, the combustion inside tuyere is strong enough to increase temperature above 2000 K. It was noticed that the lance position has a very small effect on the particle burnout at the end of the raceway. This is important information, because the lance can be moved towards the tuyere nose, which reduces the ablation and fouling of tuyere walls and increases the lifetime of the tuyere. With PC, the blast velocity does not pose a problem, because maximum velocities are in the range of 210 m/s.

As a concluding remark, this thesis provides valuable scientific information about the combustion of auxiliary fuel injection in a blast furnace. The thesis describes validated methodologies for heavy oil atomization, heavy oil combustion modeling and PC combustion modeling. The models have been applied to study different nozzle geometries to advance mixing of heavy oil with air blast and to improve heavy oil and PC combustion via optimization of the lance position in a tuyere.

In the immediate future, the work will continue with the model development using alternative auxiliary fuels (charcoal) and dusts from a blast furnace, as well as, coking processes containing fine coke dust and iron oxides. These methods can be used to lower $CO_2$ emissions and to increase material efficiency in the steel mill. The reactions for the iron oxides and phase changes should be taken into account in the blast furnace burden modeling to improve the accuracy of heat transfer and to get more accurate solution for the chemical species. The long-term goal is to create a model that can utilize DEM for the particle phase, which makes it possible to model the effect of auxiliary fuels and air blast velocity on the raceway shape and size. Furthermore, this kind of a model could be used to predict position of the cohesive zone in the blast furnace.

# References


Andahazy, D., Slaby, S., Löffler, G., Winter, F., Feilmayr, C., & Bürgler, T. (2006a). Governing processes of gas and oil injection into the blast furnace. *ISIJ International, 46*(4), 496-502.

ANSYS Inc. (2017). *ANSYS fluent user's guide 18.0*. Canonsburg, PA: Ansys Inc.

ANSYS Inc. (2017a). *ANSYS fluent theory guide 18.0*. Canonsburg, PA: ANSYS Inc.

ANSYS Inc. (2017b). *CFX-solver theory guide 18.2*. Canonsburg, PA: ANSYS Inc.

Ariyama, T., Sato, M., Yamakawa, Y., Yamada, Y., & Suzuki, M. (1994). Combustion behavior of pulverized coal in tuyere zone of blast furnace and influence of injection lance arrangement on combustibility. *ISIJ International, 34*(6), 476-483.

Baosteel (2017). PCI for blast furnace. Retrieved from http://bsee.baosteel.com/english/tech3.htm

Bartok, W., & Sarofim, A. F. (1991). *Fossil fuel combustion : A source book*. New York: John Wiley.

Bejan, A., & Kraus, A. D. (2003). *Heat transfer handbook*. New York: Wiley.

Carpenter, A. M., & IEA Coal Research. (1988). *Coal classification* IEA Coal Research.

Chatterjee, A. (2012). *Sponge iron production by direct reduction of iron oxide* PHI Learning Pvt. Ltd.

Chui, E. H. (2005). Applications of CFD modeling in Canadian industries. *Fourth International Conference on CFD in the Oil and Gas, Metallurgical and Process Industries, SINTEF/NTNU Trondheim, Norway.*

Du, S., & Chen, W. (2006). Numerical prediction and practical improvement of pulverized coal combustion in blast furnace. *International Communications in Heat and Mass Transfer, 33*(3), 327-334.

Ergun, S. (1952). Fluid flow through packed columns. *Chemical Engineering Progress, 48*(2), 89-94.

Field, M., Gill, D., Morgan, B., & Hawksley, P. (1967). *The combustion of pulverized coal*. London: British Coal Utilization Research Association.

Frenklach, M., Wang, H., Goldenberg, M., Smith, G. P., Golden, D. M., Bowman, C. T., Gardinier, W. C., & Lissianski, V. (1995). *GRI-mech – an optimized detailed chemical reaction mechanism for methane combustion.* (No.GRI-95/0058). Gas Research Institute.

Frenklach, M., Wang, H., Yu, C. L., Goldenberg, M., Bowman, C. T., Hanson, R. K., Gardinier, W. C., & Lissianski, V. (2016). GRI-mech. Retrieved from http://www.me.berkeley.edu/gri_mech/

Geerdes, M., Chaigneau, R., & Kurunov, I. (2015). *Modern blast furnace ironmaking: An introduction (third edition, 2015)* IOS Press.

Gonçalves dos Santos, R., Lecanu, M., Ducruix, S., Gicquel, O., Iacona, E., & Veynante, D. (2008). Coupled large eddy simulations of turbulent combustion and radiative heat transfer. *Combustion and Flame, 152*(3), 387-400.

Gu, M., Chen, G., Zhang, M., (Frank) Huang, D., Chaubal, P., & Zhou, C. Q. (2010). Three-dimensional simulation of the pulverized coal combustion inside blast furnace tuyere. *Applied Mathematical Modelling, 34*(11), 3536-3546.

Gu, M., Zhang, M., Selvarasu, N. K. C., Zhao, Y., & Zhou, C. Q. (2008). Numerical analysis of pulverized coal combustion inside tuyere and raceway. *Steel Research International, 79*(1), 17-24.

Guildenbecher, D., López-Rivera, C., & Sojka, P. (2009). Secondary atomization. *Experiments in Fluids, 46*(3), 371-402.

Guo, B., Zulli, P., Rogers, H., Mathieson, J. G., & Yu, A. (2005). Three-dimensional simulation of flow and combustion for pulverised coal injection. *ISIJ International, 45*(9), 1272-1281.

Guo, K., Li, H., & Yu, Z. (2016). In-situ heavy and extra-heavy oil recovery: A review. *Fuel,* 185, 886-902.

Hakala, J., & Paloposki, T. (1996). *Small scale model experiments on the injection of heavy fuel oil into the blast furnace*. Espoo: Teknillinen korkeakoulu.

Harasek, M., Jordan, C., Winter, F., Aichinger, G., Feilmayr, C., & Schuster, S. (2007). Evaluation of the high temperature conversion of plastic particles after injection into blast furnace raceway using CFD simulations. *AIChE Conference Proceedings, Annual meeting.*

Hellberg, P., Jonsson, T. L. I., & Jönsson, P. G. (2005). Mathematical modelling of the injection of coke oven gas into a blast furnace tuyere. *Scandinavian Journal of Metallurgy, 34*(5), 269-275.

Helle, M., & Saxen, H. (2002). Identification of the combustion degree of oil in the blast furnace tuyeres. *ISIJ International, 42*(10), 1185-1187.

Ishii, K. (2000). *Advanced pulverized coal injection technology and blast furnace operation*. Oxford, UK: Elsevier/Pergamon.

Iwanga, Y., & Takatan, K. (1989). Mathematical model analysis for oxidation of cokeat high temperature. *ISIJ International, 29*(1), 43-48.

Kobayashi, H., Howard, J. B., & Sarofim, A. F. (1977). Coal devolatilization at high temperatures. *Symposium (International) on Combustion, 16*(1), 411-425.

KPMG. (2017). *Coal price and FX consensus forecasts.* Switzerland: KPMG.

Law, C. K., Makino, A., & Lu, T. F. (2006). On the off-stoichiometric peaking of adiabatic flame temperature. *Combustion and Flame, 145*(4), 808-819.

Li, Y., Zhang, X., Zhang, J., Zhou, J., & Yan, H. (2014). Numerical simulation and optimization of pulverized coal injection with enriched oxygen into blast furnace. *Applied Thermal Engineering, 67*(1–2), 72-79.

Liao, D. (1998). *Analysis and modelling study of raceway phenomena including oil injection*. Oulu: [D. Liao].

Lockwood, F. C., Rizvi, S. M. A., & Shah, N. G. (1986). Comparative predictive experience of coal firing. Proceedings of the Institution of Mechanical Engineers, Part C: Journal of Mechanical Engineering Science, 200(2), 79-87.

Magnussen, B. F. (1981) On the structure of turbulence and a generalized eddy dissipation concept for chemical reaction in turbulent flow. *Nineteeth AIAA Meeting,* St. Louis.

Magnussen, B. F., & Hjertager, B. H. (1976) On mathematical models of turbulent combustion with special emphasis on soot formation and combustion. *Sixteenth Symposium (Int.) on Combustion,* 719-729.

Majeski, A., Runstedtler, A., D'alessio, J., & Macfadyen, N. (2015). Injection of pulverized coal and natural gas into blast furnaces for iron-making: Lance positioning and design. *ISIJ International, 55*(7), 1377-1383.

Markets Insider. (2017). CO2 european emission allowances. Retrieved from http://markets.businessinsider.com/commodities/co2-emissionsrechte

Marshall, E. M., & Bakker, A. (2004). Computational fluid mixing John Wiley & Sons, Inc., Hoboken, NJ.

Martin, S., & Williams, J. R. (2009). *Multiphase flow research* Nova Science Publishers.

Mathieson, J. G., Truelove, J. S., & Rogers, H. (2005). Toward an understanding of coal combustion in blast furnace tuyere injection. *Fuel, 84*(10), 1229-1237.

Moszkowicz, P., Witzel, L., & Claus, G. (1996). Modelling of very fast pyrolysis of heavy fuel oil droplets. *Chemical Engineering Science, 51*(17), 4075-4086.

Nightingale, R., Dippenaar, R., & Lu, W. (2000). Developments in blast furnace process control at port kembla based on process fundamentals. *Metallurgical and Materials Transactions B, 31*(5), 993-1003.

Nogami, H., Yamaoka, H., & Takatani, K. (2004). Raceway design for the innovative blast furnace. *ISIJ International, 44*(12), 2150-2158.

Nomura, S. (1986). Simple treatment on the geometry of raceway zone. *ISIJ International, 26*(2), 107-113.

Nozawa, K., Kasai, A., Matsui, Y., Kitayama, S., Kitano, S., & Shibata, K. (2011). Combustion behaviors of fine coal and its impact on gas permeability at lower part of blast furnace under high pulverized coal rate operation. *ISIJ International, 51*(8), 1336-1343.

Peters, N. (2000). *Turbulent combustion*. Cambridge, England: Cambridge University Press.

Platts. (2015). Pulverized coal injection eyes foray into thermal coal market on price rout. Retrieved from https://www.platts.com/news-feature/2015/metals/pci-thermal-coal-switch/index

Pope, S. B. (1985). PDF methods for turbulent reactive flows. Progress in Energy and Combustion Science, 11(2), 119-192.

Reitz, R. D. (1987). Modeling atomization processes in high-pressure vaporizing sprays. *Atomisation and Spray Technology, 3*(4), 309-337.

Reitz, R. D., & Beale, J. C. (1999). Modeling spray atomization with the kelvin-helmholtz/rayleigh-taylor hybrid model. *Atomization and Sprays*, 9(6), 623-650.

Sazhin, S. S. (2006). Advanced models of fuel droplet heating and evaporation. *Progress in Energy and Combustion Science, 32*(2), 162-214.

Shen, Y., Guo, B., Yu, A., Maldonado, D., Austin, P., & Zulli, P. (2008). Three-dimensional modelling of coal combustion in blast furnace. *ISIJ International, 48*(6), 777-786.

Shen, Y. S., Maldonado, D., Guo, B. Y., Yu, A. B., Austin, P., & Zulli, P. (2009). Computational fluid dynamics study of pulverized coal combustion in blast furnace raceway. *Industrial & Engineering Chemistry Research, 48*(23), 10314-10323.

Shen, Y. S., Guo, B. Y., Yu, A. B., & Zulli, P. (2009a). A three-dimensional numerical study of the combustion of coal blends in blast furnace. *Fuel, 88*(2), 255-263.

Shen, Y. S., Guo, B. Y., Yu, A. B., & Zulli, P. (2009b). Model study of the effects of coal properties and blast conditions on pulverized coal combustion. *ISIJ International, 49*(6), 819-826.

Shen, Y. S., Guo, B. Y., Yu, A. B., Austin, P. R., & Zulli, P. (2011). Three-dimensional modelling of in-furnace coal/coke combustion in a blast furnace. *Fuel, 90*(2), 728-738.

Shen, Y. S., Yu, A. B., Austin, P. R., & Zulli, P. (2012). CFD study of in-furnace phenomena of pulverised coal injection in blast furnace: Effects of operating conditions. *Powder Technology, 223*(0), 27-38.

Shen, Y., Yu, A., Austin, P., & Zulli, P. (2012). Modelling in-furnace phenomena of pulverized coal injection in ironmaking blast furnace: Effect of coke bed porosities. *Minerals Engineering, 33*, 54-65.

Shen, Y., Shiozawa, T., Austin, P., & Yu, A. (2014). Model study of the effect of bird's nest on transport phenomena in the raceway of an ironmaking blast furnace. Minerals Engineering, 63(0), 91-99.

Shen, Y. S., & Yu, A. B. (2016). Modelling of injecting a ternary coal blend into a model ironmaking blast furnace. *Minerals Engineering, 90*, 89-95.

Shih, T., Liou, W., Shabbir, A., Yang, Z., & Zhu, J. (1994). A new k-epsilon eddy viscosity model for high reynolds number turbulent flows: Model development and validation. *Computers and Fluids, 24*(3), 227-238.

Spalding, D. B. (1971). Mixing and chemical reaction in steady confined turbulent flames. *Symposium (International) on Combustion*, 13(1) 649-657.

Takeda, K., & Lockwood, F. C. (1996a). Gas flow calculation with a turbulence model in a packed bed. *Tetsu-to-Hagane, 82*(6), 28-33.

Takeda, K., & Lockwood, F. C. (1996b). Stochastic model of flow and dispersion of fine particles in a packed bed. *Tetsu-to-Hagane, 82*(6), 34-39.

Takeda, K., & Lockwood, F. C. (1997). Integrated mathematical model of pulverised coal combustion in a blast furnace. *ISIJ International, 37*(5), 432-440.

Ubhayakar, S. K., Stickler, D. B., Von Rosenberg, C. W., & Gannon, R. E. (1977). Rapid devolatilization of pulverized coal in hot combustion gases. *Symposium (International) on Combustion, 16*(1), 427-436.

Versteeg, H. K., & Malalasekera, W. (2007). *An introduction to computational fluid dynamics: The finite volume method.* Harlow, England: Pearson Education Ltd.

Vuokila, A., Riihimäki, M., & Muurinen, E. (2014). CFD-modeling of heavy oil injection into blast furnace – atomization and mixing in raceway-tuyere area. *Steel Research International, 85*(11), 1544-1551.

Vuokila Ari, Mattila Olli, Keiski Riitta Liisa, & Muurinen Esa. (2016). CFD modeling of pulverized coal combustion in blast furnace test rig. *Industrial Combustion, 201603* Retrieved from http://www.industrial.combustion.ifrf.net/paper_download.html?paperId=136

Vuokila, A., Mattila, O., Keiski, R. L., & Muurinen, E. (2017). CFD study on the heavy oil lance positioning in the blast furnace tuyere to improve combustion. *ISIJ International, 57*(11). *1911-1920.*

Yeh, C., Du, S., Tsai, C., & Yang, R. (2012). Numerical analysis of flow and combustion behavior in tuyere and raceway of blast furnace fueled with pulverized coal and recycled top gas. *Energy, 42*(1), 233-240.

Zhang, Y., Wei, X., Zhou, L., & Sheng, H. (2005). Simulation of coal combustion by AUSM turbulence-chemistry char combustion model and a full two-fluid model. *Fuel, 84*(14), 1798-1804.

Zhou, C. (2008). *Computational fluid dynamics (CFD) modeling for high rate pulverized coal injection (PCI) into the blast furnace.* Hammond, IN 46321: Purdue University-Calumet, Department of Mechanical Engineering.

Zhou, L., & Huang, X. (1990). Prediction of confined turbulent gas-particle jets by an energy equation model of particle turbulence. *Science China Mathematics, 33*(1), 52-59.

# Original publications

I Vuokila A, Riihimäki M & Muurinen E (2014) CFD-modeling of Heavy Oil Injection into Blast Furnace – Atomization and Mixing in Raceway-Tuyere Area. *Steel Research International 85*(11): 1544-1551.

II Vuokila A, Mattila O, Keiski RL & Muurinen E (2017) CFD study on the heavy oil lance positioning in the blast furnace tuyere to improve combustion. *ISIJ International 57*(11): 1911-1920.

III Vuokila A, Mattila O, Keiski RL & Muurinen E (2016) CFD modeling of pulverized coal combustion in blast furnace test rig. *Industrial Combustion. Article No. 201603: 1.*

IV Vuokila A, Mattila O, Keiski RL & Muurinen E (2018) CFD modeling on the effect of double lance position on pulverized coal combustion in blast furnace tuyere-raceway area. Manuscript.



Original publications are not included in the electronic version of the dissertation.

624. Mustonen, Miia (2017) Analysis of recent spectrum sharing concepts in policy making

625. Visuri, Ville-Valtteri (2017) Mathematical modelling of chemical kinetics and rate phenomena in the AOD Process

626. Lappi, Tuomas (2017) Formation and governance of a healthy business ecosystem

627. Samarakoon, Sumudu (2017) Learning-based methods for resource allocation and interference management in energy-efficient small cell networks

628. Pargar, Farzad (2017) Resource optimization techniques in scheduling : applications to production and maintenance systems

629. Uusitalo, Pauliina (2017) The bound states in the quantum waveguides of shape Y, Z, and C

630. Palosaari, Jaakko (2017) Energy harvesting from walking using piezoelectric cymbal and diaphragm type structures

631. Mononen, Petri (2017) Socio-economic impacts of a public agency – enhancing decision support for performance management

632. Kärkkäinen, Marja-Liisa (2017) Deactivation of oxidation catalysts by sulphur and phosphorus in diesel and gas driven vehicles

633. Viittala, Harri (2017) Selected methods for WBAN communications — FM-UWB and SmartBAN PHY

634. Akram, Saad Ullah (2017) Cell segmentation and tracking via proposal generation and selection

635. Ylimäki, Markus (2017) Methods for image-based 3-D modeling using color and depth cameras

636. Bagheri, Hamidreza (2017) Mobile clouds: a flexible resource sharing platform towards energy, spectrum and cost efficient 5G networks

637. Heikkinen, Kari-Pekka (2018) Exploring studio-based higher education for T-shaped knowledge workers, case LAB studio model

638. Joshi, Satya Krishna (2018) Radio resource allocation techniques for MISO downlink cellular networks

639. Shashika Manosha Kapuruhamy Badalge, (2018) Convex optimization based resource allocation in multi-antenna systems

640. Koskela, Pekka (2018) Energy-efficient solutions for wireless sensor networks

Book orders:
Granum: Virtual book store
http://granum.uta.fi/granum/

UNIVERSITY OF OULU P.O. Box 8000 FI-90014 UNIVERSITY OF OULU FINLAND

# ACTA UNIVERSITATIS OULUENSIS



UNIVERSITY of OULU
OULUN YLIOPISTO

ISBN 978-952-62-1769-7 (Paperback)
ISBN 978-952-62-1770-3 (PDF)
ISSN 0355-3213 (Print)
ISSN 1796-2226 (Online)